

Beam Position Monitoring System In Accelerators

Department of Electrical and Information Technology
Lund University

&

European Spallation source

Lund, Sweden

Elham Vafa

Rouhina Behpour

Supervisors: Anders Karlsson and Andreas Jansson

January, 2012

Abstract

This thesis is done in collaboration with European Spallation Source (ESS) in Lund, Sweden which will be one of the largest accelerator research centers in the world using the neutron scattering technique. The ESS facility is anticipated to open in 2019 and will be fully operational in 2025.

A particle accelerator speeds up the charged particles by using electromagnetic fields to propel particles to high speed close enough to the speed of light. For the proton Linear accelerator, the design is based on the operating frequency of 352.2 MHz due to the accessibility of high power RF sources, and to avail the collaboration with Cern [1].

An essential part of each accelerator is the Beam Position Monitoring system, BPM, which provides information about the beam size and shape. BPM is usually composed of four electrodes installed around the accelerator wall. The purpose of this thesis is to study the relations between the BPM electrodes voltages and the proton beam size and shape to determine the system accuracy.

Different tolerances like temperature variations or fabrication errors can occur on the BPM electrode dimensions and position. Hence, BPM calibration is highly needed in order to get high accuracy. In doing so, finding a correlation between the errors in the coupling from the beam to the electrodes and the errors in the coupling between the electrodes can be useful. Hence, S-parameter matrices obtained from a BPM as a four port system with an internal source are compared with an off internal source BPM system. Interestingly, the results for both cases are in a good agreement.

At an early step of this work, in order to confirm the accuracy of the results, a basic BPM model is simulated in CST Microwave Studio software and compared to the same simulated model in Comsol Multiphysics software. Afterward, the rest of the models are done mostly in Comsol to get the required information.

Since ESS and its partners are currently engaged in technical design review, the BPM model has not been designed yet. Therefore, numerical simulations are done based on BPM equipment characteristics used in Max-Lab at Lund University.

Acknowledgement

We would like to express our deep gratitude to those who have guided and assisted us in the present work and manuscript. The work presented in this thesis would not have been possible without their feedback and support.

We wish to extend our appreciation to our supervisors, Anders Karlsson and Andreas Jansson who showed us the correct way of approaching the problems. We are very grateful to the whole team at the accelerator division at ESS for giving us the great opportunity to work with them.

Finally we would like to thank our parents and family for giving us love and support.

Table of Contents

1. Introduction	1
2. Theory	3
2.1 Beam Position Monitoring	3
2.2 Beam position measurement	4
2.3 BPM button voltage	5
3. BPM Simulations	7
3.1 2D simulations	7
3.2 3D simulations	9
4. Practical models	14
4.1 Variations of electrode outer and inner radius	14
4.2 Variations of electrode inner radius	16
4.3 Variations of electrode outer radius	19
4.4 Insertions of electrode inner cylinder inside the pipe	22
4.5 Displacements of electrode inner cylinder (Radially/longitudinally)	24
5. Beam multipole expansions	31
5.1 Beam displacements along the vertical axis	32
5.2 Beam Displacements along a line between the horizontal and vertical axes	35
5.3 Elliptic beam	37
6. Conclusions	40
A. Basic physics behind an accelerator	41
B. Beam position measurement	43
B.1 BPM button voltage	43
B.2 Multipole expansions	44
B.3 S-parameters	45
C. Modeling instructions	47
C.1 2D simulation (Comsol)	47
C.2 3D simulation (Comsol and CST)	47
D. Basic consideration	55
D.1 Mesh	55
D.2 Frequency	56
D.3 Beam size	57
E. S-parameters tables with considering Renormalization	59

F. S-parameters tables without considering Renormalization-----66

7. References-----83

List of Figures

1.1 Visualization of ESS in Lund	1
1.2 Quadrupole magnets at SLAC, Magnets are used to confine beam	1
2.1 Two more important types of BPM instruments	3
2.2 Button BPM unit	3
2.3 Horizontal and Vertical Button electrodes	4
2.4 Schematic of a Schematic of a displaced beam	4
2.5 Geometry of a capacitive BPM	5
3.1 2D structure of the button electrode, provided by Max-lab	8
3.2 2D structure of the button electrode in Comsol	8
3.3 Transmission from the input port to the output port of the electrode, figure 3.1	9
3.4 A BPM system with the beam in the pipe center by using two softwares: a) Comsol Multi-physics and b) CST Microwave Studio	9
3.5 A BPM system without the beam, PEC wire, in the pipe center	11
3.6 A BPM system a) pipe cross section of the pipe b) with the PEC inside the pipe	11
3.7 A BPM system a) pipe cross section of the pipe b) without the PEC inside the pipe	12
3.8 Manufacture tolerances of electrode number 2 , for the case with the inner conductor inside the pipe	12
3.9 S-parameters for different tolerances of electrode number 2, provided by Max-lab, for the case with the inner conductor inside the pipe	13
4.1 Variation of both inner and outer radiuses of electrode number 2 ,with the PEC wire in the pipe center	15
4.2 S-parameters for different inner and outer radiuses of electrode number 2, with the inner conductor inside the pipe	15
4.3 Horizontal errors for different inner and outer radiuses of electrode number 2, with the inner conductor inside the pipe	15
4.4 Variation of both inner and outer radius of the electrode number 2 ,with the PEC wire in the pipe center	16
4.5 S-parameters for different inner and outer radiuses of electrode number 2, without the inner conductor inside the pipe	16

4.6 Horizontal error for different inner and outer radiuses of electrode number 2, without the inner conductor inside the pipe	16
4.7 Variation of inner radius of electrode number 2, with the PEC wire in the pipe center.....	17
4.8 S-parameters for different inner radiuses of electrode number 2, with the inner conductor inside the pipe	18
4.9 Horizontal error for different inner radiuses of electrode number 2, with the inner conductor inside the pipe	18
4.10 Variation of inner radius of electrode number 2,without the PEC wire in the pipe center	18
4.11 S-parameters for different inner radiuses of electrode number 2, without the inner conductor inside the pipe	19
4.12 Horizontal Error for different inner radiuses of electrode number 2, without the inner conductor inside the pipe	19
4.13 Variation of outer radius of electrode number 2, with the PEC wire in the pipe cente.....	20
4.14 S-parameters for different outer radiuses of electrode number 2, with the inner conductor inside the pipe.	20
4.15 Horizontal error for different outer radiuses of electrode number 2, with the inner conductor inside the pipe	21
4.16 Variation of outer radius of electrode number 2, without the PEC wire in the pipe center.....	21
4.17 S-parameters for different outer radiuses of electrode number 2, without the inner conductor inside the pipe	21
4.18 Horizontal error for different outer radiuses of electrode number 2, without the inner conductor inside the pipe	22
4.19 Schematic of a capacitive BPM	22
4.20 Insertion of the inner cylinder of electrode 2 inside the pipe, with the PEC wire in the pipe center.....	23
4.21 S-parameters for different insertions of electrode number 2, with the inner conductor inside the pipe	23
4.22 Horizontal error for different insertions of electrode number 2, with the inner conductor inside the pipe	23
4.23 Insertion of the inner cylinder of electrode 2 inside the pipe, without the PEC wire in the pipe center	24
4.24 S-parameters for different insertions of electrode number 2, without the PEC wire in the pipe center	24

4.25 Horizontal error for different insertions of electrode number 2, without the PEC wire in the pipe center	24
4.26 Eccentricity of the inner conductor inside the coaxial cable	25
4.27 Radial displacements of the inner cylinder of electrode number 2 toward port 4, with the PEC wire in the pipe center	26
4.28 S-parameters for different radial displacements of electrode number 2, with the PEC wire in the pipe center.....	26
4.29 Horizontal errors for different radial displacements of electrode number 2, with the PEC wire in the pipe center	26
4.30 Radial displacements of the inner cylinder of electrode number 2, without the PEC wire in the pipe center: a) Clockwise and b) counter Clockwise	27
4.31 S-parameters for different radial displacements of electrode number 2, without the PEC wire in the pipe center: a) Clockwise and b) counter clockwise	27
4.32 Horizontal errors for different radial displacements of electrode number 2, without the PEC wire in the pipe center: a) Clockwise and b) counter clockwise	27
4.33 Longitudinal displacements of the inner cylinder of electrode number 2 toward input port, with the PEC wire in the pipe center	28
4.34 S-parameters for different longitudinal displacements of electrode number 2, with the PEC wire in the pipe center	28
4.35 Horizontal errors for different longitudinal displacements of electrode number 2, with the PEC wire in the pipe center	28
4.36 Longitudinal displacements of the inner cylinder of electrode number 2 toward input port, without the PEC wire in the pipe center	29
4.37 S-parameters for different longitudinal displacements of electrode number2, without the PEC wire in the pipe center	29
4.38 Horizontal errors for different longitudinal displacements of electrode number 2, without the PEC wire in the pipe center	29
4.39 Comparison between the clock wise and counter clockwise radial displacements and longitudinal displacements of electrode number 2, without the inner conductor inside the pipe	30
5.1 Displacement of the inner PEC wire along the vertical axis z	32
5.2 S-parameters for different displacements of the beam along the vertical axis by: a) adding extra electrode to the button and b) using the Lumped port	32
5.3 Transmission through buttons 2 and 3 for different displacements of the beam along the vertical axis by: a) adding extra electrode to the button and b) using the Lumped port	33

5.4 Dipole moments for different displacements of the beam along the z-axis by: a) adding extra electrode to the button and b) using the Lumped port	34
5.5 Dipole signals for different displacements of the beam along the z-axis by: a) adding extra electrode to the button and b) using the Lumped port	34
5.6 Displacement of the inner pipe along the line $y = z$	35
5.7 S-parameters for different displacements of the beam along the line $y=z$ by: a) adding extra electrode to the button and b) using the Lumped port	35
5.8 Transmission through port 2 and 3 for different displacements of the beam along the line $y=z$ by: a) adding extra electrode to the button and b) using the Lumped port	35
5.9 Dipole moments for different displacements of the beam along the line $y=z$ by: a) adding extra electrode to the button and b) using the Lumped port	36
5.10 Comparison of the Dipole moments and Dipole signals for displacement of the beam along the line $y=z$ by: a) adding extra electrode to the button and b) using the Lumped port.....	37
5.11 Ellipse shape of the beam with the horizontal diameter $2a$ and vertical diameter $2b$	37
5.12: Buttons transmissions on vertical and horizontal axis by: a) adding extra piece to the electrode and b) using the Lumped port. , 300MHz, [dB]	38
5.13: The quadrupole moments of Elliptic beam with different semimajor axis a , and semiminor axis b , in horizontal and vertical axes vs the quadrupole signals $[(S41 dB+ S51 dB)-(S21 dB+ S31 dB)]$ by: a) adding extra piece to the electrode and b) using the Lumped port,300MHz [dB]	38
5.14: The Quadrupole moments vs quadrupole signals of Elliptic beam with different semimajor axis a , and semiminor axis b , in horizontal and vertical axes vs the quadrupole signals $[(S41 dB+ S51 dB)-(S21 dB+ S31 dB)]$ by: a) adding extra piece to the electrode and b) using the Lump port. , 300MHz, [dB]	39

List of Tables:

3.1 Transmission from the input port to the output port of the electrode	9
3.2 BPM parameters	10
3.3 S-parameters before renormalization and after using renormalization in CST and COMSOL	10
3.4 S-parameters for different tolerances of electrode number 2, provided by Maxlab, for the case with the inner conductor inside the pipe	12
5.1 Linear charge (Monopole) on the inner pipe surface for different displacements of the beam along the vertical axis	33
5.2 Linear charge (Monopole) on the inner pipe surface for different displacements of the beam along the line $y = z$	36

Chapter 1:

Introduction

In 1928, Wideröe built the first linear ion accelerator based on alternating voltage applied on a tube. The produced potential differences could accelerate the ions. Then in 1930, the first small circular accelerator established by Lawrence and Livingston [2]. Since the late twenties, some kinds of accelerator schemes have been designed such as circular and linear accelerators and also two main subgroups of accelerators which are electron and proton accelerators [3, 4]. Accelerators are used by a very wide range of applications like optics and light sources for chemistry in scientific fields and medical applications in cancer therapy, radiology, and isotope production [5]. Today, there are number of research accelerator facilities around the world such as Spallation Neutron Source (SNS) in USA, CERN in Geneva and European Spallation Source (ESS) in Sweden. In 2001, ESS Scandinavia is established by Scandinavian neutron scattering associations. ESS is a joint venture of 17 European countries and it aims to be the brightest neutrons source in the world. ESS laboratory is based on a linear accelerator (Linac) in which protons accelerate and then strike a heavy metal target resulting intensive pulses of neutrons (Figure 1.1) [6].



Figure 1.1: Visualization of ESS in Lund [7]

In summary, at the pulsing heart of ESS, there is one ion source producing proton pulses. This intense proton pulse is injected into the linear accelerator. Ideally the beam should be located at the center of the pipe. The centering of the beam is done by using a lattice of quadrupole magnets. Figure 1.2 depicts a quadrupole magnet used to focus the beam.

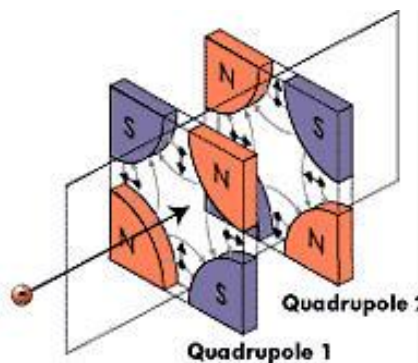


Figure 1.2: Quadrupole magnets at SLAC, Magnets are used to confine beam [8]

The beam trajectory may be deflected from the pipe center due to a variety of reasons. That is why having a beam position monitoring system is highly needed in accelerators. The beam position monitoring system (BPM) is the system that determines the position of the beam. There are different kinds of BPM systems. For instance, a number of strip lines or buttons may be welded to the accelerator wall to pick up the induced voltages. The voltages are further processed to derive the exact position of the beam. The BPMs are calibrated mostly before installation to determine the offsets of their electrical and mechanical centers [9]. All beam positions are measured with respect to the electrical center where the normalized voltage difference is zero [10].

In this thesis a BPM system based on button electrodes is analyzed. This BPM structure is simulated to find the relations between the beam characteristics and voltage on the electrodes in order to determine the accuracy of the system.

Chapter two introduces the BPM structure and the BPM button voltage. It is followed by a brief explanation of the dependence of the results to the mesh size, frequency range and beam size. Different errors induced by fabrication, temperature or other errors on the BPM are analyzed in chapter four. Attention is paid to the BPM simulations at different transverse beam positions in chapter five. Finally, the conclusions are presented in chapter six, which follows by some appendixes for more information, about the theoretical part, modeling instruction of the simulations in both CST microwave Studio (MWS) and COMSOL multiphysics and some other simulation information.

Chapter 2:

Theory

2.1 Beam Position Monitoring

As the beam passes through the accelerator vacuum tube, it produces electromagnetic fields that depend on the beam position and geometry. The beam locations are detected by a number of electrodes around the beam pipe called the beam position monitor (BPM) device. The beam should be ideally located at the pipe center. To assure proper positioning of the beam, the beam position should be monitored continuously in real time.

A BPM normally provides information about the beam phase and beam transverse position by using position sensitive detectors (PSDs). In most accelerators, each BPM setup consists of four PSDs symmetrically placed 90 degrees apart, followed by an electronic system for signal processing in order to determine the beam transverse position. The beam position is achieved by comparing the picked up voltages of either horizontal or vertical directions [10]. The two more important types of PSD instruments are buttons and strip lines as shown in Figure 2.1 [11].

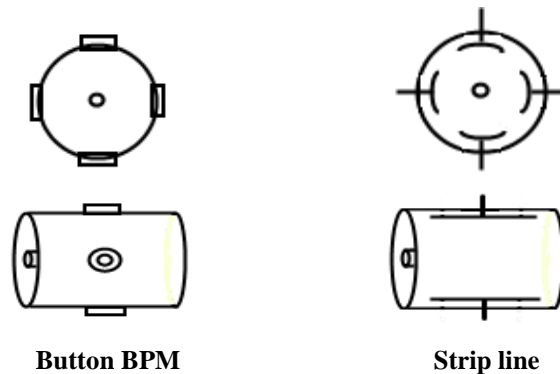


Figure 2.1: Two more important types of BPM instruments

PSDs used in this project are button electrodes that consist of two pairs, one pair located in the horizontal diameter of the pipe and the other pair located in the vertical diameter to determine the Y and Z position of the beam (Figure 2.2) [12]. Buttons are usually terminated with an impedance of 50 Ω . In comparison to the strip lines, buttons have lower coupling impedance [15]. Usually buttons are the best choice due to the high accuracy in fabrication and installation [16].

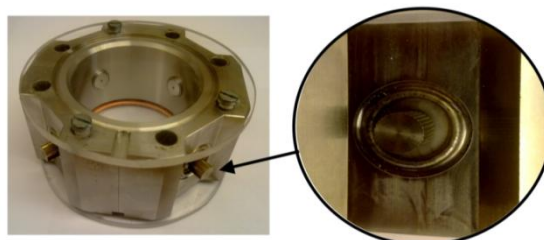


Figure 2.2: Button BPM unit

The beam current induces magnetic field and electric so the main issue is to investigate how button electrodes respond to the beam and detect the displacement of the beam from the center of the pipe. In

other words, Beam position is extracted by comparing the voltages which has been picked up either on horizontal or vertical directions as shown in figure 2.3.

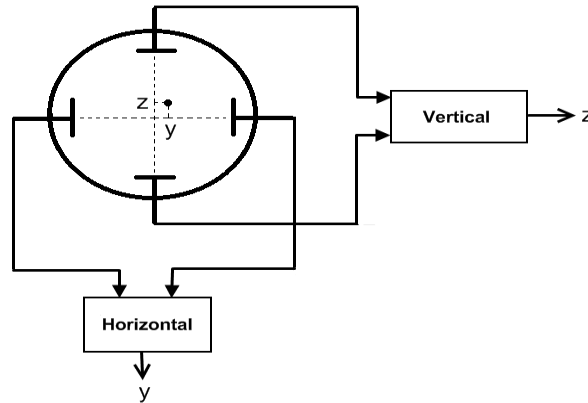


Figure 2.3: Horizontal and Vertical Button electrodes

For the BPM implementation, there are many considerations like electronics, signals processing, calibrations and also mechanics. One important design consideration for a BPM system is minimizing mechanical deformation to improve accuracy [17].

There are two kinds of different characteristics with BPMs [18, 19]:

1. Position resolution is the most important character of the BPM. It corresponds to the smallest deflection of the beam that is detectable by the BPM. The position sensitivity can be obtained from S-parameters calculated in frequency domain.
2. The time resolution is the time needed for the BPM to get ready for the next bunch detection. It is defined by the bandwidth of the signal: $\tau = \frac{1}{\pi \times BW}$ [s]

2.2 Beam position measurement:

As a result of the beam passing through the accelerator tube, an image charge appears on the beam pipe wall as shown in figure 2.4 (see appendix A). The variation of the image charge distribution is a key to find the beam position. The beam position is determined from the relative amplitudes of the signals induced in the electrodes [20]. For a capacitive coupling, the voltage difference of four pickups in two opposite plates for horizontal(Y) and vertical (Z) directions ($\Delta V_y = V_{right} - V_{left}$ or $\Delta V_z = V_{up} - V_{down}$) determines the deviation of the beam center from the pipe center. If the beam is exactly located in the center of the vacuum tube, the charged distribution on the pipe wall is exactly uniform, so the pickup voltages of the buttons are the same [21, 22].

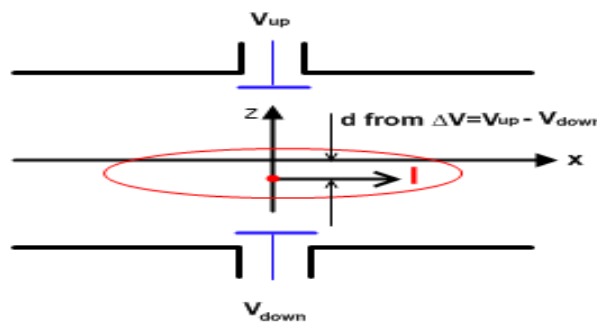


Figure 2.4: Schematic of a displaced beam along the z-axis

Non –equal current distribution on the pipe wall for small displacements is proportional to the beam position, but for large beam displacements, there is no linear dependence anymore. One of the methods to extract the beam position from BPM signals is (Δ / Σ) method [23]. The horizontal and vertical displacements can be calculated by the following equations [24]:

$$Z = \frac{1}{S_z} \times \frac{V_{up} - V_{down}}{V_{up} + V_{down}} \equiv \frac{1}{S_z} \times \frac{\Delta V_z}{\Sigma V_z} \quad (\text{Vertical})$$

$$Y = \frac{1}{S_y} \times \frac{V_{right} - V_{left}}{V_{right} + V_{left}} \equiv \frac{1}{S_y} \times \frac{\Delta V_y}{\Sigma V_y} \quad (\text{Horizontal})$$

Both Y and Z are independent of the beam intensity that means beam intensity does not affect the position information. The proportional constants S_z and S_y between the beam movement and the evaluated voltage difference is called position sensitivity with unit of [%/mm] for linear processing and [dB/mm] in logarithmic case. It is defined as the response of the BPM to the displacement of the beam.

$$S_z(z) = \frac{d}{dz} \left(\frac{\Delta V_z}{\Sigma V_z} \right) = [\%/mm] \quad (\text{Linear})$$

$$S_z(z) = \frac{d}{dz} \left(\log \frac{V_{up}}{V_{down}} \right) = [dB/mm] \quad (\text{Logarithmic})$$

For small beam displacements, the position signal is a linear function of the displacement. If the beam displacement is large compared to the beam size, the signal has a nonlinear dependence of the vertical and horizontal directions. The position signal is a function of vertical and horizontal displacement and also of frequency, i.e. $S(y,z,\omega)$. The electric center is derived by equal output voltages on both buttons in a plate. A small asymmetry in BPM structure leads to an offset of the geometrical origin compared to the electrical center. Position signal can be different for the vertical and the horizontal plane due to the small non symmetries for both directions. By a perfect mechanical design, the frequency dependence of the position signal and the offset can be minimized.

2.3 BPM Button voltage:

The induced surface charge density ρ_s (C/m²) on the conducting shell, for a centered beam can be obtained by the following formula [24, 25]:

$$\rho_s = \frac{\rho_l}{\text{Duct circumference}} = \frac{\rho_l}{2\pi R_p} \quad , \text{ Where } \rho_l \text{ (C/m) is the line charge density of the beam.}$$

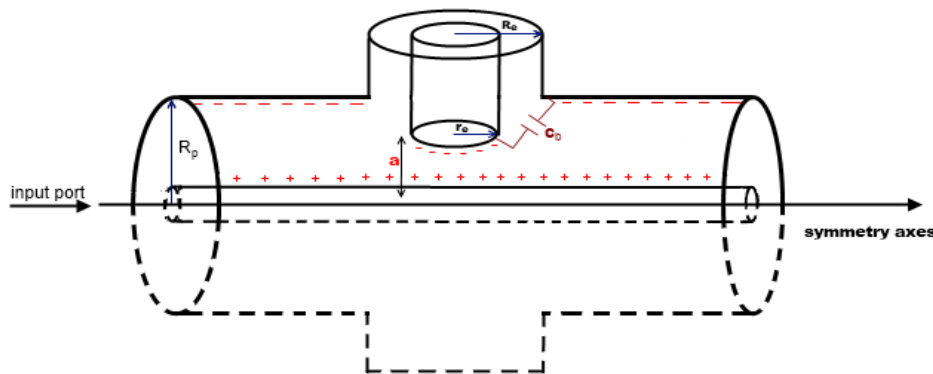


Figure 2.5: Geometry of a capacitive BPM

The voltage induced on each electrode depends on the transfer impedance which is given by:

$$|Z_t| = \frac{1}{\beta c} \times \frac{1}{C_b} \times \frac{\pi r_e^2}{2\pi a} \times \frac{\frac{\omega}{\omega_{cut}}}{\sqrt{1 + \frac{\omega^2}{\omega_{cut}^2}}}$$

Where $\omega_{cut} = 2\pi f_c$ and f_c is the cut-off frequency. Notice that Z_t act as a first order high pass filter with cut off frequency f_c .

The button voltage formula for frequencies below and above the cut off frequency is obtained as follows:

At high frequencies, $f \gg f_c$,

$$Z_t \propto \frac{\frac{\omega}{\omega_{cut}}}{\sqrt{1 + \frac{\omega^2}{\omega_{cut}^2}}} \rightarrow 1$$

And the resulting voltage is equal to:

$$V_{button} = \frac{\pi r_e^2}{2\pi R_p} \times \frac{1}{\beta c} \times \frac{1}{C_b} \times I_{beam}(\omega) \quad (2.1)$$

In the low frequency range, $f \ll f_c$, the transfer impedance is proportional to:

$$Z_t \propto \frac{\frac{i\omega}{\omega_{cut}}}{1 + \frac{i\omega}{\omega_{cut}}} \rightarrow \frac{i\omega}{\omega_{cut}}$$

The voltage is independent of the capacitance:

$$V_{button} = \frac{\pi r_e^2}{2\pi R_p} \times \frac{Z_{coax}}{\beta c} \times i\omega \times I_{beam}(\omega) \quad (2.2)$$

Formula 2.1 and 2.2 illustrate that the button voltage depends on the beam current, frequency, the cross section area of the electrode, the impedance seen by button, and the distance between the beam and accelerator pipe wall (see appendix B.1).

Chapter 3

BPM Simulations:

During this work, several simulations have been done under the condition that the general properties should be the same for all the models. Some of the general characteristics such as the mesh size, frequency and the beam size are explained in appendix D.

Analysis softwares like Comsol or CST, partition the model into small units called “mesh”. In Comsol, it is possible to choose the element size either by default mesh definitions, extremely coarse, extra coarse, coarser, coarse, normal, fine, extra fine, extremely fine or by using custom option and entering the desired value. In this thesis, the common mesh size used for all models is finer (in Comsol 4.2) which provides small and more symmetric units and small errors.

According to the formula 2.1 and 2.2, the button voltage and as a result the induced S-parameters are frequency dependent, therefore any change in the frequency affects the result. S-parameters for different frequencies in the interval 200 MHz to 400 MHz with step of 50 MHz are presented in appendix D. In all other simulations the BPM behavior is studied at the frequency 300 MHz while the beam radius used for all 3D simulations is equal to 1mm.

At an early step of the design process, the button electrode simulation was performed using Comsol Multi-physics, 2D axial symmetry. After that the BPM was simulated in 3D by using CST Microwave Studio and Comsol programs. The modeling instructions in 2D and 3D are presented in appendix C.

3.1 2D simulations:

The geometry design comes from figure 3.1 provided by Maxlab. It can be seen from this figure that the BPM electrode geometry is complicated. This makes it hard to obtain a high accuracy by simulation softwares such as Comsol and CST. According to figure 3.1, each electrode can be considered as two successive coaxial transmission lines with different characteristic impedances due to the different radius sizes. The input port of the electrode has the inner and outer radiuses equal to 5.4 and 5.65mm which correspond to 2.71Ω characteristic impedance. The characteristic impedance of the Coaxial line is geometry dependent. Hence, the mentioned errors in figure 3.1 change the characteristic impedance of the coaxial line attached to the pipe wall. Moreover, the upper $50\ \Omega$ coaxial line is attached to a SMA connector.

This section is devoted to study the S-parameters behavior when geometrical deviations appear on the BPM electrode coaxial line.



BPM Electrode Feedthrough ESRF-85.50.0056.C (version C)

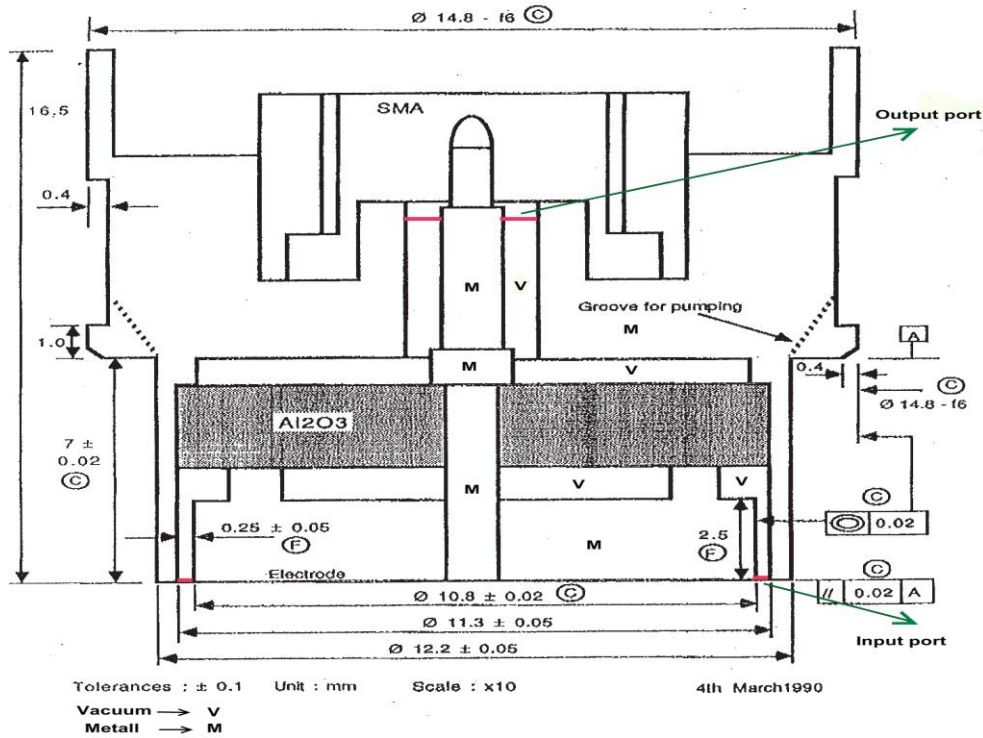


Figure 3.1: 2D structure of the button electrode, provided by Max-lab

Figure 3.2 shows the simplified figure of the button electrode depicted in figure 3.1 in 2D axial symmetry mode of Comsol.

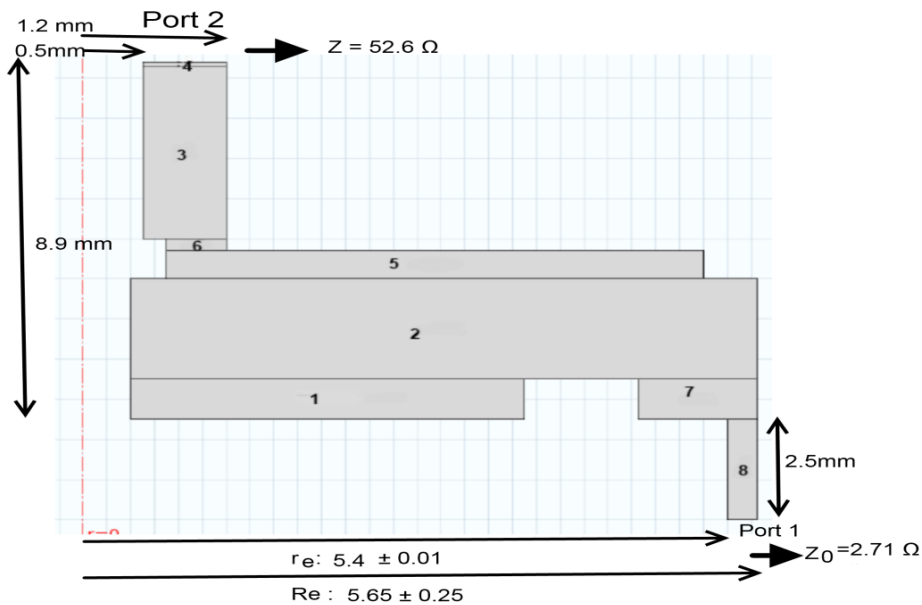


Figure 3.2: 2D structure of the button electrode in Comsol

The outer radius is symbolized with 'Re' and the inner one with 're'. Table 3.1 shows transmission from port 1 to port 2, S_{21} , for different inner and outer radiuses, as indicated in figure 3.2.

Table 3.1: Transmission from the input port to the output port of the electrode (see figure 3.1)

	Radiuses[mm]	S_{21} [dB]
1	Re:5.625 , re:5.39, (d:0,235)	-7.5156
2	Re:5.65 , re:5.4, (d:0.25)	-7.285
3	Re:5.675 ,re:5.41, (d:0,265)	-7.0696

According to the formula 2.2, an increase of the electrode area results in more transmission. The 2D simulation results confirm this theory, as shown in figure 3.3.

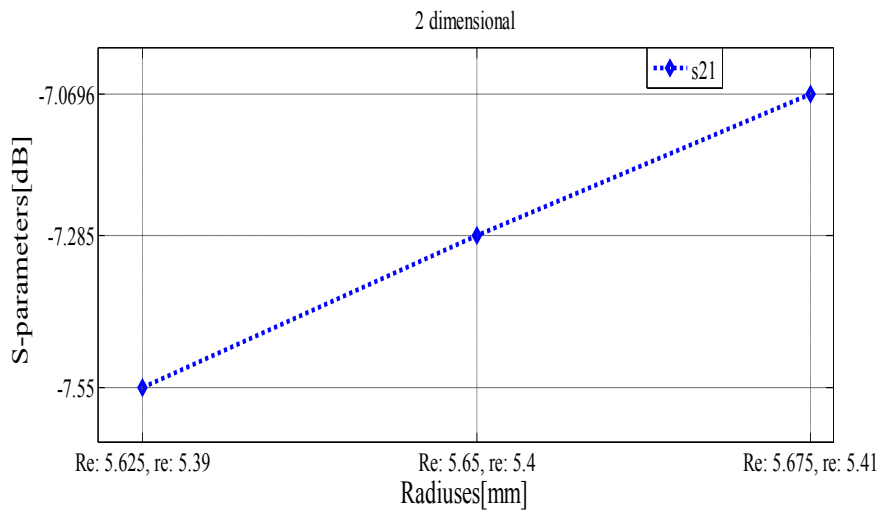


Figure 3.3: Transmission from the input port to the output port of the electrode, figure 3.1

The main advantage of setting up the model in 2D is that it solves much faster and uses less memory in order to get the results. The drawback is that it can only be used for axially symmetry geometries. That is why this thesis is mostly focused on 3D simulations.

3.2 3D simulations:

The BPM can be viewed as a four port system with an internal source, the beam. Coaxial structure is used for the main pipe with the beam in its center as well as the electrodes.

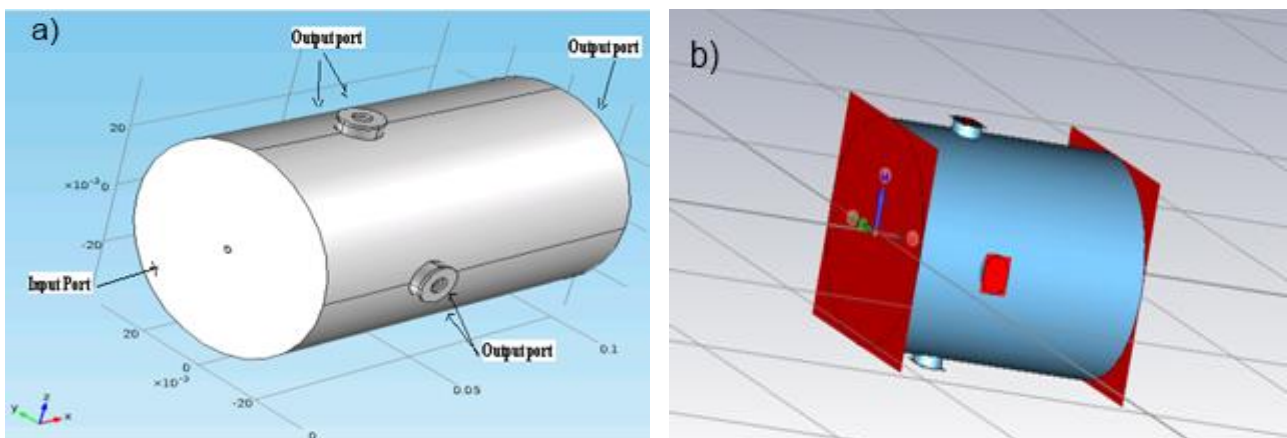


Figure 3.4: A BPM system with the beam in the pipe center by using two softwares: a) Comsol Multi-physics and b) CST Microwave Studio.

A view of the final schematic of the BPM is shown in figure 3.4. The BPM parameters are presented in table 3.2.

Table 3.2: BPM parameters

Electrode radiuses	Value [mm]	Description
R_p	32.5	Vacuum tube outer radius
r_p	1	Vacuum tube inner radius, beam
L	100	Vacuum tube Length
$R_{e i}$	5.65	2.71 Ω coaxial outer radius
$r_{e i}$	5.4	2.71 Ω coaxial inner radius
$R_{e o}$	5.65	50 Ω coaxial outer radius
$r_{e o}$	2.45	50 Ω coaxial inner radius
In	0.9	Electrode insertion inside the vacuum tube
L1	3.7	2.71 Ω coaxial cable length
L2	1	50 Ω coaxial cable length

A part of this thesis is devoted to study the effect of the electrode geometry variations, on the S-parameters. At the early step of the simulations, according to figure 3.1 each button electrode was considered to be a 2.71 Ω coaxial line. The electrode geometry variations change both load and electrode characteristic impedances. Hence, the results are a combination of two different effects; one is due to the variation in electrode size and the other one is because of the load variations. Therefore, in order to remove the load impedance effect and having a pure effect of electrode geometry variations, the load impedance should be kept constant. In reality the electrode is hooked up to the cable with constant 50 Ω characteristic impedance. Thus, all electrodes ports impedances are renormalized to 50 Ω . In CST Microwave Studio, by using S-parameter renormalization option, the results convert to the real values. In Comsol Multiphysics, there is no S-parameter renormalization option so by adding a short constant 50 Ω coaxial cable, attached to the electrode or using lumped port definition, the renormalized results are obtained. The outcomes from these different ways are in good agreement, as shown in table 3.3. S_{n1} shows the coupling between the beam, port 1, to the electrode number 'n'. In other words, S_{n1} shows the transmission through the nth electrode.

Table 3.3: S-parameters before renormalization and after using renormalization in CST and COMSOL

CST	Before Renormalization	After Renormalization
S_{21}	-66.496091	-54.49993
S_{31}	-66.477514	-54.491521
S_{41}	-66.530012	-54.484455
S_{51}	-66.519306	-54.513899
COMSOL	Before Renormalization	After Renormalization
S_{21}	-66.3007	-54.5103
S_{31}	-66.301	-54.5099
S_{41}	-66.3008	-54.5098
S_{51}	-66.3009	-54.5102

The simulation results before using renormalization are presented in appendix F.

One of the goals of this work is to find a relation between two different cases in a BPM system:

- 1- A BPM system with a beam in the pipe center.
- 2- A BPM system without a beam in the pipe center (an empty vacuum tube).

The comparison results might be used for calibration

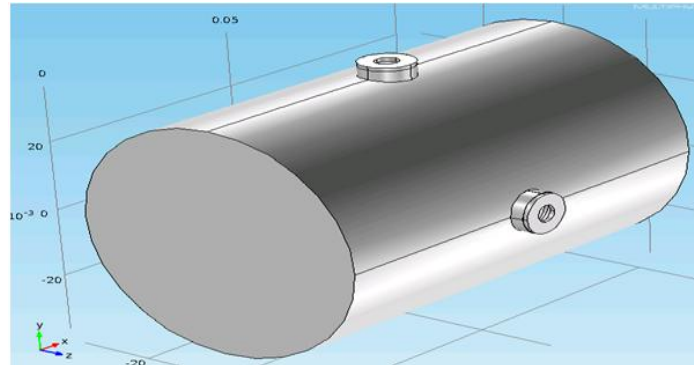


Figure 3.5: A BPM system without the beam, PEC wire, in the pipe center

Therefore, all simulations have been done for two different cases:

1. A vacuum tube with a beam, in its center which is modeled by a coaxial structure; In this case, the input port is the entrance of the vacuum tube, called port 1, whereas the exit of the vacuum tube, port 6 and also all of the electrode ports are defined as output ports, figure 3.6. In doing so, the target is to find the coupling between the beam, PEC wire in the pipe center and the electrodes installed around the pipe wall.

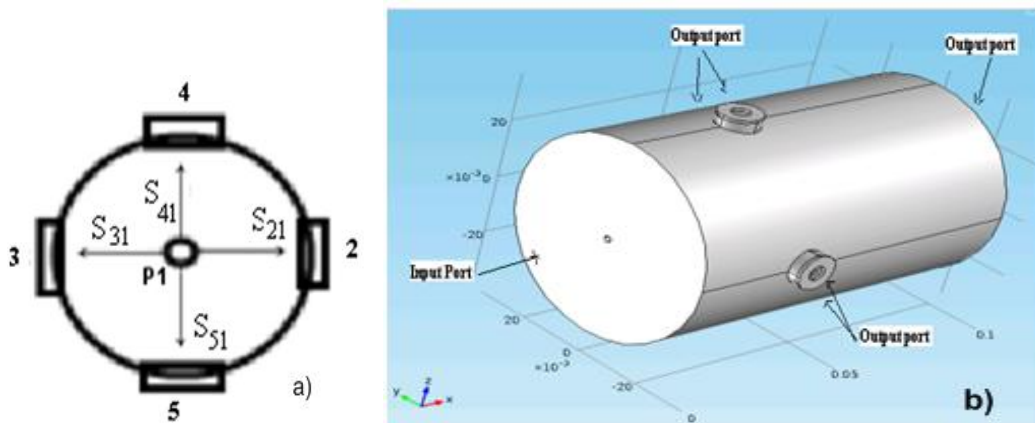


Figure 3.6: A BPM system a) cross section of the pipe b) with the PEC inside the pipe

2. There is no PEC wire (beam) inside the tube, i.e. it is an empty vacuum tube. One of the electrodes is considered to be the input port, port 1, and the other three electrodes are output ports. In this case, the aim is to find the coupling between port 1, and the three other electrodes, as illustrated in figure 3.7.

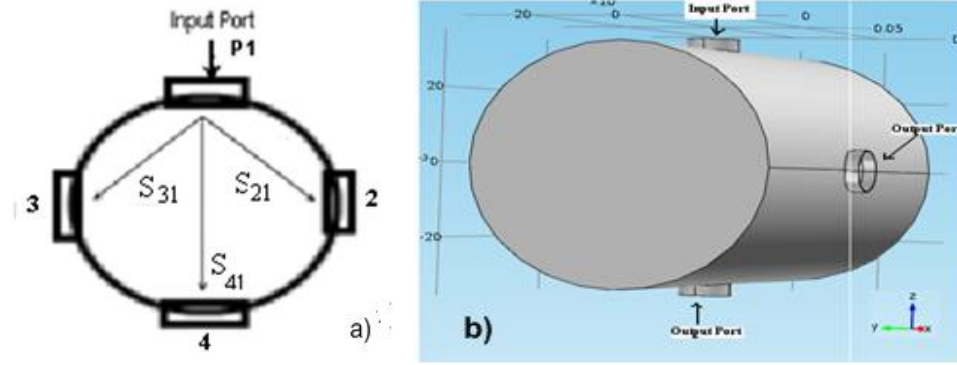


Figure 3.7: A BPM system a) cross section of the pipe b) without the PEC inside the pipe

In this part the electrode manufacture tolerances provided by Maxlab are studied in three dimensional simulations as it has been studied for two dimensional in section 3.1.

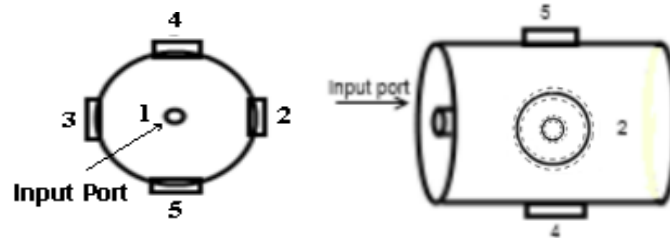


Figure 3.8: Manufacture tolerances of electrode number 2 , for the case with the inner conductor inside the pipe

Table 3.4: S-parameters for different tolerances of electrode number 2, provided by Maxlab, for the case with the inner conductor inside the pipe (see figure 3.8).

Size[mm]	S_{21} [dB]	S_{31} [dB]	S_{41} [dB]	S_{51} [dB]	$ S_{31} - S_{21} $ [dB]	$ S_{51} - S_{41} $ [dB]
Re: 5.625 re: 5.39 (d: 0.235)	-54.6108	-54.51	-54.5101	-54.5101	0.1936	0
Re: 5.65 re: 5.4 (d: 0.25)	-54.5103	-54.5099	-54.5098	-54.5102	0.0004	0.0004
Re: 5.675 re: 5.41 (d: 0.285)	-54.3752	-54.5096	-54.5096	-54.5096	0.1344	0

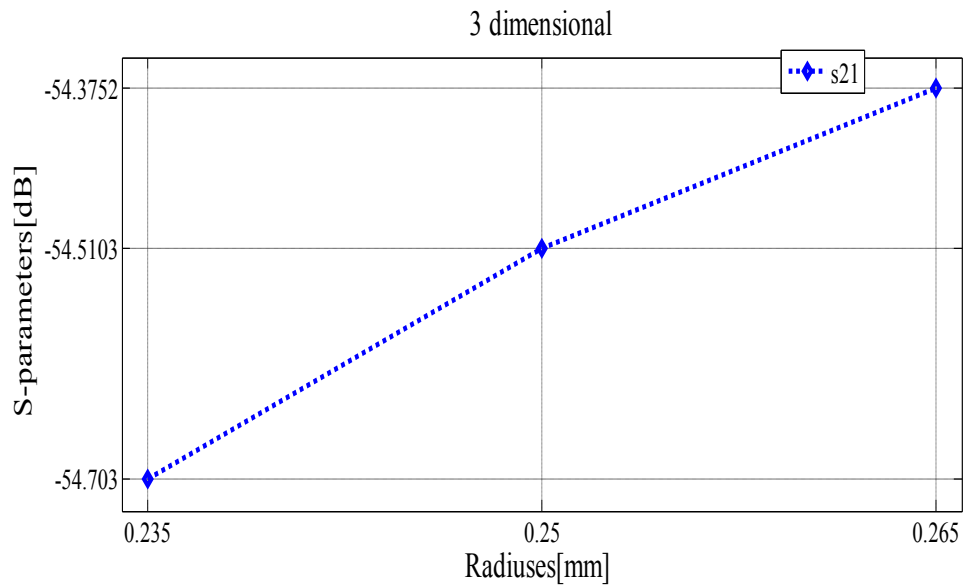


Figure 3.9: S-parameters for different tolerances of electrode number 2, provided by Max-lab, for the case with the inner conductor inside the pipe (see figure 3.8).

As shown in figure 3.9, the transmission behavior for 3D simulation is exactly the same as 2D simulations. An increase of the electrode cross section area increases the transmission.

Chapter 4

Practical Models:

The effect of the environment temperature changes, i.e. condensation or thermal expansion, and fabrication errors on BPM system can cause deformation and change in electrode geometry. The S-parameters dependence of the electrode geometry is investigated in this chapter. The first three sections are devoted to study the electrode inner and outer radius variations. In section 4.4 different insertion of the electrode inner cylinder inside the pipe are studied. The last part is devoted to the inner cylinder displacements in the radial or longitudinal directions. For studying the S-parameter variations in each type of the errors, a number of models have been simulated for two different cases; when there is an inner conductor inside the vacuum tube and when there is not.

For each case with the inner conductor inside the vacuum tube, one table is provided representing the couplings from the beam, port 1, to the electrodes around the pipe, i.e. S_{21} , S_{31} , S_{41} and S_{51} , figure 3.6. We are interested to study the variations in S_{21} behaviour compared with the transmission through the other electrodes when electrode number 2 varies .

In the models without the inner conductor the source port is one of the electrodes, named port 1, Figure 3.7. Couplings from one electrode to the other electrodes around the pipe, i.e. S_{21} , S_{31} , S_{41} are presented. In this case, the change in coupling from the source electrode, to the variable electrode number 2, i.e. S_{21} , has been studied.

These two different cases are compared with each other, in order to find a relation between them for system calibration. All S-parameter tables related to the figures are presented in appendix E .

4.1 Variations of electrode outer and inner radius

This part is devoted to study the S-parameter behavior for the variations of both internal and external radiuses of electrode number 2. In this case, the distance between the cylinders is constant, 0.25 mm, (figures 4.1 and 4.4).

As seen in figures 4.2 and 4.5 by increasing the inner and the outer radiuses of electrode number 2, transmission i.e. S_{21} , through this electrode increases. The blue line in these figures shows the constant transmission through the three other invariable electrodes. This behavior is in accordance with what we expect. According to formula 2.2, electrode voltage and as a result the transmission are related to the electrode area. Therefore, while the inner radius of the electrode increases, the electrode area increases, which results in more transmission from the variable electrode.

The starting point in figures 4.2 and 4.5 is when the inner and the outer radiuses are equal to 4.9 and 5.15mm, respectively. In this case, the variable electrode has the maximum deviation compared to the constant electrodes which means that the maximum error occurs here, as seen from figures 4.3 and 4.6. By increasing the radiuses, the difference between electrode number 2 and the other electrodes decreases, so the horizontal error decreases. In the case with the outer and inner radiuses equal to 5.65 and 5.4 mm, electrode number 2 has the same geometry as the other electrodes. That is why the horizontal error is almost equal to zero at this point. After this cross point, again the difference

between the variable electrode and the other electrode increases which results in an increasing horizontal errors.

In the case with and without inner PEC wire inside the main pipe, the S-parameters and horizontal error behavior are exactly the same, as shown in figures 4.2, 4.3, 4.5 and 4.6.

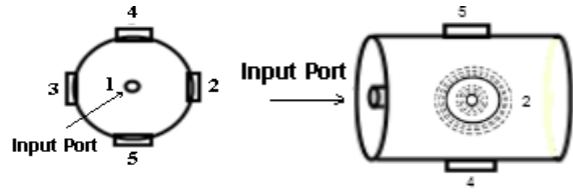


Figure 4.1: Variation of both inner and outer radiuses of electrode number 2 ,with the PEC wire in the pipe center

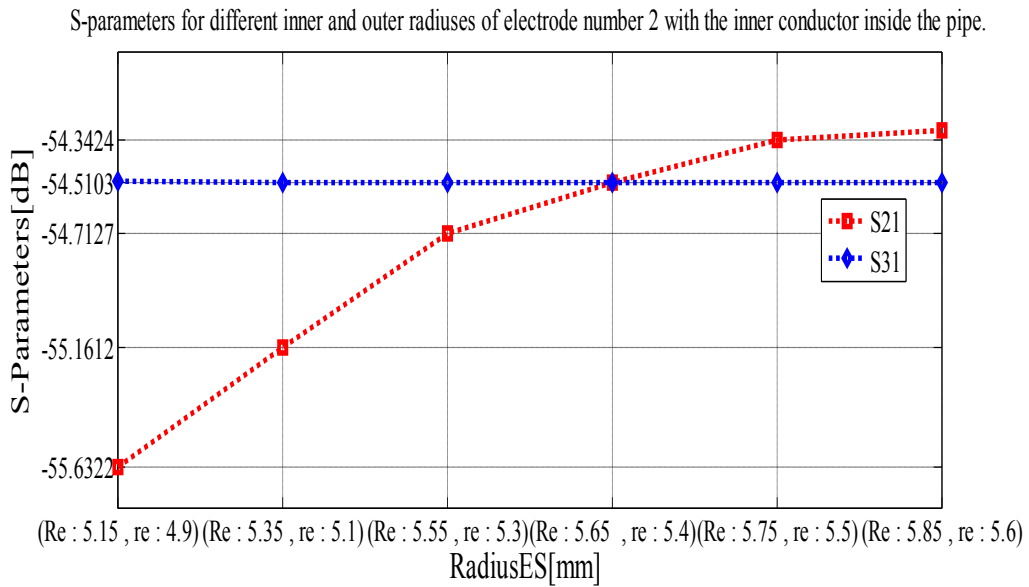


Figure 4.2: S-parameters for different inner and outer radiuses of electrode number 2, with the inner conductor inside the pipe (see Figure 4.1).

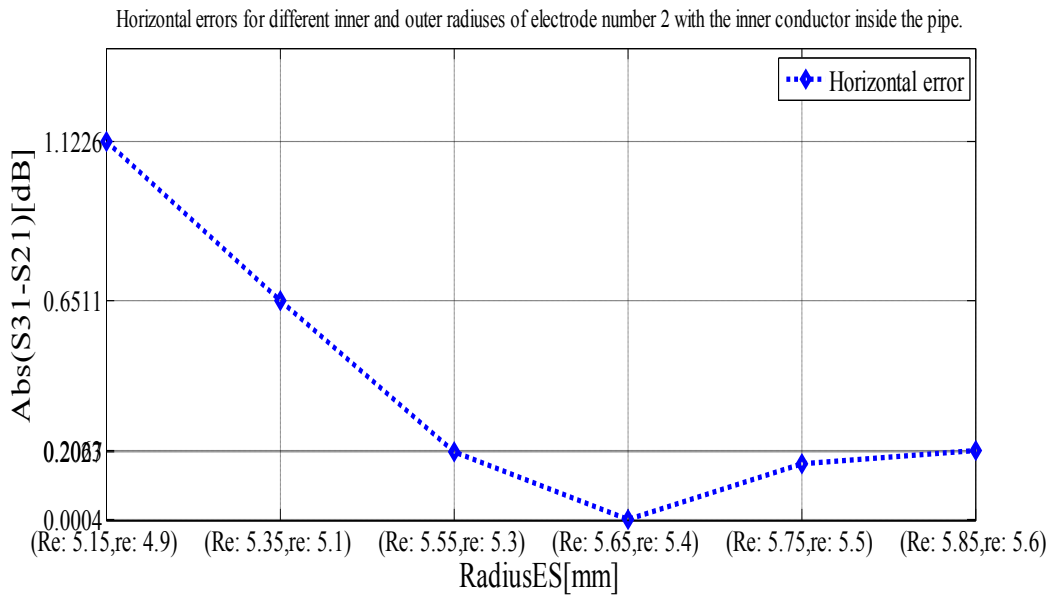


Figure 4.3: Horizontal errors for different inner and outer radiuses of electrode number 2, with the inner conductor inside the pipe (see Figure 4.1).

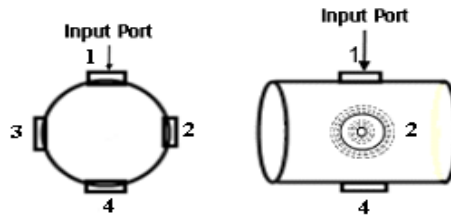


Figure 4.4: Variation of both inner and outer radius of electrode number 2, with the PEC wire in the pipe center

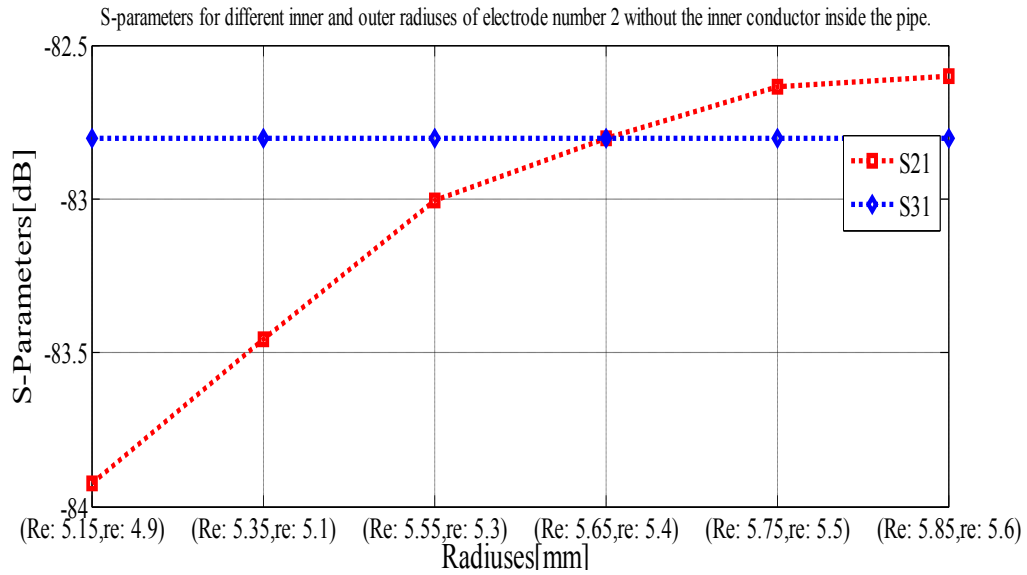


Figure 4.5: S-parameters for different inner and outer radii of electrode number 2, without the inner conductor inside the pipe (see Figure 4.4).

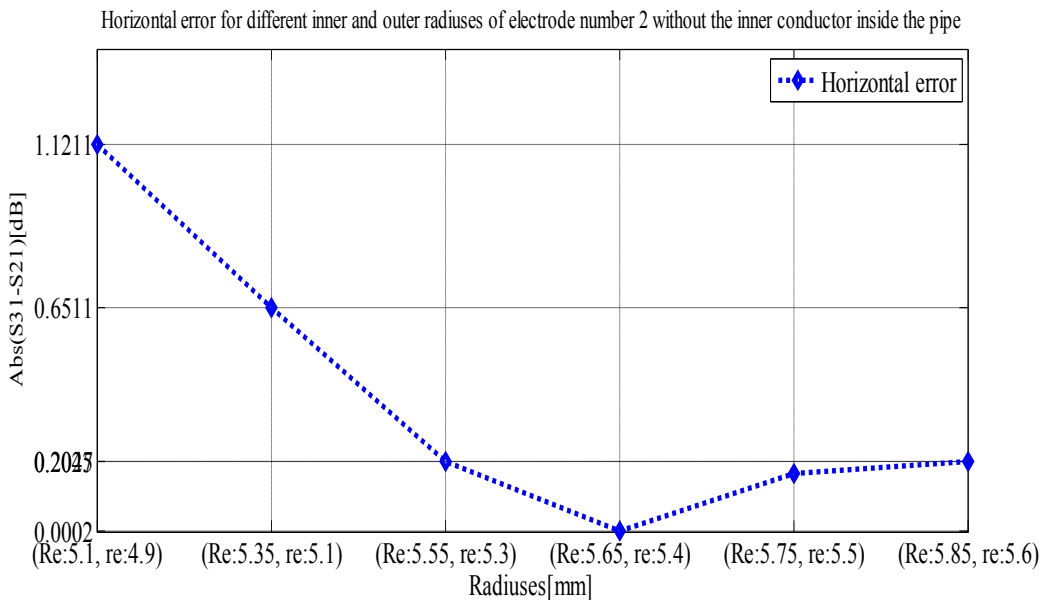


Figure 4.6: Horizontal error for different inner and outer radii of electrode number 2, without the inner conductor inside the pipe (see Figure 4.4).

4.2 Variations of electrode inner radius

The other one of the errors happens when the electrode outer radius is constant and the inner one increases. In this part, the outer radius for electrode number 2 has been kept constant, 5.65mm, while

the inner radius varies from 4.9mm to 5.55mm. The increase of the inner radius increases the electrode cross section area, and hence increases the transmission through the variable electrode. There is another factor which may affect the transmission and that is the ratio of the outer radius to the inner radius, i.e. $\frac{R_e}{r_e}$. This radius ratio appears in the coaxial capacitance formula: $C = \frac{2\pi\epsilon_0}{\ln(R_e/r_e)}$

At the starting point, the size of the inner cylinder is small, 4.9mm, which results in a small cross section area and less transmission. The distance between the two concentric cylinders has increased. Consequentially, there is a large radius ratio, $\frac{R_e}{r_e}$. According to the coaxial capacitance formula, a large radius ratio leads to a small capacitance between the internal and external cylinders and in contrast, large amount of characteristic impedance. Hence, the impedance seen by the electrode becomes large, resulting in more transmission. In this case, the dominant factor is the small cross section area of the electrode which results in less transmission. As the inner radius increases, the electrode cross section area becomes larger and therefore there is more transmission through the variable electrode number 2, as shown in figures 4.8 and 4.11.

At the point where the inner radius starts to be larger than 5.3 mm, the electrode transmission decreases, due to the small distance between the internal and external cylinders dominates the electrode area. Since the inner radius becomes much closer to the outer radius, the distance between the cylinders gets very small so the radiuses ratio, $\frac{R_e}{r_e}$, decreases which results in a small impedance seen by the electrode and consequently less signal transmission according to formula 2.2.

As seen in figures 4.8 and 4.11 there are two cross points where the transmission through the variable electrode is the same as the transmission through the other constant electrodes. Hence the horizontal error in these point is almost equal to zero, See figures 4.9 and 4.12. An interesting observation is that the transmission behaviour and horizontal errors for the vacuum tube with and without PEC in its center, are exactly the same according to figures 4.8 - 4.11, and 4.9- 4.12.

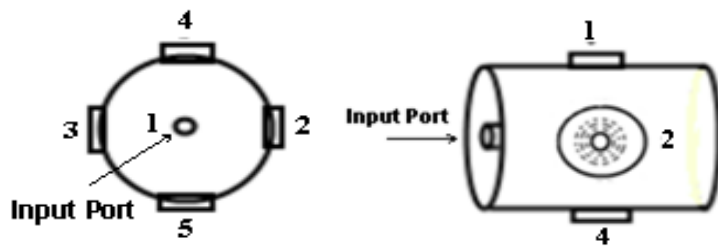


Figure 4.7: Variation of inner radius of electrode number 2, with the PEC wire in the pipe center

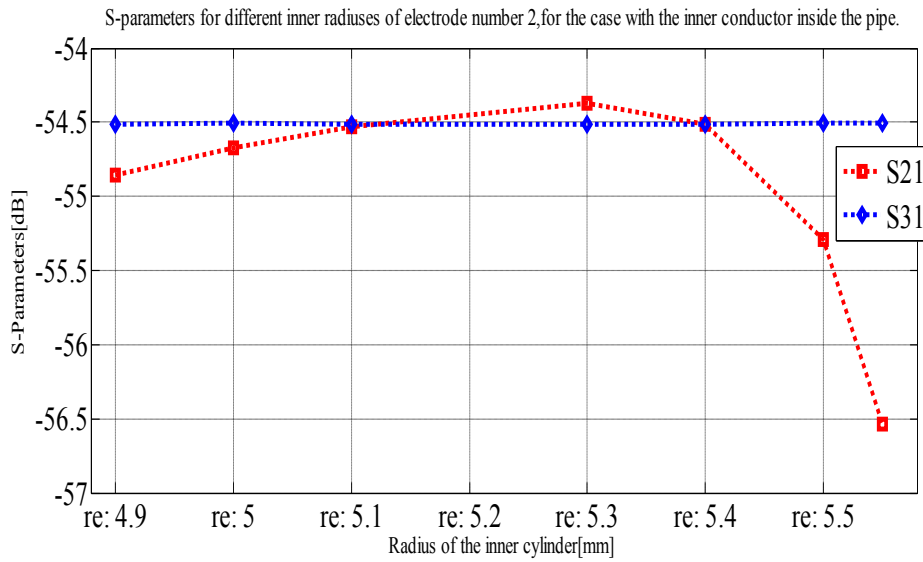


Figure 4.8: S-parameters for different inner radii of electrode number 2, with the inner conductor inside the pipe (see Figure 4.7).

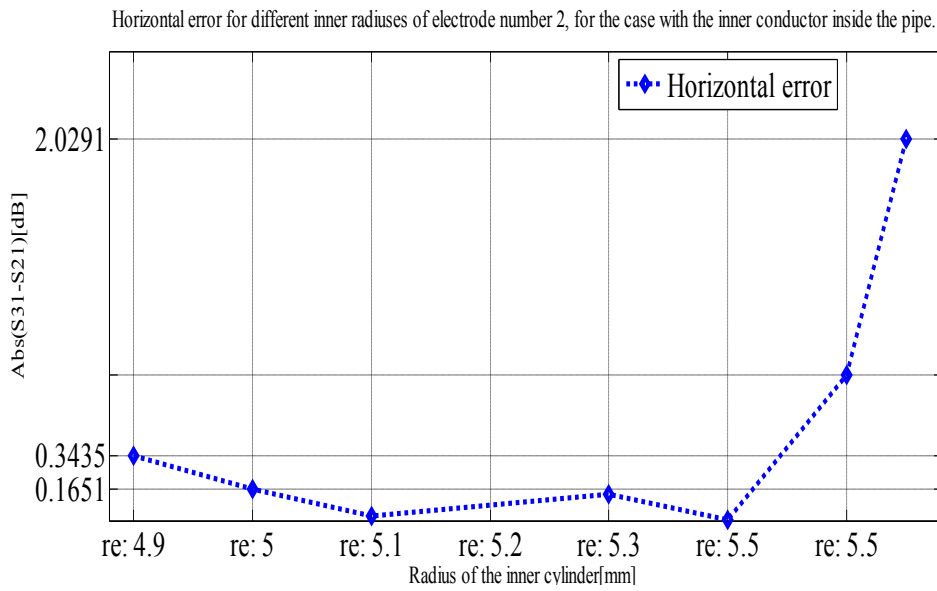


Figure 4.9: Horizontal error for different inner radii of electrode number 2, with the inner conductor inside the pipe (see Figure 4.7).

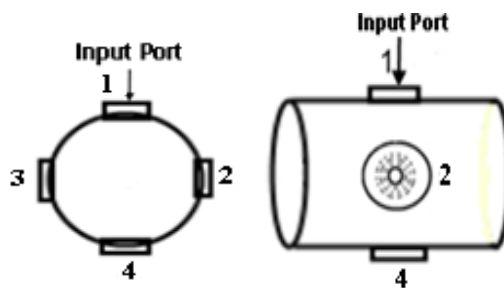


Figure 4.10: Variation of inner radius of electrode number 2, without the PEC wire in the pipe center

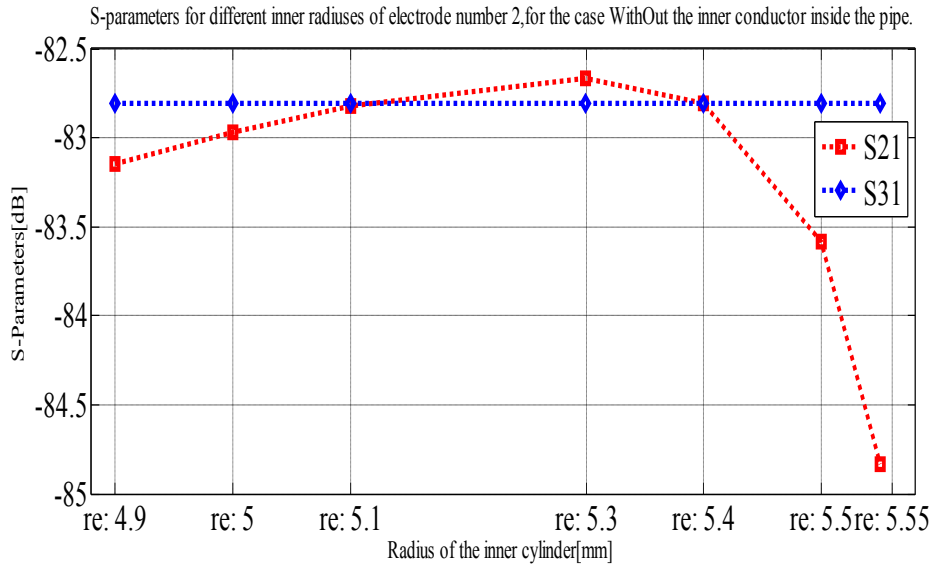


Figure 4.11: S-parameters for different inner radiuses of electrode number 2, without the inner conductor inside the pipe (see Figure 4.10).

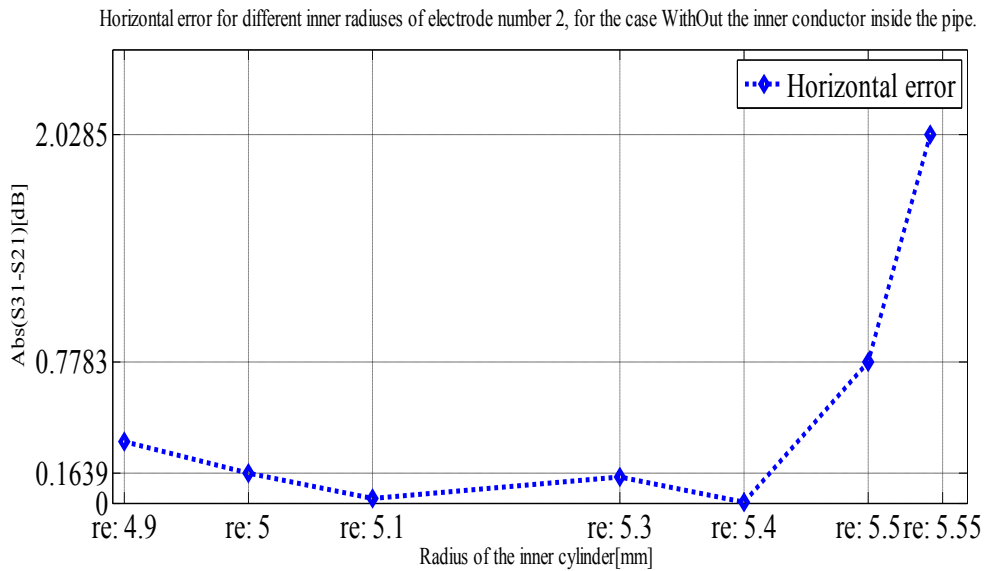


Figure 4.12: Horizontal Error for different inner radiuses of electrode number 2, without the inner conductor inside the pipe (see Figure 4.10).

4.3 Variations of electrode outer radius

In the next step of the simulations, the inner radius of electrode number 2 is kept constant, 5.4mm, while the outer radius varies from 5.45mm to 5.75mm, as shown in figures 4.13 and 4.17. The constant inner radius results in a constant electrode cross section area. Hence, the electrode area has no effect on the transmission.

When the outer radius is equal to 5.45mm, the distance between the inner and outer cylinders is very small, 0.05 mm. This small distance between the internal and external cylinders implies a small radius ratio, $\frac{R_e}{r_e}$, ensuing small impedance and a large capacitance. Hence, the impedance seen by the electrode decreases resulting in less transmission through the variable electrode. The increase in outer radius results in less capacitance and more transmission (figures 4.14 and 4.17). As seen from figures

4.15 and 4.18, the maximum horizontal error occurs at the first point. By increasing the outer radius to 5.65 mm, the horizontal error decreases to zero since the variable electrode resembles the other electrodes. Once, the outer radius of the variable electrode number 2 increases from 5.65 mm, the horizontal errors increase.

For the case without the beam in the pipe center, the behavior of transmission and the horizontal errors resembles the corresponding curves for the case with PEC in the pipe center (see figures 4.17 and 4.18).

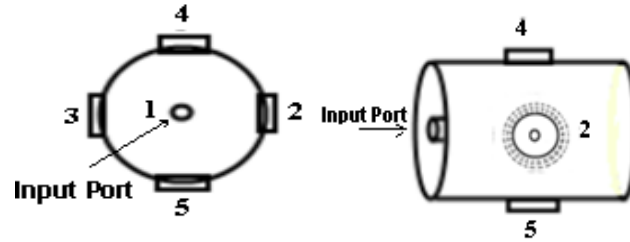


Figure 4.13: Variation of outer radius of electrode number 2, with the PEC wire in the pipe center

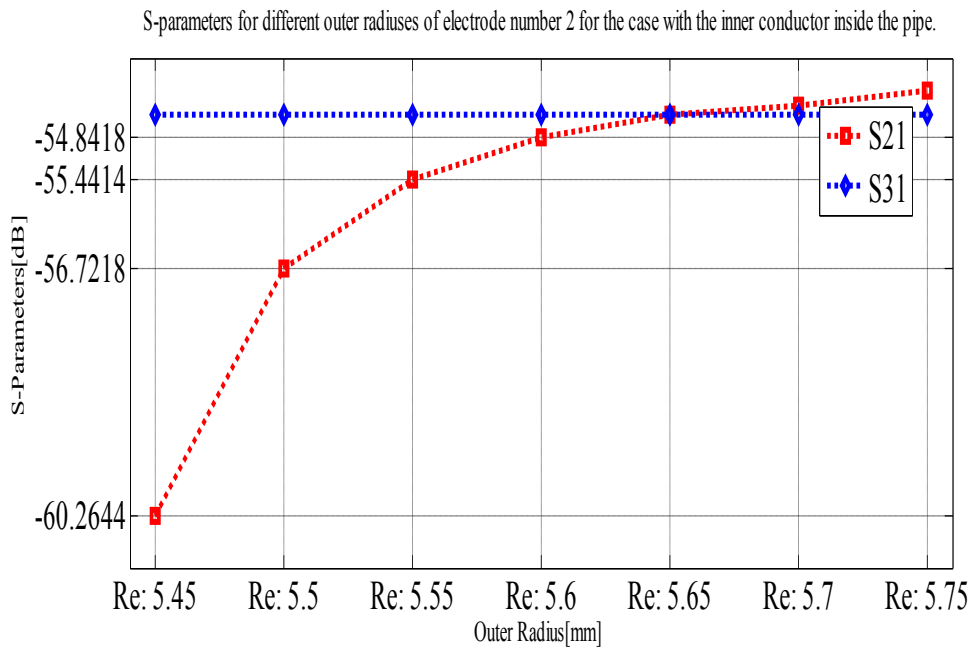


Figure 4.14: S-parameters for different outer radiuses of electrode number 2, with the inner conductor inside the pipe (see Figure 4.13).

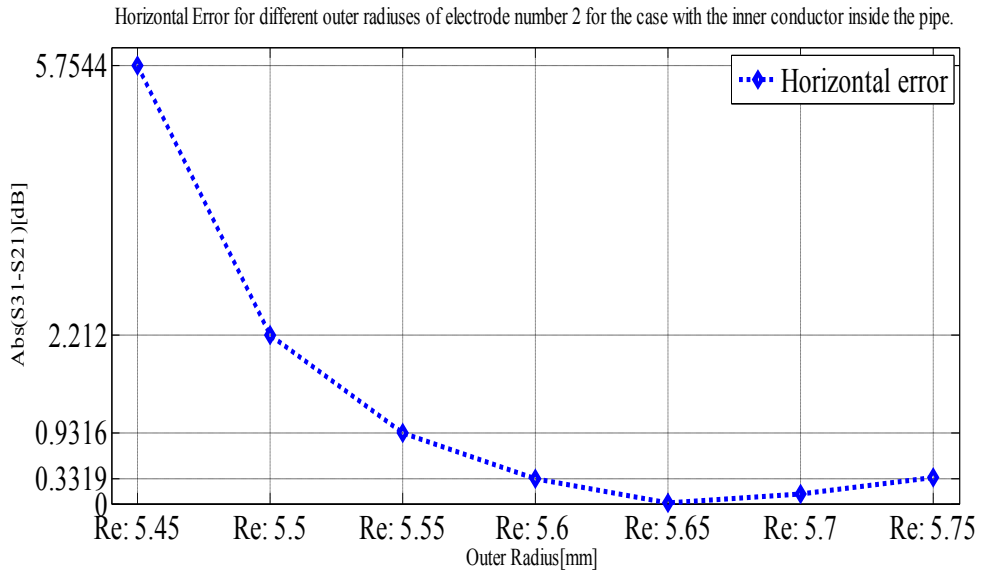


Figure 4.15: Horizontal error for different outer radiuses of electrode number 2, with the inner conductor inside the pipe (see Figure 4.13).

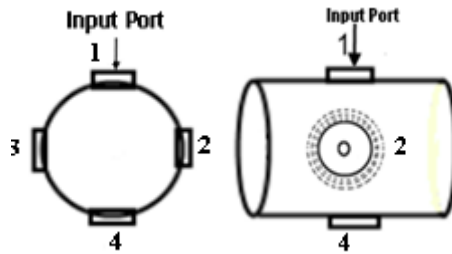


Figure 4.16: Variation of outer radius of electrode number 2, without the PEC wire in the pipe center

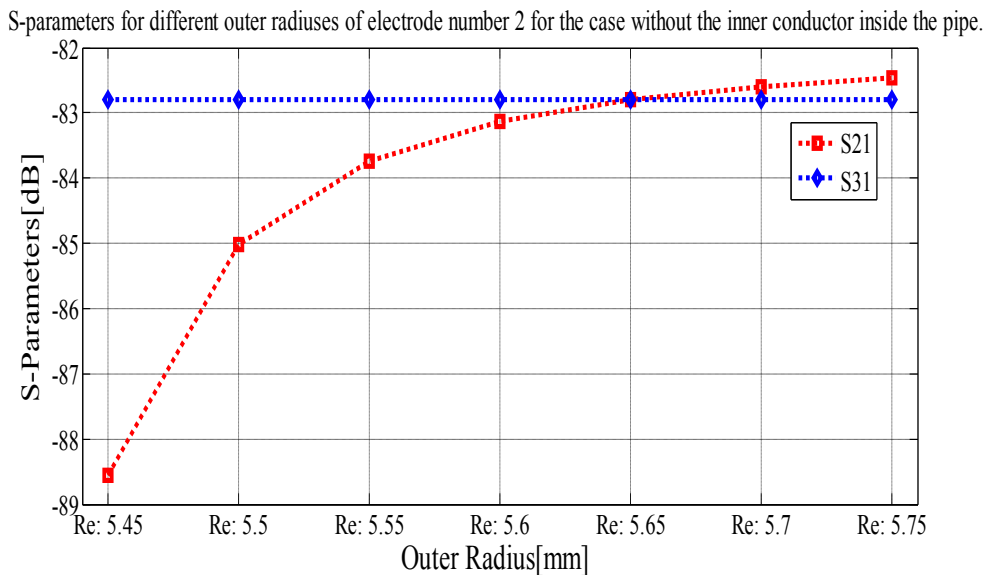


Figure 4.17: S-parameters for different outer radiuses of electrode number 2, without the inner conductor inside the pipe (see Figure 4.16).

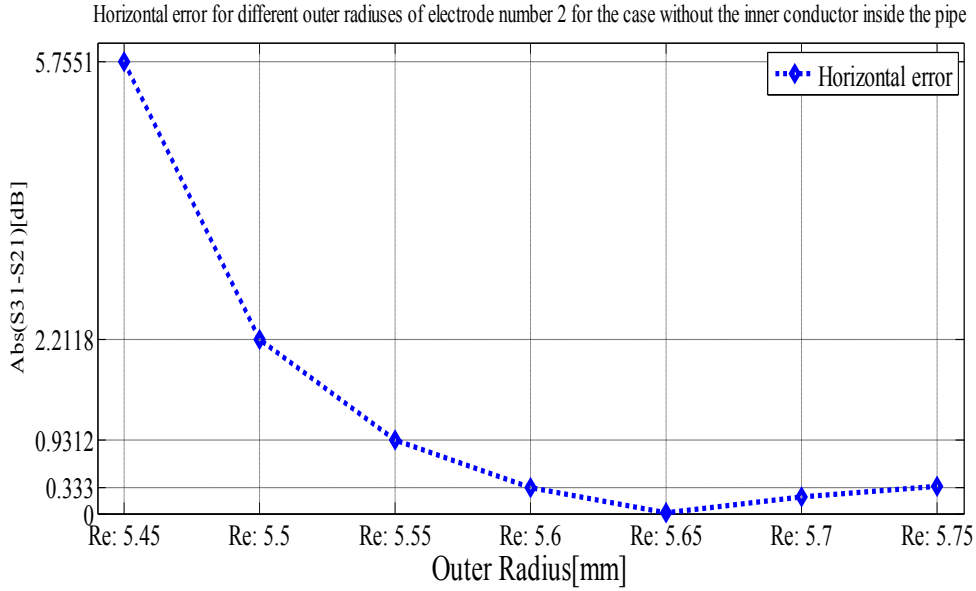


Figure 4.18: Horizontal error for different outer radiuses of electrode number 2, without the inner conductor inside the pipe (see Figure 4.16).

4.4 Insertions of electrode inner cylinder inside the pipe

In addition to the variations of the electrode inner and outer radiuses, different depths of the inner cylinder of electrode are of interest. In the prototype model, the inner cylinder insertion of all electrodes inside the main pipe is equal to 0.9mm. In this section more insertions of the inner cylinder of electrode number 2 have been investigated.

For the case with the inner PEC wire inside the vacuum tube, as the electrode inner cylinder moves down, the distance between the PEC wire and the electrode inner cylinder decreases. According to the button voltage formula 2.2, there is an indirect relation between the distance of the PEC wire and the electrode inner cylinder:

$$V_{button} = \frac{\pi r_e^2}{2\pi(R_p - \ln)} \times \frac{60 \ln(R_e/r_e)}{\beta c} \times i\omega \times I_{beam}(\omega)$$

Where ‘ln’ shows the amount of the insertions inside the main pipe.

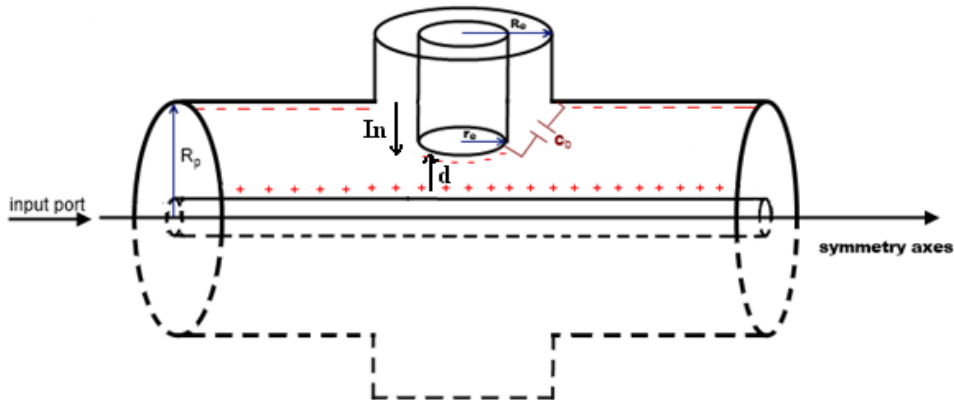


Figure 4.19: Schematic of a capacitive BPM

As the inner cylinder insertions increase, the distance, $d = R_p - R_i$, between the PEC wire in the vacuum tube center and the inner cylinder cross section, decreases. According to the button voltage formula, the decrement in denominator results an electrode voltage increment and consequently in an increase of the transmission. For the case without the PEC wire in the pipe center, the behavior is exactly the same. Figures 4.21 and 4.24 confirm that by having more insertion inside the vacuum tube, the transmission from the variable electrode increases. It is noticeable that as the insertion inside the main pipe increases, the horizontal error increases due to the more dissimilarity between the variable electrode and the other constant electrodes. The results are confirmed by figures 4.22 and 4.25.

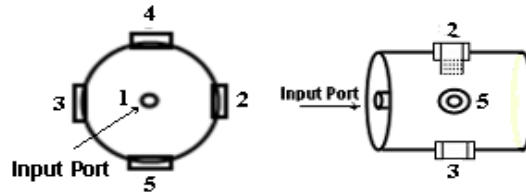


Figure 4.20: Insertion of the inner cylinder of electrode 2 inside the pipe, with the PEC wire in the pipe center

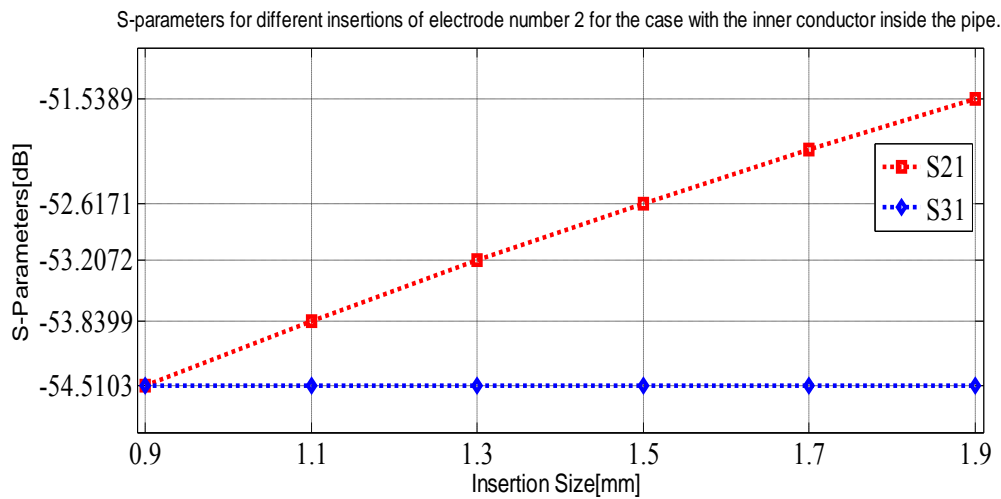


Figure 4.21: S-parameters for different insertions of electrode number 2, with the inner conductor inside the pipe (see Figure 4.20).

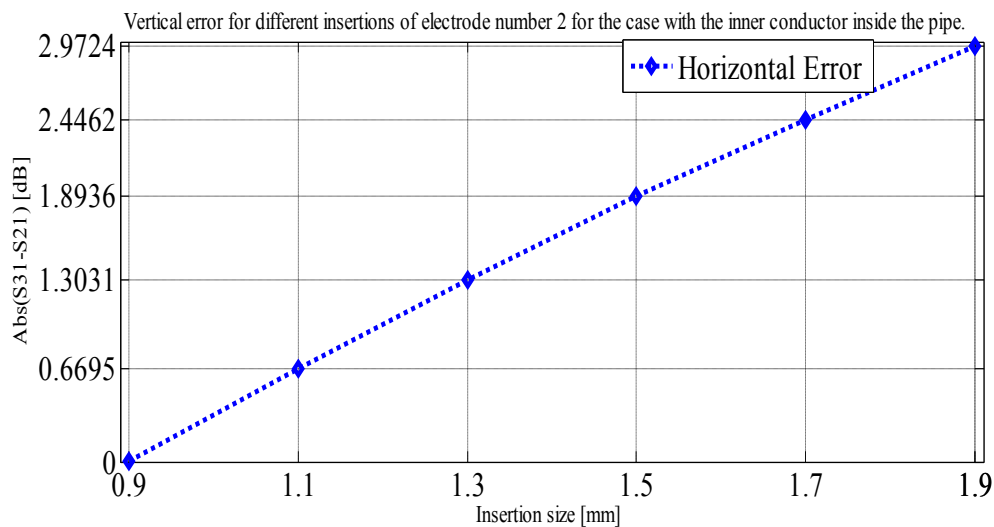


Figure 4.22: Horizontal error for different insertions of electrode number 2, with the inner conductor inside the pipe (see Figure 4.20).

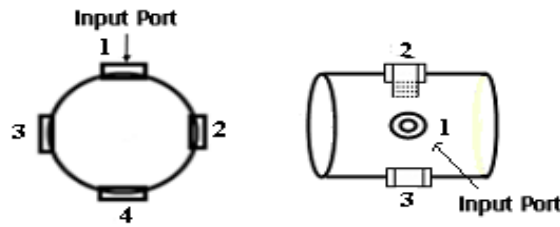


Figure 4.23: Insertion of the inner cylinder of electrode 2 inside the pipe, without the PEC wire in the pipe center

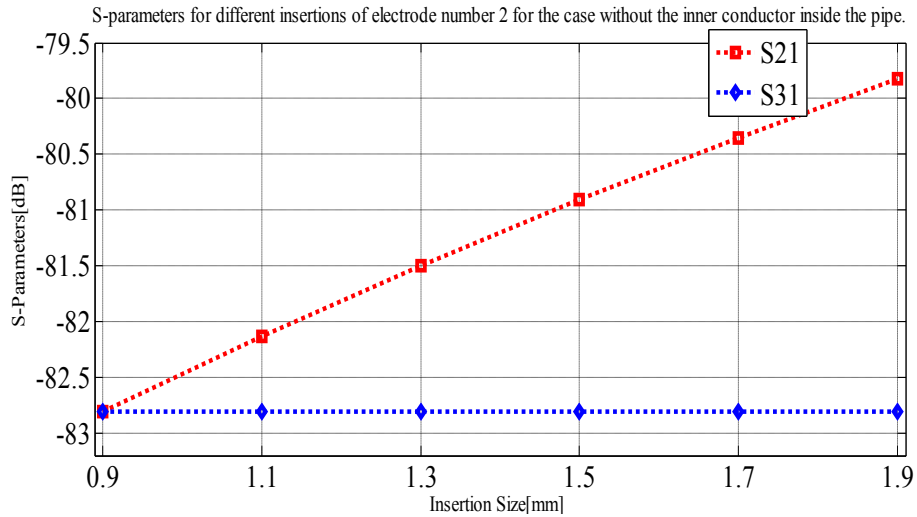


Figure 4.24: S-parameters for different insertions of electrode number 2, without the PEC wire in the pipe center (see Figure 4.23).

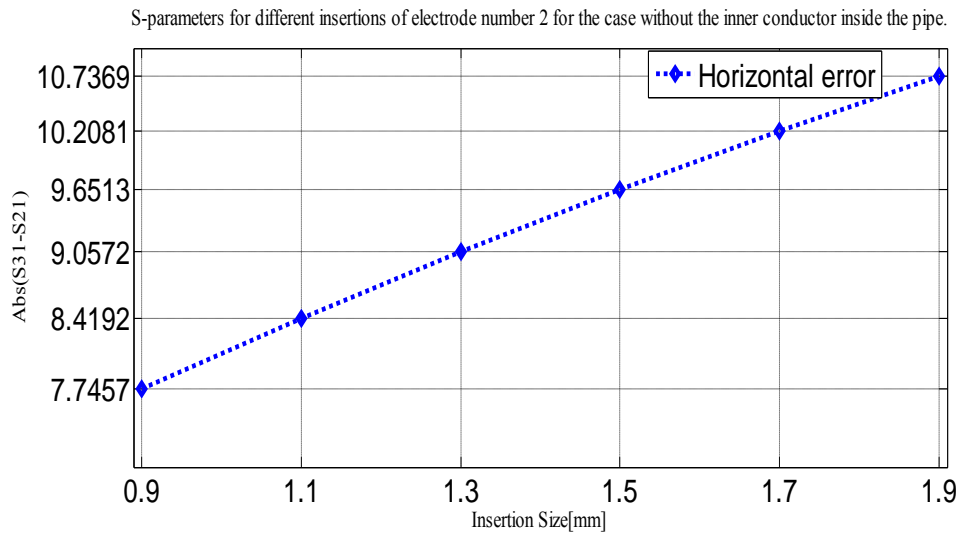


Figure 4.25: Horizontal error for different insertions of electrode number 2, without the PEC wire in the pipe center (see Figure 4.23).

4.5 Displacements of electrode inner cylinder

One of the other kind of constructing errors which may occur on the BPM system is the electrode inner cylinder displacements. The inner cylinder displacement makes the coaxial line a non-concentric coaxial line with some specific inner conductor eccentricity. Studying the capacitance in an

eccentric coaxial line requires more precision. Once the electrode inner cylinder is displaced, the capacitance on one side increases while it on the opposite side decreases. Hence, in general the effect of capacitance is probably neutralized. This is an increasing need to be able to measure the characteristic impedance for non symmetric coaxial cable, Figure 4.26.

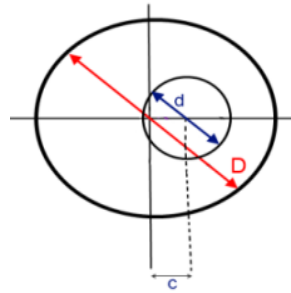


Figure 4.26: Eccentricity of the inner conductor inside the coaxial cable

Coaxial cable impedance can only decrease if the inner conductor is off center [26, 27]. Characteristic impedance of off-center coaxial cable can be expressed as:

$$Z_{coax} = \frac{60}{\sqrt{\epsilon_r}} \ln (x + \sqrt{x^2 - 1}) \quad (4.1)$$

Where
$$x = \frac{d^2 + D^2 - 4c^2}{2Dd}$$

Parameter c shows the eccentricity while the outer and inner diameters are symbolized by D and d, respectively. If c is equal to zero, the characteristic impedance is the same as the normal coaxial cable characteristic impedance:

$$Z_{coax} = \frac{60}{\sqrt{\epsilon_r}} \ln \left(\frac{D}{d} \right)$$

It is evident from formula 4.1 that since the inner conductor gets far from the vacuum tube center, the amount of x, and therefore the characteristic impedance is weakened. According to the electrode voltage formula (2.2), decrement in the characteristic impedance results a reduction of the impedance seen by the electrode. Consequently, it results in a reduction in the button voltage and in the transmission through the variable electrode. In this section, the inner cylinder displacements of electrode number 2 in radial and longitudinal directions have been investigated.

In the case of passing the beam through the pipe center, the results for the variable electrode inner cylinder displacements in both clockwise and counter clockwise radial directions are the same due to symmetry. Hence, for this case clockwise radial direction is studied. However for the case without beam in the pipe center, the system is not symmetric. Therefore, the clockwise and counter clockwise radial displacements of electrode number 2 are investigated, separately.

Figures 4.28, 4.31 for radial displacements and figures 4.34 and 4.37 for longitudinal displacements confirm that while the eccentricity of the inner cylinder is increased, the coupling from the source to that variable electrode decreases. It is obvious that as the eccentricity grows, the dissimilarity between the variable electrode number 2 and the other constant electrodes increases, and as a result horizontal error increases. We refer to figures 4.29, 4.32 for the radial case and 4.35, 4.38 for the longitudinal case.

- Radial displacements of the electrode inner cylinder (With the inner PEC wire)

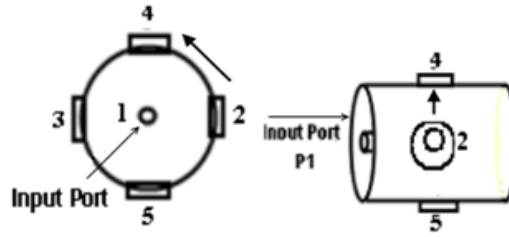


Figure 4.27: Radial displacements of the inner cylinder of electrode number 2 toward port 4, with the PEC wire in the pipe center

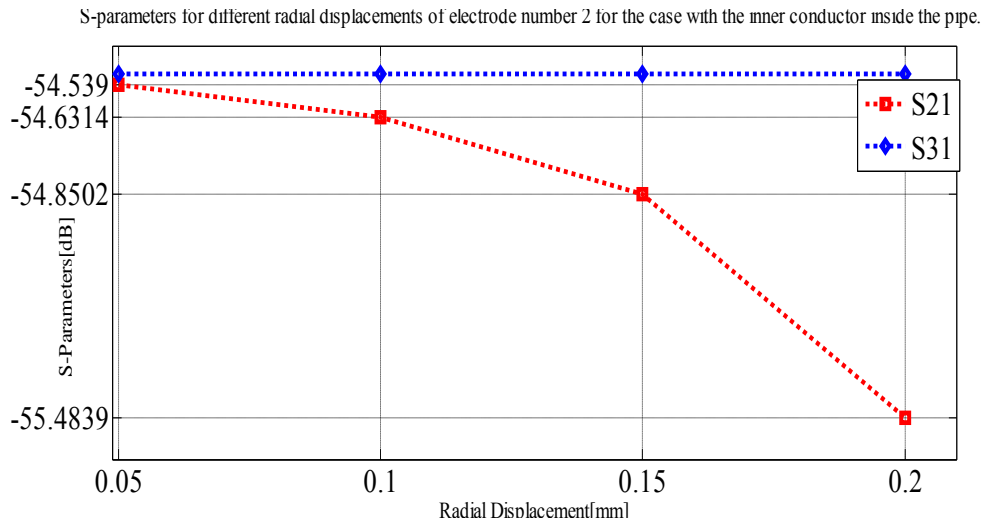


Figure 4.28: S-parameters for different radial displacements of electrode number 2, with the PEC wire in the pipe center (see Figure 4.27).

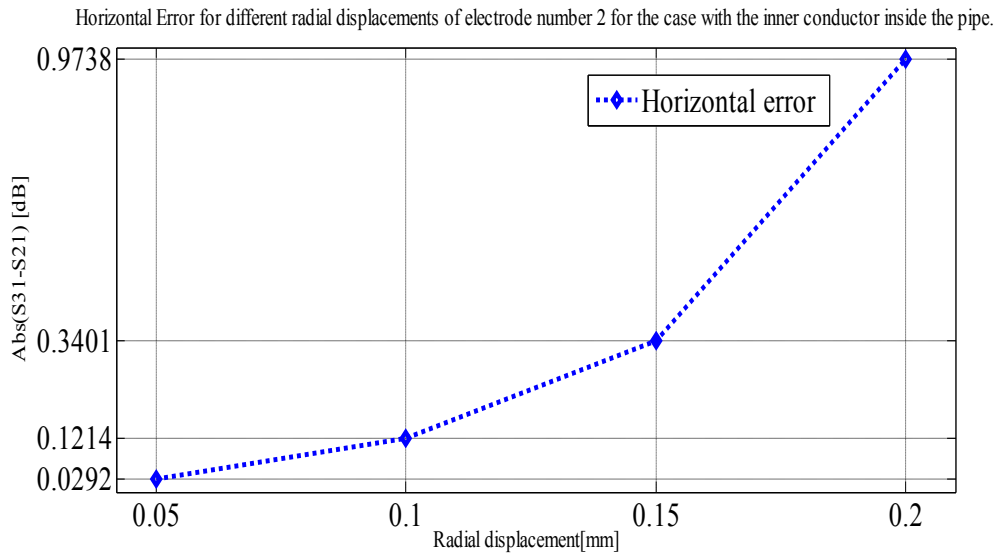


Figure 4.29: Horizontal errors for different radial displacements of electrode number 2, with the PEC wire in the pipe center (see Figure 4.27).

- Radial displacements of the electrode inner cylinder (Without the inner PEC wire)

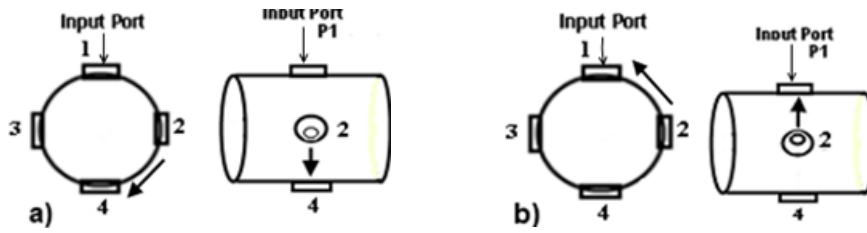


Figure 4.30: Radial displacements of the inner cylinder of electrode number 2, without the PEC wire in the pipe center: a) Clockwise and b) counter Clockwise

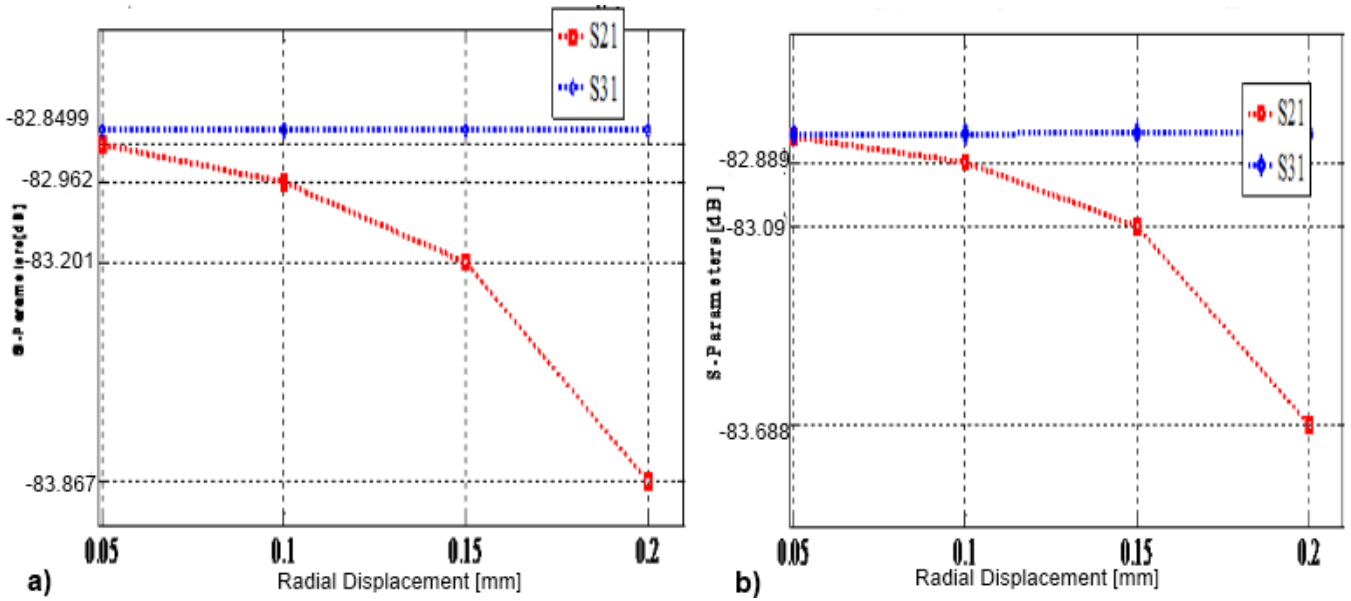


Figure 4.31: S-parameters for different radial displacements of electrode number 2, without the PEC wire in the pipe center: a) Clockwise and b) counter clockwise (see Figure 4.30).

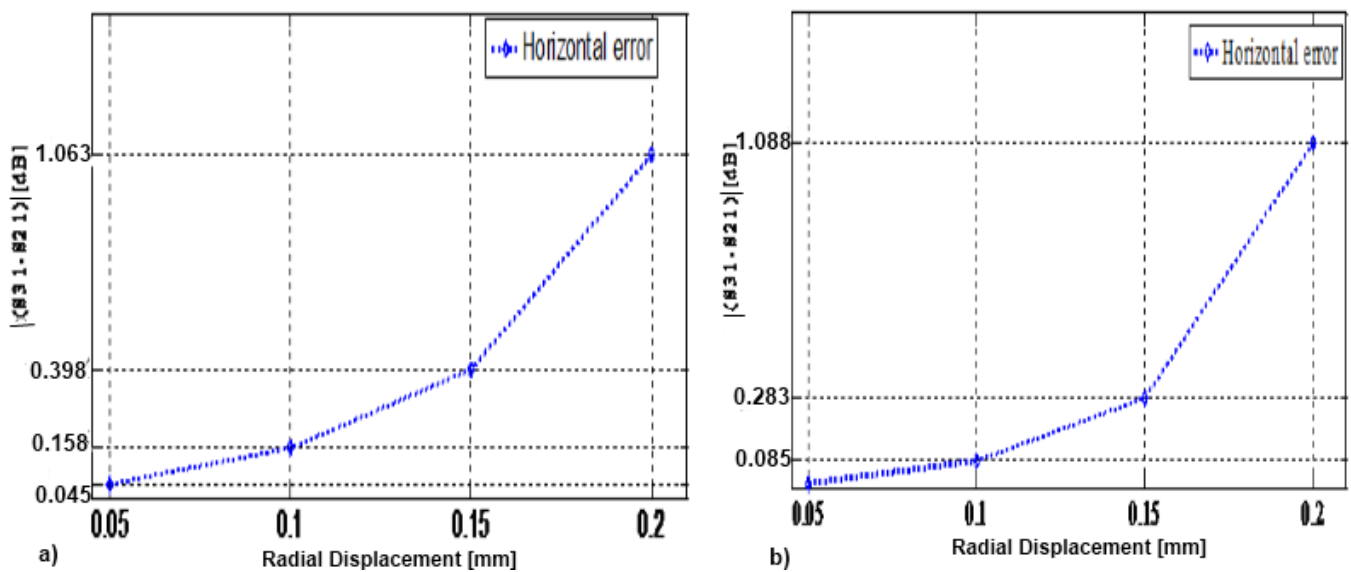


Figure 4.32: Horizontal errors for different radial displacements of electrode number 2, without the PEC wire in the pipe center: a) Clockwise and b) counter clockwise (see Figure 4.30).

- Longitudinal displacements of the electrode inner cylinder (With the inner PEC wire)

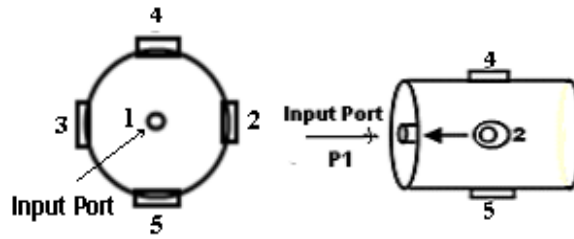


Figure 4.33: Longitudinal displacements of the inner cylinder of electrode number 2 toward input port, with the PEC wire in the pipe center

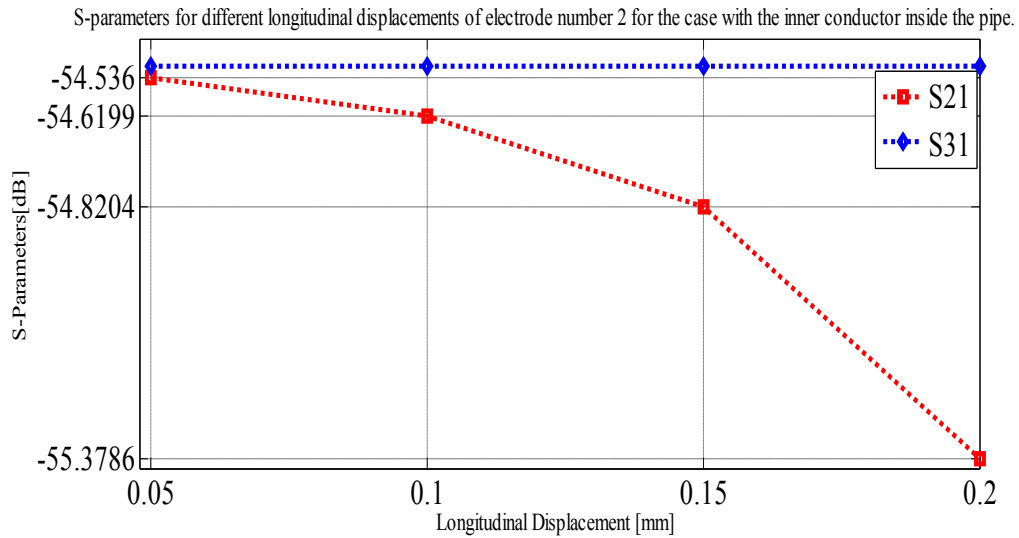


Figure 4.34: S-parameters for different longitudinal displacements of electrode number 2, with the PEC wire in the pipe center (see Figure 4.33).

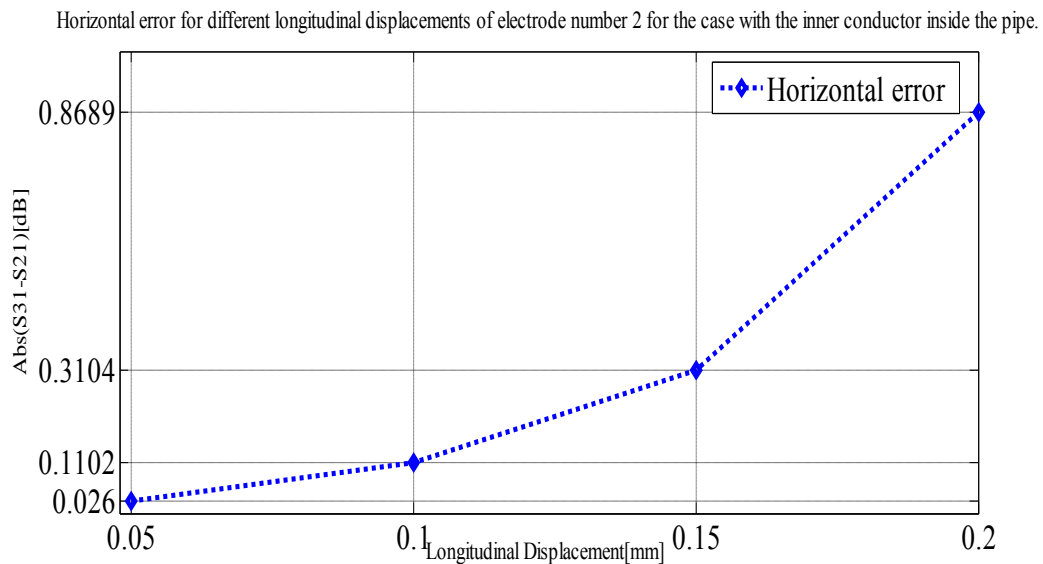


Figure 4.35: Horizontal errors for different longitudinal displacements of electrode number 2, with the PEC wire in the pipe center (see Figure 4.33).

- Longitudinal displacements of the electrode inner cylinder (Without the inner PEC wire)

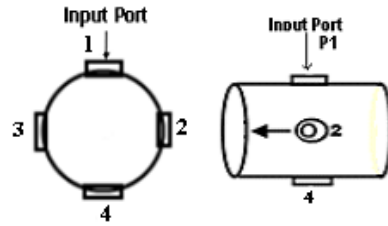


Figure 4.36: Longitudinal displacements of the inner cylinder of electrode number 2 toward input port, without the PEC wire in the pipe center

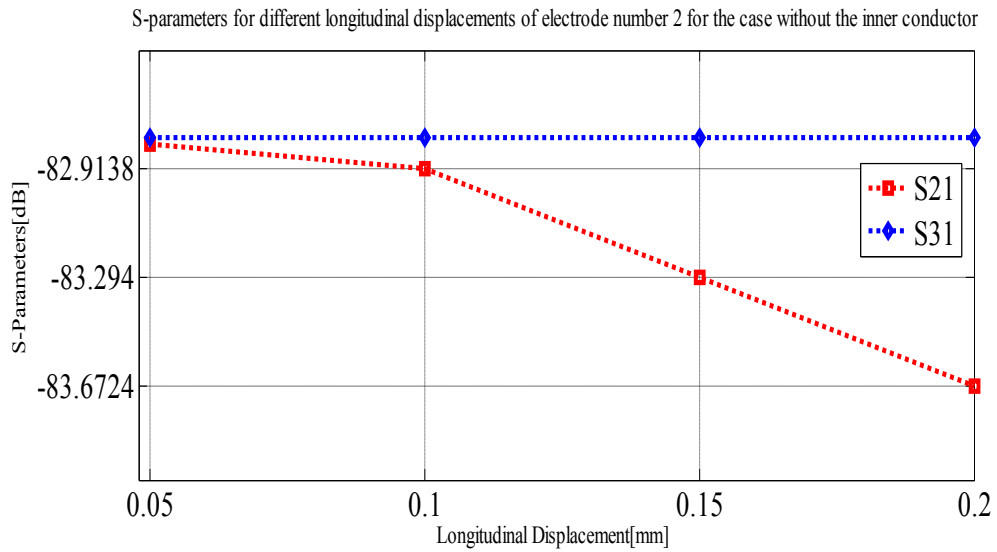


Figure 4.37: S-parameters for different longitudinal displacements of electrode number 2, without the PEC wire in the pipe center (see Figure 4.36).

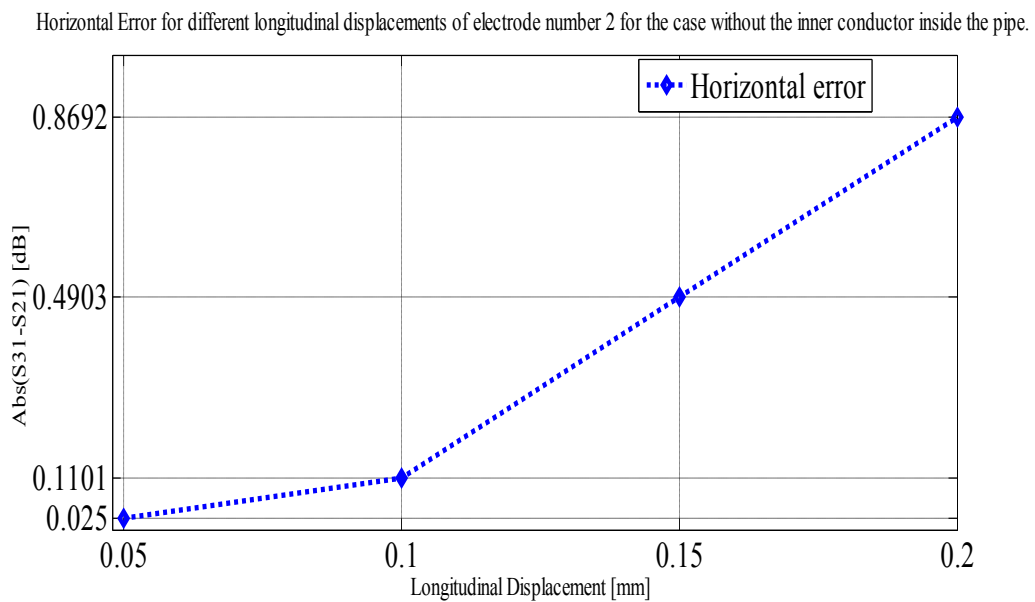


Figure 4.38: Horizontal errors for different longitudinal displacements of electrode number 2, without the PEC wire in the pipe center (see Figure 4.36).

Comparing Clockwise and Counter Clockwise and longitudinal for radial displacements of the inner cylinder of the electrode 2

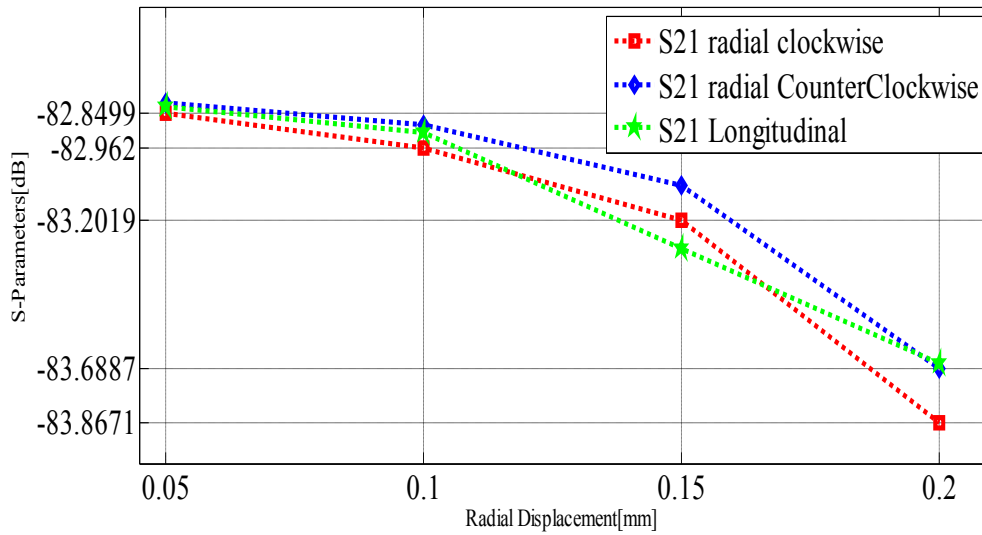


Figure4.39: Comparison between the clock wise and counter clockwise radial displacements and longitudinal displacements of electrode number 2, without the inner conductor inside the pipe

Figure 4.39 illustrates the difference between two different clock wise and counter clockwise radial direction displacements, for the case without the inner PEC wire inside the main pipe compared with longitudinal displacements. The electrode inner cylinder displacements toward the electrode source, i.e. counter clockwise radial displacements, results in more transmission compared with the case of the inner cylinder moving in opposite direction.

Chapter 5

Beam multipole expansions:

Multiple expansions are widely used in problems involving the propagation of electromagnetic waves and electric and magnetic fields of current and charge distributions. The basic idea is to decompose the particles into groups which can provide us information about the shape and position of the beam. BPM converts the induced voltage on the electrodes into a position offset from the center in order to measure the position of the beam. Since the coaxial cable is used in this work, there are two surface charge distributions on the outer and inner conductors. A two dimensional charge distribution $\rho(y, z)$ inside the circle with radial coordinate $r_c = \sqrt{y^2 + z^2}$ is considered. The induced electrostatic potential from the inner conductor in point $r = (y, z)$ can be expanded in a Taylor series in terms of the charge distribution on the inner conductor (see appendix B.2) [28]:

$$V(r) = -\frac{1}{2\pi\epsilon_0} (\rho_l \ln(r_c) - \rho_y \frac{y}{r_c^2} - \rho_z \frac{z}{r_c^2} + (Q_{yy} - Q_{zz}) \frac{z^2 - y^2}{2r_c^4} - 2Q_{yz} \frac{yz}{r_c^4}) + O(r_c^{-3}) \quad (5.1)$$

The source point is symbolized by r' and the total charge is described by the zero order moment called the monopole moment, which is the charge per unit length: $\rho_l = \int_{\Gamma} \rho_s(r') dl$

P_y and P_z are the first order moments called dipole moments that illustrate the center-of-charge measurements:

$$p_y = \int_{\Gamma} y' \rho_s(r') dl \quad , \quad p_z = \int_{\Gamma} z' \rho_s(r') dl$$

The information about displaced beam is given by the dipole moments which depend linearly on the beam position [29]. Position pick-ups are usually optimized with respect to the linear behavior by the beam displacements [30].

$Q_{yy}, Q_{zz}, Q_{zy}, Q_{yz}$ are the second order moments so-called quadrupole moments and changed by variation of the beam cross section shape [31]:

$$Q_{yy} = \int_{\Gamma} y'^2 \rho_s(r') dl \quad , \quad Q_{zz} = \int_{\Gamma} z'^2 \rho_s(r') dl \quad , \quad Q_{zy} = Q_{yz} = \int_{\Gamma} z' y' \rho_s(r') dl$$

The quadrupole moments contain information about the shape of the beam cross section.

Both the beam offset from the pipe centre and the beam cross-section varying to non-circular shape result in a non-constant distributed charge on the pipe surface. The picked up voltage for each electrode varies due to this uneven charge distribution and generation of differential field. The information collected by the BPM system gives position offsets by measuring the various voltages. The dependency of the potential (formula 5.1) to the dipole moments is easy to study by Comsol models but the major problem is to investigate the quadrupole moments dependency. In fact, simulating one wire as a beam and moving it around the pipe center or towards the electrodes is a better way to consider how the pickups respond to the beam, instead of simulating several positions of the beam. It is difficult to measure the electrode pickups due to coupling between the wires when several wires are considered simultaneously. The following models have been simulated by two different methods and the results are compared, either by adding an extra piece of electrode to the

button and terminate it to 50Ω or by using Lumped port and set the impedance to 50Ω (see appendix C for more information).

Two different kinds of beam displacements have been investigated in this part in order to determine the dependence of the induced voltage to linear charge distribution on the pipe surface and the dipole moment according to formula 2.2.

- 1- Beam displacements along the vertical axis.
- 2- Beam displacements along a line between the horizontal and vertical axes.

5.1 Beam displacements along the vertical axis:

As mentioned before, one of the targets in accelerators is to keep the beam in the pipe center. However, due to the different reasons, beam may displace from its ideal location. Sections 5.1 and 5.2 are devoted to find a relation between a displaced beam and the induced voltage on the electrodes as well as the multipole expansion variations, in two different directions.

In this section, the inner cylinder gets closer to electrode number 2, along the vertical axis, z , by 0.5, 0.75, 1, 1.25 and 1.5 millimeters (figure 5.1).

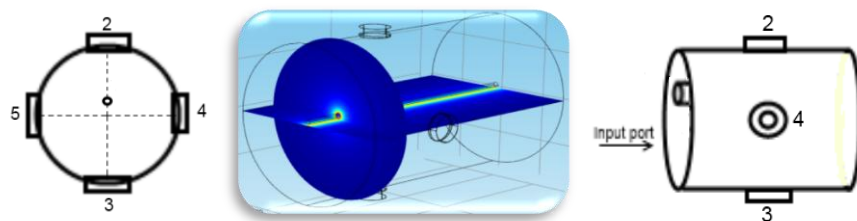


Figure 5.1: Displacement of the inner PEC wire along the vertical axis z

The beam that is located on the pipe center generates a constant distribution on the pipe wall. Once the beam gets away from the pipe center, the uniform charge distribution on the pipe wall will be disturbed.

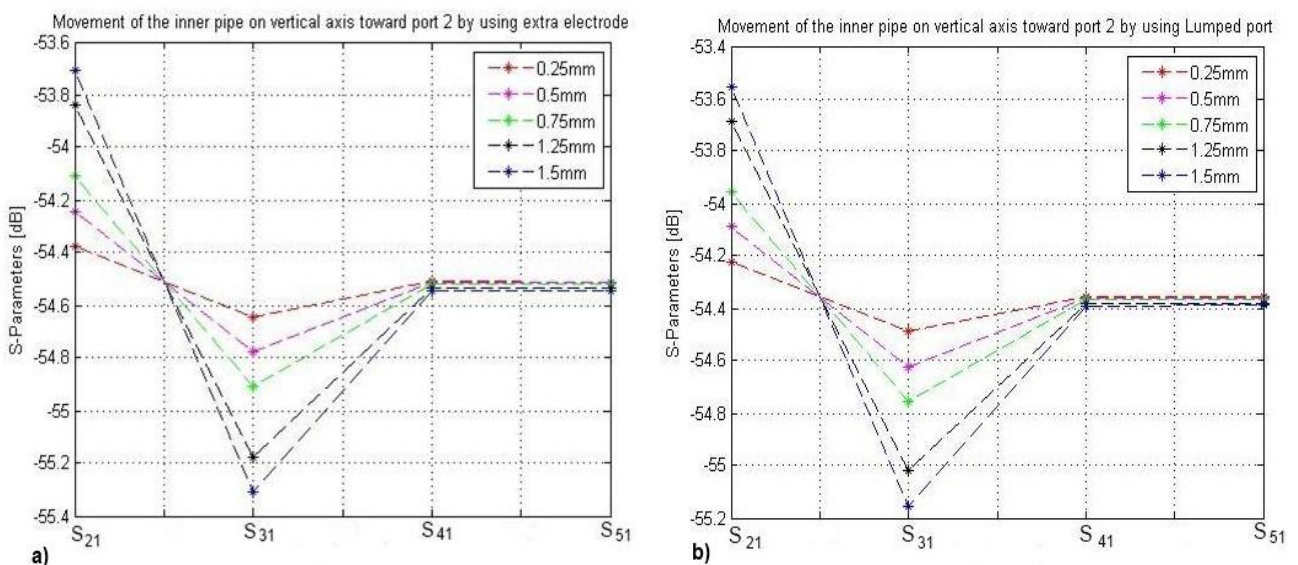


Figure 5.2: S-parameters for different displacements of the beam along the vertical axis by: a) adding extra electrode to the button and b) using the Lumped port (See figure 5.1).

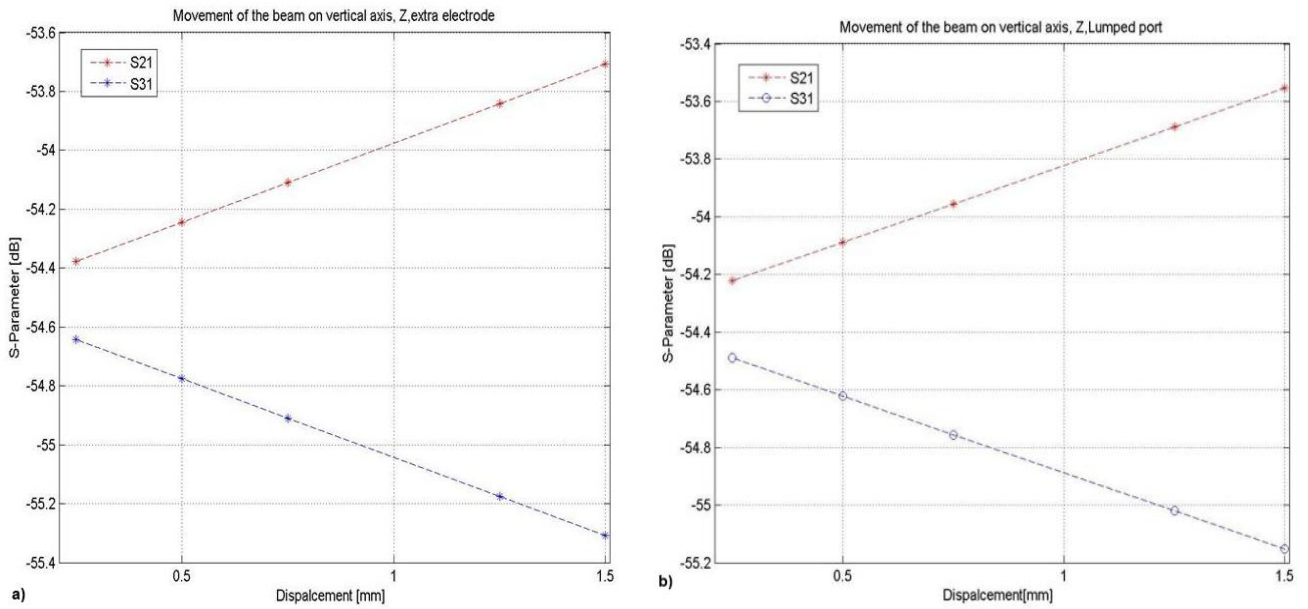


Figure 5.3: Transmission through buttons 2 and 3 for different displacements of the beam along the vertical axis by: a) adding extra electrode to the button and b) using the Lumped port (See Figure 5.1).

Figures 5.2 and 5.3 confirm that as the beam moves toward electrode number 2, the S_{21} , coupling between the beam and that electrode increases while for the opposite electrode, the S_{31} , transmission is reduced with the same ratio.

Table 5.1 depicts the distributed linear charges of the inner pipe for different beam displacements on the vertical axis. The monopole moment is not beam position dependent and it is constant while its distribution is changed by shifting the beam.

Table 5.1: Linear charge (Monopole) on the inner pipe surface for different displacements of the beam along the vertical axis (See Figure 5.1).

Displacement of the beam (mm)	0.25	0.5	0.75	1.25	1.5
ρ_l (v*m)	1.61144758e-9	1.61018963e-9	1.6105145e-9	1.61180131e-9	1.61116604e-9

Figure 5.4 compares the dipole moments for different displacements of the inner pipe along the z-axis. The dipole signal is shown in figure 5.5.

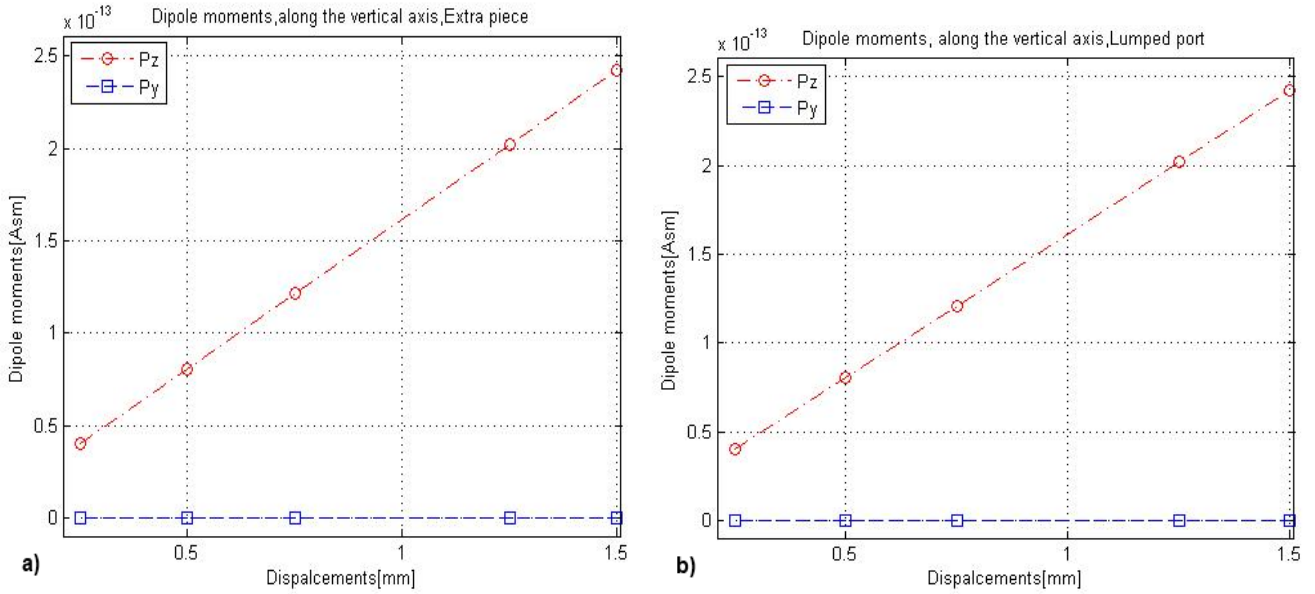


Figure 5.4: Dipole moments for different displacements of the beam along the z-axis by: a) adding extra electrode to the button and b) using the Lumped port (See Figure 5.1)

Moving along z direction toward electrode number 2, results in increasing negative charges on that side and less negative charges on the opposite side. As a result, the dipole moment in the z-direction increases slightly while the dipole moment in the y-direction is almost constant (figure 5.4).

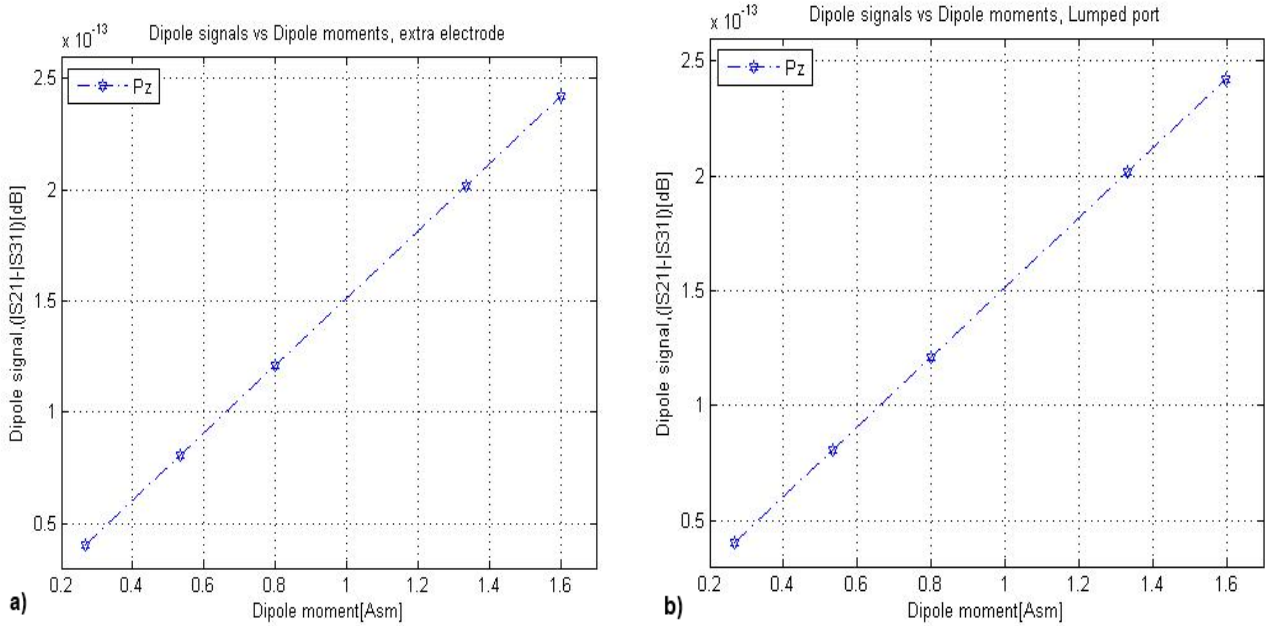


Figure 5.5: Dipole signals for different displacements of the beam along the z-axis by: a) adding extra electrode to the button and b) using the Lumped port (See Figure 5.1).

Figure 5.5 illustrates the dipole signal, which is the difference between two signals of electrode 2 and 3 on the opposite sides. The signal increases linearly as the dipole moment is enhanced on the z-axis. Consequently, the induced voltage on electrode number 2 raises if the beam is displaced towards that electrode, according to formula 2.2.

5.2 Beam displacements along a line between the horizontal and vertical axes

In this part, the beam position is displaced along the line $y=z$ and moved toward electrode 2 and 4 (Figure 5.6).

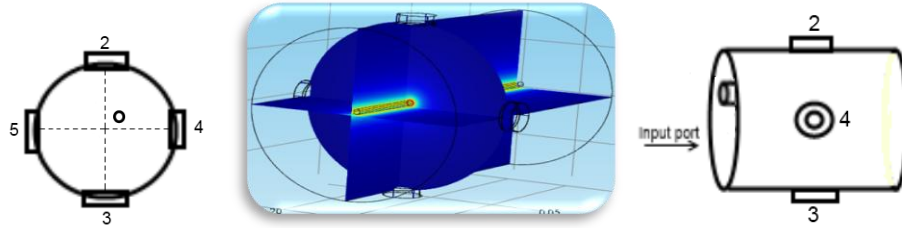


Figure 5.6: Displacement of the inner pipe along the line $y = z$

Figure 5.7 shows the S-parameters for different displacements of the inner pipe along the line $y = z$ on the pipe cross section. Also the transmissions through two ports (2 and 3) that are placed in the opposite directions are illustrated in figure 5.8.

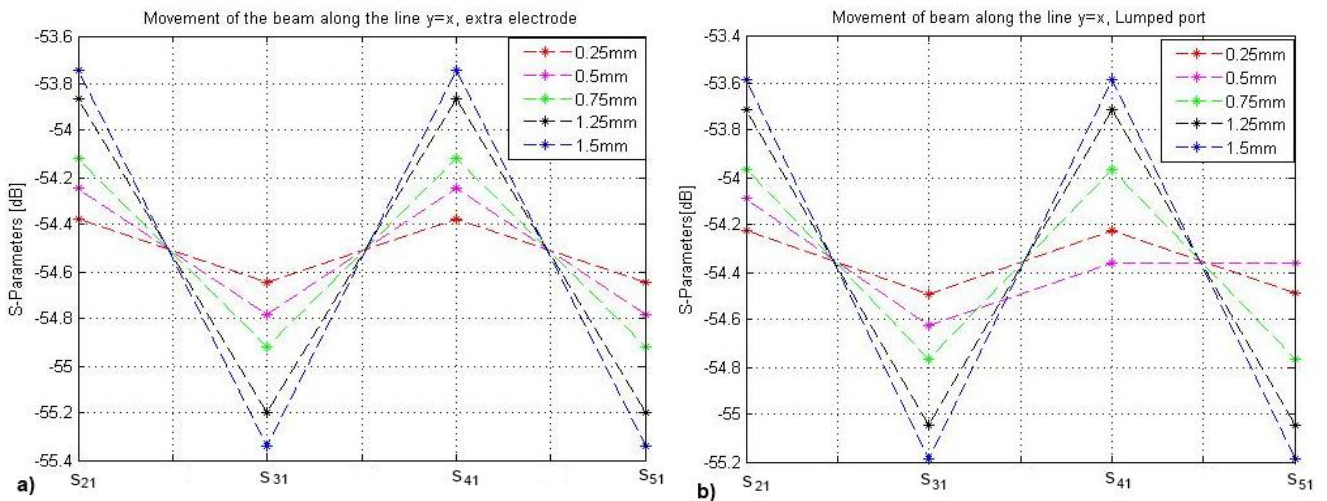


Figure 5.7: S-parameters for different displacements of the beam along the line $y=z$ by: a) adding extra electrode to the button and b) using the Lumped port (see figure 5.6).

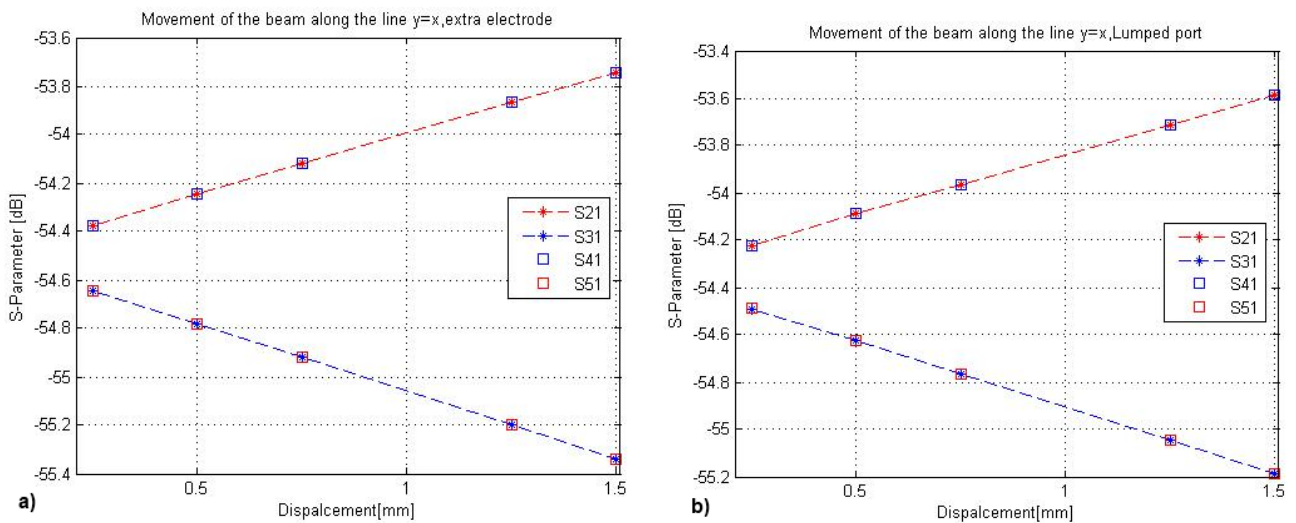


Figure 5.8: Transmission through port 2 and 3 for different displacements of the beam along the line $y=z$ by: a) adding extra electrode to the button and b) using the Lumped port (see figure 5.6)

It is obvious from figures 5.7 and 5.8 that moving along the line $y=z$ results in equal coupling from the beam source to the electrodes number 2 and 4, $S_{21}=S_{41}$. By increasing the movements along the 45 degree line, for the two opposite electrodes, transmission reduction occurs with the same ratio, $S_{31}=S_{51}$.

Table 5.2 shows the distributed linear charges of the inner pipe. It is obvious that the monopole moment is constant for different displacements of the beam along the line $y=z$ but the charge distribution will change by moving the beam.

Table 5.2: Linear charge (Monopole) on the inner pipe surface for different displacements of the beam along the line $y=z$ (see figure 5.6)

Displacement of the beam [mm]	0.25	0.5	0.75	1.25	1.5
ρ_l (v*m)	1.60987269e-9	1.6104e-9	1.61121773e-9	1.6110926e-9	1.6125893e-9

Figure 5.9 illustrates the dipole moments for different displacements of the inner pipe along the line $y=z$. furthermore, the dipole signal is shown in figure 5.10.

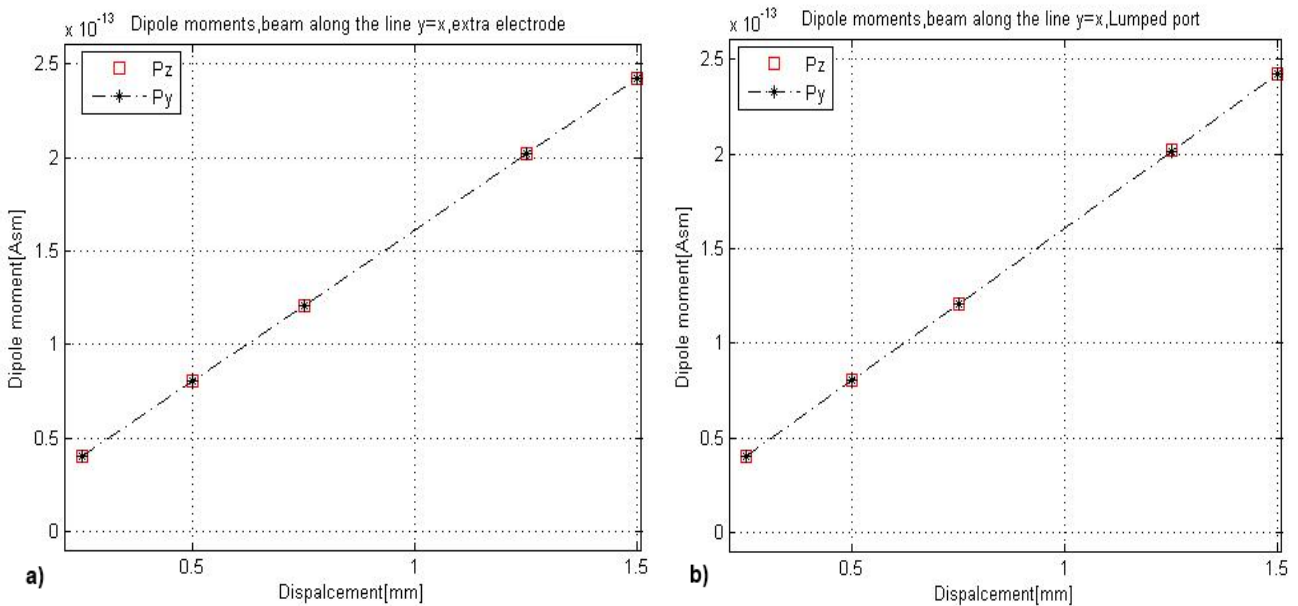


Figure 5.9: Dipole moments for different displacements of the beam along the line $y=z$ by: a) adding extra electrode to the button and b) using the Lumped port (see figure 5.6)

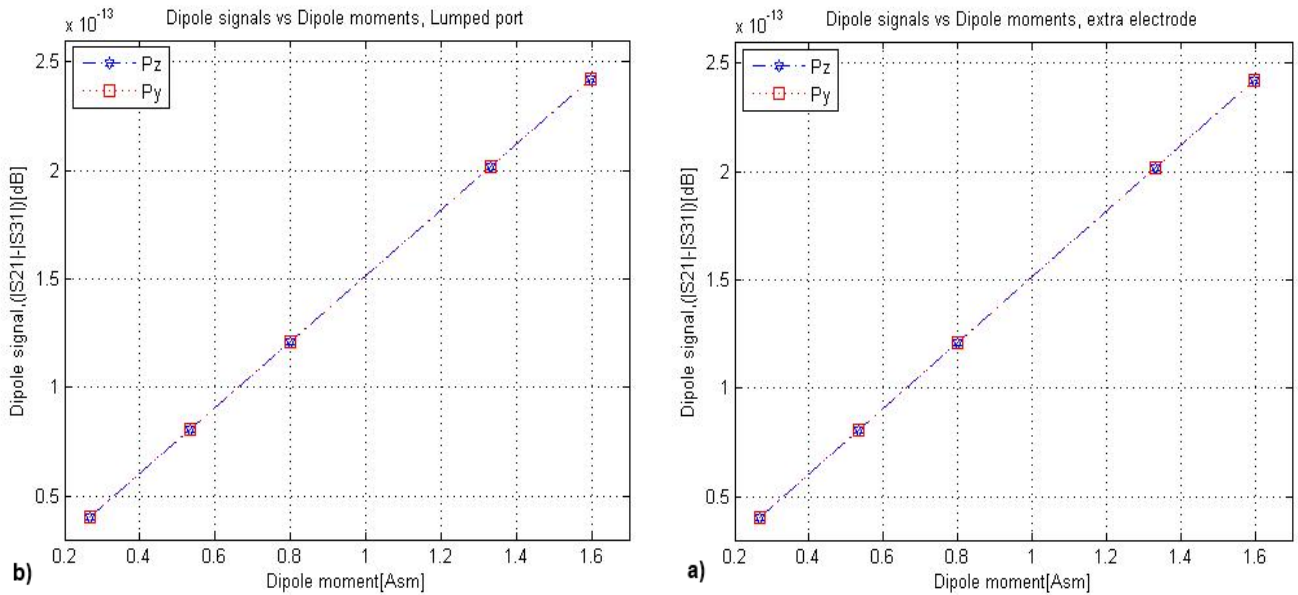


Figure 5.10: Comparison of the Dipole moments and Dipole signals for displacement of the beam along the line $y=z$ by: a) adding extra electrode to the button and b) using the Lumped port (see figure 5.6).

Figure 5.9 shows that the amount of dipole in the y and z directions is the same, and as the beam gets far from the pipe center, the dipole moment is enlarged. Moreover, figure 5.10 proves that the dipole signal increases by increases the dipole moment and it enhanced the induced voltage on electrode number 2 and 4 more than the other electrodes in opposite direction.

In general, the induced electrode voltage changes by displacing the beam due to the varying linear charge distribution on the inner pipe surface and dipole moment. Also the quadrupole moment around the pipe center compare to the dipole moment is negligible when the beam with a circular cross section is only displaced slightly from the pipe center.

5.3 Elliptic beam

The quadrupole quantity depends on the beam dimension more than the beam position. therefore any problem related to this dependency can be solved only by appropriate centering of the beam in the BPM [33, 34]. The quadrupole signal contribution of the displaced beam can be either corrected for good accuracy or neglected if the displacement of the beam from the center of the pipe is small in comparison to the beam dimensions. Therefore, the beam is assumed to have a noncircular cross section such as elliptic shape and induce signal on each electrode (Figure 5.11).

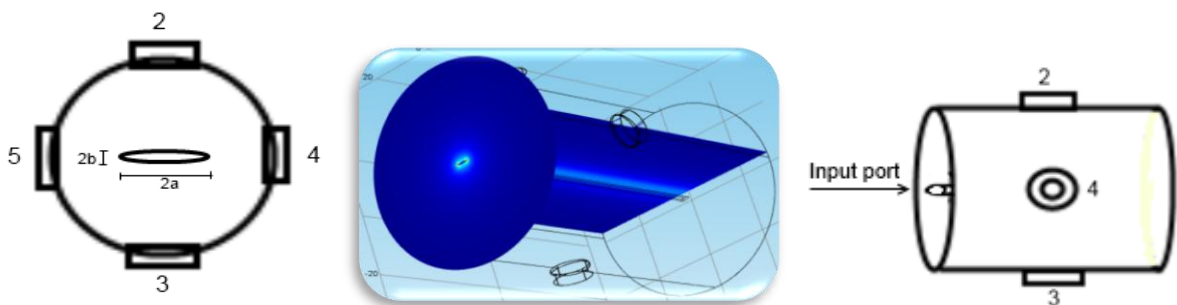


Figure 5.11: Ellipse shape of the beam with semimajor axis a and semiminor axis b

It is an important issue that the area of the beam should be constant and the same as the beam area in the other simulated models with circular cross section (The beam area $\approx 634 \text{ mm}^2$). By this assumption, only the beam cross section shape variation will be considered. Figure 5.12 shows the S-parameters for Elliptic beam with semimajor axis a and semiminor axis b in 300MHz.

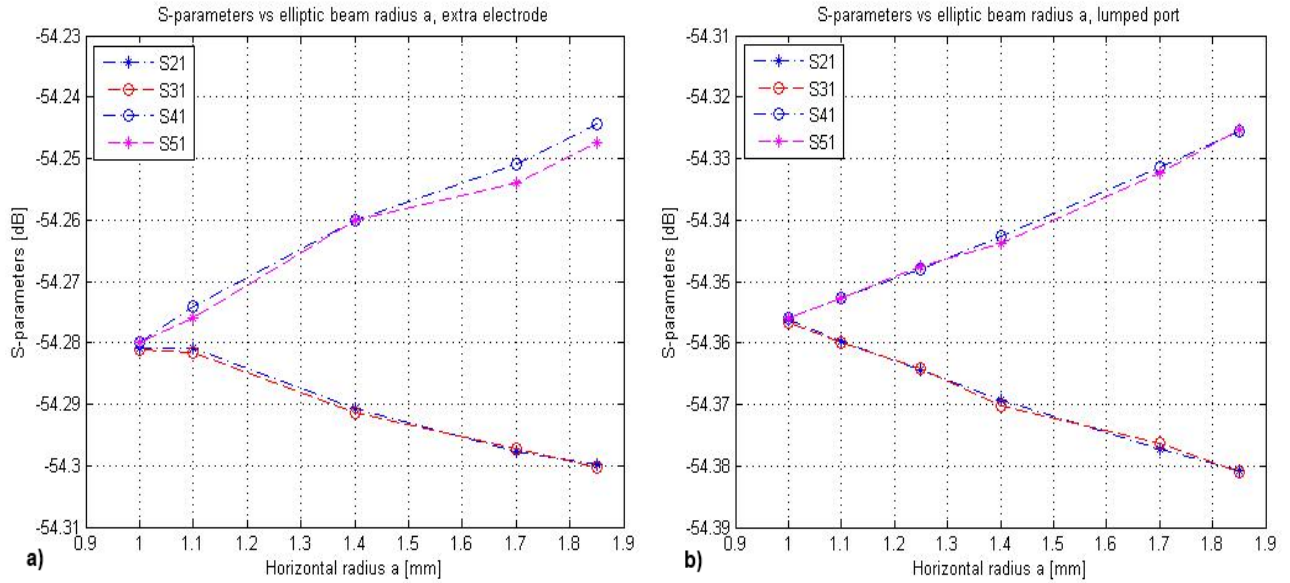


Figure 5.12: Buttons transmissions on vertical and horizontal axis by: a) adding extra piece to the electrode and b) using the Lumped port. , 300MHz, [dB] (see figure 5.11)

As shown in figure 5.12, the coupling to the electrodes located on the horizontal axis increases by elongating the elliptical beam in this direction and it is vice versa for the electrodes on the vertical axis, $S_{21}=S_{31}$ and $S_{41}=S_{51}$.

Some information about the multipole moments for different displacements of the elliptic beam are shown in figures 5.13 and 5.14 which can be explained according to the quadrupole moments formulas.

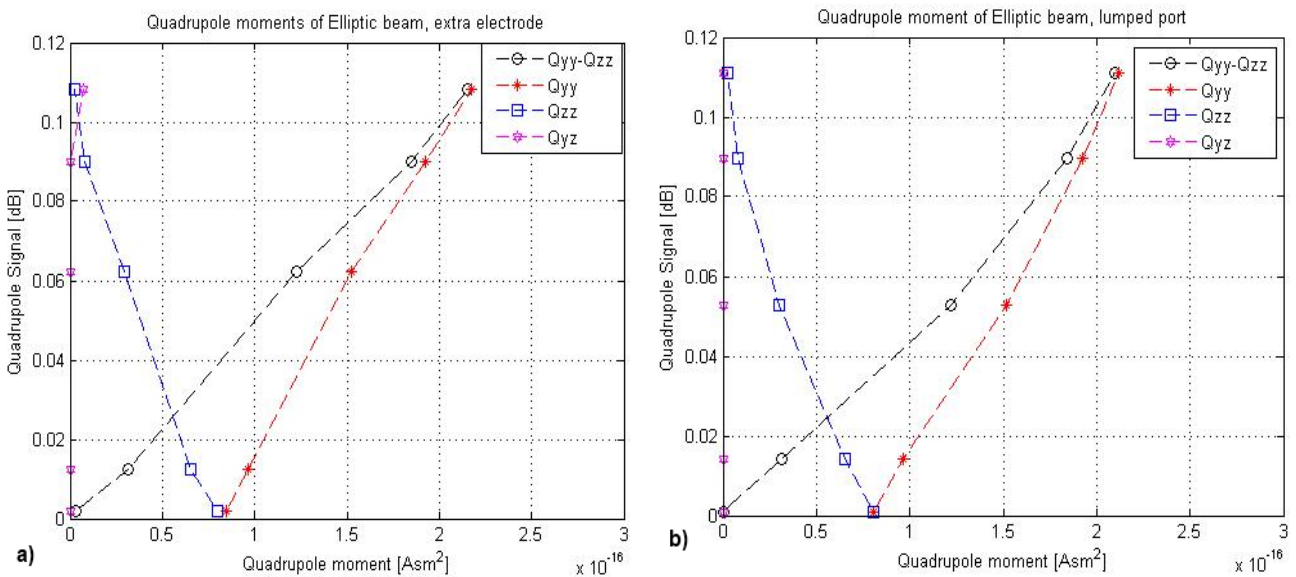


Figure 5.13: The quadrupole moments of Elliptic beam with different semimajor axis a , and semiminor axis b , in horizontal and vertical axes vs the quadrupole signals $[(|S_{41}| \text{dB} + |S_{51}| \text{dB}) - (|S_{21}| \text{dB} + |S_{31}| \text{dB})]$ by: a) adding extra piece to the electrode and b) using the Lumped port. , 300MHz, [dB] (see figure 5.11)

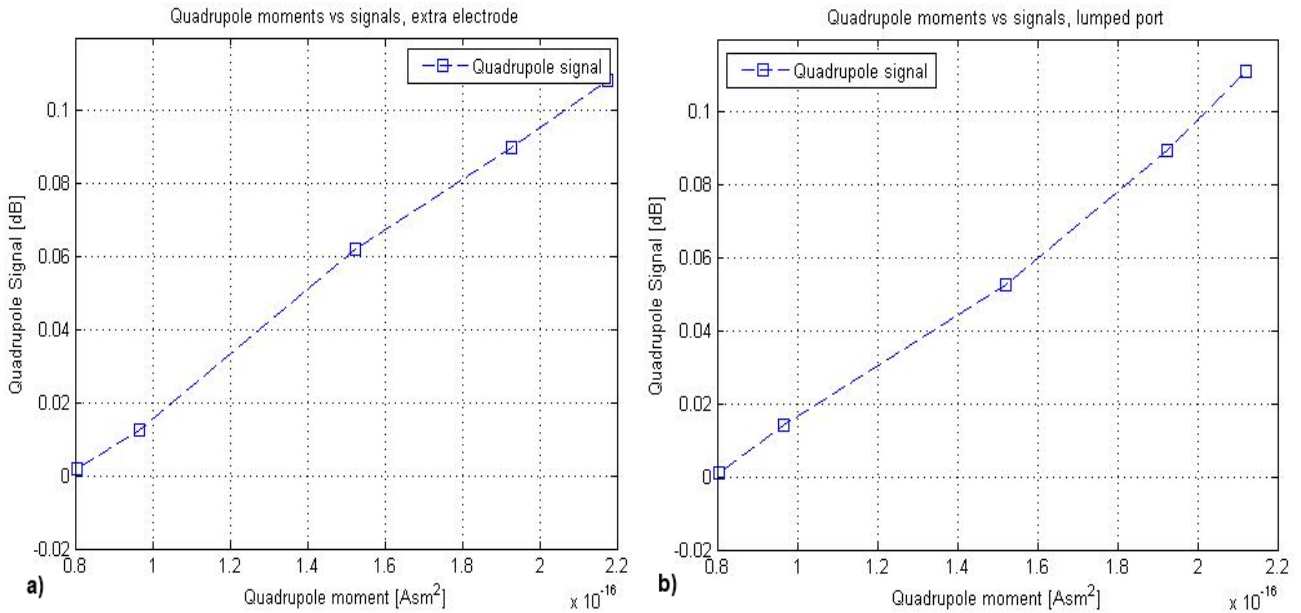


Figure 5.14: The Quadrupole moments vs quadrupole signals of Elliptic beam with different semimajor axis a , and semiminor axis b , in horizontal and vertical axes vs the quadrupole signals $[(|S_{41}|_{\text{dB}}+|S_{51}|_{\text{dB}})-(|S_{21}|_{\text{dB}}+|S_{31}|_{\text{dB}})]$ by: a) adding extra piece to the electrode and b) using the Lumped port. , 300MHz, [dB] (see figure 5.11)

Quadrupole signal is defined as the difference value between sum of the S-parameters in horizontal axis and the sum of the S-parameters in vertical axis.

It is evident from figure 5.13 that the quadrupole moment on y-axis, Q_{yy} , increases by elongating the ellipse horizontally but it drops along the vertical direction, Q_{zz} . Therefore, the difference of quadrupole moment in y and z directions ($Q_{yy} - Q_{zz}$) is enhanced slightly. The intersection point of Q_{yy} and Q_{zz} shows that those amounts are equal and this equality happens when the quadrupole signal is almost equal to zero. It means the sum of the S parameters in y and z directions are equal and the beam has a circular cross section shape.

Moreover, the quadrupole signal rises in y-direction as the moment increases (figure 5.14). It is clear that the quadrupole moment depends on beam cross section shape more than displacement of the beam from the pipe center. Since the beam is centered inside the pipe then the dipole moment is negligible in this model.

6. Conclusion

A BPM system consisting of a vacuum tube and four button electrodes installed around its wall is analyzed in Comsol and CST with good accuracy. One of the main aims in this thesis is to study the deviation of the electrode geometry due to the temperature variations and fabrication tolerances giving errors that affect the measured values of the beam position and cross section. In doing so, two different cases are investigated:

- 1- When there is a very narrow PEC wire instead of beam in the vacuum pipe center. In this case the couplings between the PEC wire and four button electrodes are studied.
- 2- When there is no PEC wire in the vacuum tube center. In this case, one of the electrodes is defined as input source and coupling between this electrode and the three other electrodes are studied.

These two different cases are compared for all types of the simulations, in order to find a relation between their results. An important result is that the errors in s-parameters due to the variations of the electrode geometries follow the same behavior in both cases. It might be possible to use this agreement for calibrating the BPM system.

One of the other objectives in this thesis is to study the relation between multipole moment expansions strength and different displacements and shapes of the beam. By decomposing the beam into its monopole, dipole and quadrupole parts, it can be seen that the linear charge or the monopole moment ρ_l is not beam position dependent and is constant for all different displacements of the beam but the linear charge distribution is changed. The simulations show that the dipole moments can be determined from measurements, even when the errors due to the tolerances are taken into account. The induced electrode voltages from the dipole moments are used to determine the position of the beam. The induced voltages from the quadrupole moments can be used to determine the shape of the beam.

Appendix A:

Basic physics behind an accelerator:

Each particle accelerator works like a coaxial cable. We assumed that the inner conductor of coaxial cable works as the beam that passes through the pipe. It consists of two concentric cylinders which are metallic conductors with the inner pipe radius r_p and the outer pipe radius R_p (Figure A.1). Two metallic conductors are separated by vacuum with dielectric constant ϵ . The motion of the charged particles generates electromagnetic field which is characterized by $E_x = 0$ and $H_x = 0$.

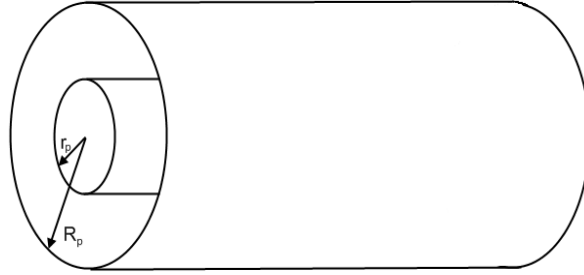


Figure A.1: A coaxial transmission line

In coaxial lines, the dominant propagation mode is the transverse electromagnetic mode (TEM) which has the lowest cutoff frequency equal to zero. In this mode the electric and magnetic field lines are normal to the transmission direction. This desirable mode can propagate at all frequencies. In addition, Characteristic impedance and phase velocity are constant over a wide range in TEM mode. TE and TM modes also can transmit along a coaxial cable. These modes are called higher order propagation modes (HOMs). These modes will be generated if the signal frequency exceeds a certain amount of so called cutoff frequency (f_c) [32, 33].

The number of propagating modes increases when the frequency increases. Accordingly, the frequency should stay below f_c in order to have just one mode, TEM, therefore smaller cable is required for providing this condition to obtain good performance at high frequencies. The cutoff wavelength and frequency are shown as [34]:

$$\lambda_c = \pi (R_p + r_p) \sqrt{\mu_r \epsilon_r} \xrightarrow{\text{for vacuum dielectric}} \lambda_c = \pi (R_p + r_p)$$

$$f_c = \frac{c}{\lambda_c} = \frac{c}{\pi (R_p + r_p) \sqrt{\mu_r \epsilon_r}} \xrightarrow{\text{for vacuum dielectric}} f_c = \frac{c}{\pi (R_p + r_p)}$$

It is important to be aware of the cutoff frequency to avoid the higher order mode propagation. The existence of higher modes can strongly affect on the transmitted power level. That is why the use of the coaxial cables should be restricted with the frequencies below the TE mode cutoff frequency.

$$f_{max} < f_c = \frac{c}{\pi (R_p + r_p)}$$

However, the frequency range in accelerators should be high enough to have small wavelength.

A coaxial transmission line has the following characteristic parameters. Characteristic impedance is [35]:

$$Z_0 = \frac{60}{\sqrt{\epsilon_r}} \ln\left(\frac{R_p}{r_p}\right) = \sqrt{\frac{L}{C}} \quad (\Omega)$$

Relative permittivity, ϵ_r , for vacuum is equal to 1. The capacitance and inductance per unit length are given by:

$$C = \frac{2\pi\epsilon_0}{\ln\left(\frac{R_p}{r_p}\right)} \quad (F/m)$$

$$L = \frac{\mu_0}{2\pi} \ln\left(\frac{R_p}{r_p}\right) \quad (H/m)$$

Where ϵ_0 , vacuum electric permittivity, is equal to $8.854 \times 10^{-12} \frac{C}{Vm}$ and vacuum magnetic permeability $\mu_0 = 4\pi \times 10^{-7} (H/m)$. The above parameters are geometry dependent.

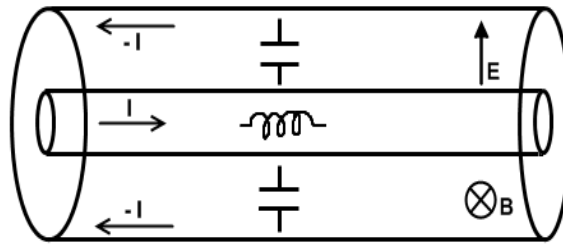


Figure A.2: Electric and magnetic fields in a coaxial cable

Appendix B:

Beam position measurement:

B.1. BPM button voltage:

As mentioned in Theory section, the voltage induced on each electrode depends on transfer impedance as following:

The Surface charge distribution ρ_s (C/m²) on the conducting shell can be obtained by the following formula [25, 36]:

$$\rho_s = \frac{\rho_l}{\text{Duct circumference}} = \frac{\rho_l}{2\pi a}$$

Where ρ_l (C/m) is line charge distribution.

In all cases of this report, the electrode cross section has the distance $a = R_p - 0.9$ mm, from the beam center. The image charge on the button depends on the linear charge density ρ_l changing gradually on the scale of the button size as follows :

$$Q_{img}(\omega) = \rho_s \times \text{area of the inner cylinder of electrode} = \frac{\rho_l(\omega)}{2\pi a} \times \pi r_e^2$$

Although the number of particles for a single bunch is normally utilized as a measure of beam current, but in this place the following formula gives the image current out of the button:

$$I_{img} = I_{button} = \frac{dQ_{img}}{dt} = \frac{\pi r_e^2}{2\pi a} \times \frac{d\rho}{dt} \quad (\text{B.1.1})$$

Indicating the linear charge density in terms of the beam current results the following formula:

$$\rho_l(\omega) = \frac{I_{beam}(\omega)}{\beta c} \rightarrow \frac{d\rho_l}{dt} = \frac{1}{\beta c} \times \frac{dI_{beam}}{dt} = \frac{1}{\beta c} \times i\omega \times I_{beam}(\omega) \quad (\text{B.1.2})$$

Where βc is the beam velocity. By replacing formula B.1.2 in B.1.1 the image current is:

$$I_{img} = I_{button}(\omega) = \frac{\pi r_e^2}{2\pi(R_p - 0.9\text{mm})} \times \frac{1}{\beta c} \times i\omega \times I_{beam}(\omega) \quad (\text{B.1.3})$$

The electrode voltage is equal to the product of the current and load impedance (Z) which is seen by the button which is the reactance of the button capacitance C_b shunted by the cable characteristic impedance of the cable. Z_{coax} is 50 Ω Cable impedance.

$$V_{button}(\omega) = Z_{\text{seen by button}} \times I_{button}(\omega) \quad (\text{B.1.4})$$

$$Z_{\text{seen by button}} = Z(\omega) = Z_{coax} \parallel \frac{1}{j\omega C_b} = \frac{z_{coax}}{1 + j\omega z_{coax} C_b} \quad (\text{B.1.5})$$

Substituting (B.1.5) in (B.1.4) gives the button voltage:

$$V_{button}(\omega) = \frac{z_{coax}}{1 + j\omega z_{coax} C_b} \times I_{button}(\omega) \quad (\text{B.1.6})$$

Button current formula (B.1.3) is replaced in (B.1.6):

$$V_{button} = \frac{\pi r_e^2}{2\pi(R_p - 0.9\text{mm})} \times \frac{1}{\beta c} \times \frac{1}{C_b} \times \frac{i\omega z_{coax} C_b}{1 + j\omega z_{coax} C_b} \times I_{beam}(\omega)$$

The transfer impedance is defined as:

$$Z_t = \frac{\pi r_e^2}{2\pi(R_p - 0.9\text{mm})} \times \frac{1}{\beta c} \times \frac{1}{C_b} \times \frac{i\omega z_{coax} C_b}{1 + j\omega z_{coax} C_b} \rightarrow |Z_t| = \frac{1}{\beta c} \times \frac{1}{C_b} \times \frac{\pi r_e^2}{2\pi(R_p - 0.9\text{mm})} \times \frac{\frac{\omega}{\omega_{cut}}}{\sqrt{1 + \frac{\omega^2}{\omega_{cut}^2}}}$$

$$V_{button} = Z_t(\omega) \times I_{beam}$$

At high frequencies $f \gg f_c$, $\therefore Z_t \propto \frac{\frac{\omega}{\omega_{cut}}}{\sqrt{1 + \frac{\omega^2}{\omega_{cut}^2}}} \rightarrow 1$

And the resulting voltage is equal to:

$$V_{button} = \frac{\pi r_e^2}{2\pi(R_p - 0.9\text{mm})} \times \frac{1}{C_b \beta c} \times I_{beam}(\omega)$$

We are more interested at low frequency range $f \ll f_c$, which the transfer impedance is proportional

to: $Z_t \propto \frac{\frac{i\omega}{\omega_{cut}}}{1 + \frac{i\omega}{\omega_{cut}}} \rightarrow \frac{i\omega}{\omega_{cut}}$

the voltage is independent of the capacitance :

$$V_{button} = \frac{\pi r_e^2}{2\pi(R_p - 0.9\text{mm})} \times \frac{z_{coax}}{\beta c} \times i\omega \times I_{beam}(\omega)$$

B.2. Multipole expansions:

The coaxial transmission lines are used for button electrodes. The TEM waves mostly propagate in lossless transmission lines. Both electric and magnetic fields are zero in the propagation direction. Furthermore, the propagation of the electromagnetic waves through these lines is analyzed by Maxwell equations [39]:

$$\nabla \times \mathbf{E}(\mathbf{r}, t) = -\partial \mathbf{B}(\mathbf{r}, t) / \partial t \quad , \quad \nabla \times \mathbf{H}(\mathbf{r}, t) = \mathbf{J}(\mathbf{r}, t) + \partial \mathbf{D}(\mathbf{r}, t) / \partial t$$

Where $\mathbf{E}(\mathbf{r}, t)$, $\mathbf{H}(\mathbf{r}, t)$, $\mathbf{D}(\mathbf{r}, t)$, $\mathbf{B}(\mathbf{r}, t)$ and $\mathbf{J}(\mathbf{r}, t)$ are the electric field [V/m], Magnetic field [A/m], electric flux density [As/m²], magnetic flux density [Vs/m²] and current density [A/m²], respectively.

The electric field, \mathbf{E} and the electric flux density, \mathbf{D} are parallel in vacuum and can be expressed as:

$$\mathbf{D} = \epsilon_0 \mathbf{E} \quad , \quad \mathbf{B} = \mu_0 \mathbf{H} \quad , \quad \text{Where } \epsilon_0 \approx 8.854 \times 10^{-12} \text{ (As/Vm)} \text{ and } \mu_0 = 4\pi \times 10^{-7} \text{ V}\cdot\text{s/(A}\cdot\text{m)}.$$

In addition the fields have the same propagator $e^{\pm i\gamma z}$ since the propagation wave is a TEM wave:

$$\mathbf{E}(x, y, z) = \mathbf{E}_T(x, y) e^{\pm i\gamma z} \quad , \quad \mathbf{H}(x, y, z) = \mathbf{H}_T(x, y) e^{\pm i\gamma z}$$

There is a potential for the field such that $\mathbf{E}_T(x, y) = -\nabla V(x, y)$.

The electrostatic potential in a point, $\mathbf{r}(y, z)$ inside a circle with radial coordinate $r_c = \sqrt{y^2 + z^2}$ where $r_c < a$ In a two-dimensional charge distribution $\rho(y, z)$ is given by:

$$V(r) = -\frac{1}{2\pi\epsilon_0} \int_S \rho(r') \ln(|r - r'|) dS$$

The surface S is the area where the charge distribution is not zero ($\rho(r) \neq 0$). By expanding the above formula in Taylor series and using the binomial theorem, the induced electric potential formula in point $r=(y,z)$ is defined by : $V(r) = -\frac{1}{2\pi\epsilon_0} (\rho_l \ln(r_c) - \rho_y \frac{y}{r_c^2} - \rho_z \frac{z}{r_c^2} + (Q_{yy} - Q_{zz}) \frac{z^2 - y^2}{2r_c^4} - 2Q_{yz} (\frac{yz}{r_c^4}) + O(r_c^{-3})$

Monopole mode:

$$\rho_l = \int_{\Gamma} \rho_s(r') dl$$

Dipole modes:

$$p_y = \int_{\Gamma} y' \rho_s(r') dl \quad , \quad p_z = \int_{\Gamma} z' \rho_s(r') dl$$

Quadrupole modes:

$$Q_{yy} = \int_{\Gamma} y'^2 \rho_s(r') dl \quad , \quad Q_{zz} = \int_{\Gamma} z'^2 \rho_s(r') dl \quad , \quad Q_{zy} = Q_{yz} = \int_{\Gamma} z' y' \rho_s(r') dl$$

The technique of using quadrupole moment information for emission measurement has been suggested by Miller [40, 41].

B.3. S-parameters:

For high frequency structures voltage and current are not well defined entities then instead of looking to current or voltage it is better to study S-parameters in terms of reflected and incident voltage waves. Scattering parameters or S-parameters describe the electrical properties, such as inductors, capacitors, signal power and energy of different networks. The parameters are very useful for systems design especially for microwave engineering and networks operating at radio frequency. These parameters are frequency dependent. Measured S-parameters at different ports of devices describe the transmission and reflection of electromagnetic fields.

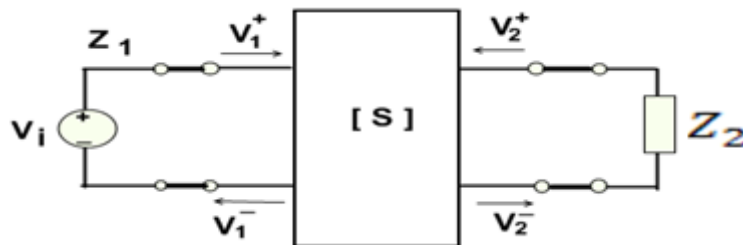


Figure B.3.1: Two ports schematic of incident and reflected waves

Each electrode as an output should be terminated with a suitable load to minimizing the reflected wave as an incident wave then the load connected to each electrode should be equal to 50Ω which has reflection coefficient equal to zero. By definition:

$$V_1^- = S_{11}V_1^+ + S_{12}V_2^+$$

$$V_2^- = S_{21}V_1^+ + S_{22}V_2^+$$

At port 1 the total voltage is:

$$V_1 = V_1^+ + V_1^-$$

S_{11} is the input port voltage reflection coefficient; S_{12} is the reverse voltage gain; S_{21} is the forward voltage gain and S_{22} is the output port voltage reflection coefficient.

In this thesis we are interested to study transmission from the pipe to the electrodes, S_{n1} . If the pipe entrance is called port 1 and each electrode with $n=1,2,3,4$. For example S_{21} is the voltage transmission coefficient from port 1 to port 2. The S-parameter is given by this formula:

$$S_{21} = \frac{V_2^-}{V_1^+}, \text{ Where } Z_1 = Z_2.$$

If the characteristic impedances of two connected transmission lines are not the same, S_{21} definition is

expressed as:
$$S_{21} = \frac{V_2^-}{V_1^+} \sqrt{\frac{Z_1}{Z_2}}$$

Appendix C: Modeling instructions

C.1 2D simulation:

In this section the modeling instructions in COMSOL 4.2, are presented.

1. *Model wizard* window → 2D asymmetric → Add Physics tree, select *Radio Frequency* → *Electromagnetic Waves (emw)* → **Preset Studies** → **Frequency Domain** → Finish
2. Material: Model Builder window, choose Material → Rename it to Air → In the Material properties tree, select Electromagnetic Models → Refractive index (n). The material **Contents** table:

Table C.1: Materials refractive indices in model

Material	Refractive index
Air	1
Aluminum (Al ₂ O ₃)	1.65

The default boundary condition is perfect electric conductor for all boundaries except the ports. All the rectangle materials are vacuum (n=1) except the rectangle number 2 in figure C.1 which is Alumina oxide with the refractive index of 1.65.

3. Ports: right-click *Electromagnetic Waves* and choose *Port* → select *Rectangular* → From the Wave excitation at this port list, select *on* for input port. Redo this step for the output port, but select *off* for the wave excitation.
4. Mesh: In the *Model Builder* window, right-click *Model 1* → *Mesh 1* and choose *Free Triangular* → Settings window for *Size* → From the Predefined list, select *extremely fine* → *Build All*
5. Frequency Domain: In the *Model Builder* window → Study 1 node, then click *Step 1: Frequency Domain* → In the Frequencies edit field, type range (2e8, 1e8, 4e8) → right-click *Study 1* and choose *Compute*.

After computation the wave propagation inside the 2D electrode looks like figure 4:

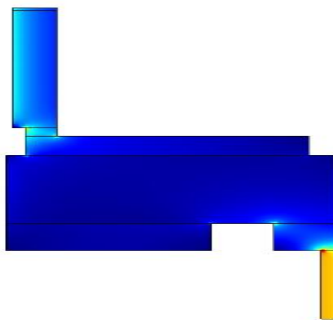


Figure C.1: wave propagation inside 2D BPM plot

C.2 3D simulation:

This section tries to give you an idea about construction of the BPM model step-by-step in both Comsol Multiphysics and CST Microwave Studio. The design is based on coaxial properties. The described model computes and compares the reflection and transmission between the coaxial pipe and the coaxial electrodes.

Comsol Multiphysics:

A drawing of the final schematic of the BPM is shown in figure 5 and 6; four similar circular button electrodes as BPM are attached on the coaxial waveguide wall. The electrodes inserted in the waveguide in order to transmit the waves.

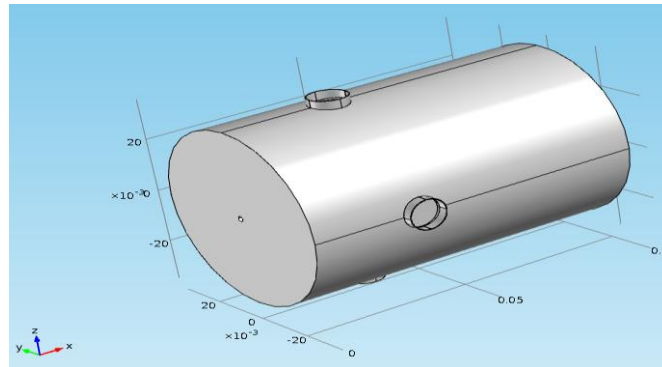


Figure C.2:BPM structure consists of a coaxial pipe and four coaxial electrodes around it without 50 ohm coaxial cables

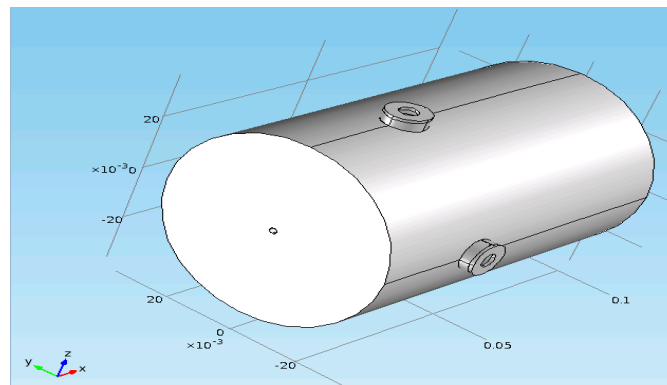


Figure C.3:BPM structure consists of a coaxial pipe and four coaxial electrodes around it with 50 ohm coaxial cables

Modeling instructions:

1. *Model Wizard* window → in the Add Physics tree, select *Radio Frequency* > *Electromagnetic Waves (emw)* → select *Preset Studies* → *Frequency Domain* → *Finish*.
2. *Model Builder* window, right-click *Global Definitions* and choose *Parameters*.

The BPM geometry parameters listed in the table 2. In order to renormalize the S-parameters the model will change by adding an extra piece to the ports by 50 Ω (table C.2) or set a *Lumped* port for a model with the same geometry.

Table C.2: BPM Geometry parameters

Rp	32.5[mm]	Radius of the outer pipe
rp	1 [mm]	Radius of the inner pipe
L	100 [mm]	pipe length
Re	5.65 [mm]	the outer radius of the electrode
re	5.4 [mm]	the inner radius of the electrode
l	3.7 [mm]	electrode length
hi	0.9 [mm]	electrode insertion inside the pipe
RL	2.45 [mm]	Inner radius of the 50 ohm coaxial cable
LL	1 [mm]	Length of the 50 ohm coaxial cable

3. *Model Builder* window, right-click *Geometry 1* → *Cylinder* → locate the Size and Shape section and build all the cylinders → *Build All*
4. *Model Builder* window, right-click *Geometry 1* and choose *Boolean Operations* → *Difference*. Then select and add outer cylinders of the coaxial cables and remove the inner ones → *Build All*.

Definition : Define a couple of boundary selections:

Selection1:

5. *Model Builder* → right-click *Definitions* → *Selection* → Rename Selection to *Metal Boundaries* → from the Geometric entity level list, select *Boundary* → All boundaries → remove all port boundaries.

Selection2:

6. *Model Builder* → right-click *Definitions* → *Selection* → Rename Selection to *Input Port* → from the Geometric entity level list, select *boundary1*.

Repeat this step for all ports separately.

Materials:

7. *Model Builder* → right-click *Materials* and choose *Material* → Rename Material to *Dielectric* → select *all domains*

Table C.3: Material properties used at BPM system

Property	Name	Value
Electric conductivity	sigma	0
Relative permittivity	Epsilon r	1
Relative permeability	Mu r	1

8. *Model Builder* → *Materials* → select *Built-In* → *Copper* → Add Material to Model → click *Copper* → from the Geometric entity level list, select *Boundary* → select *Metal Boundaries*.
9. *Model Builder* → right-click *Model 1* → *Electromagnetic Waves* → choose *Impedance Boundary Condition* → select *Metal Boundaries*.
10. *Model Builder* → right-click *Electromagnetic Waves* and choose *Port* → select *Input Port* → Locate the Port Properties → from the Type of port list, select *Coaxial* → from the Wave excitation at this port list, select *on*. Do this step for other output ports as well with *Off Wave* excitation.

Mesh

Analysis software like Comsol or CST, divide the model into small units called “mesh” (Figure D.5). Mesh is a small unit of model and mesh size is one of the most important features in simulation process which is determined by the size and the shape of the geometry. In Comsol, for example, it is possible to choose element size either by selecting extremely coarse, extra coarse, coarser, coarse, normal, fine, extra fine, extremely fine or opening custom check box and entering the desired value. Obviously, the smaller and more symmetric mesh size, the better precision. Moreover, it strongly

depends on physical RAM memory of computer. Out of memory error occurs when Comsol requests for more memory, for running the model.

The S-parameters are evaluated by integrals over the port boundaries. The more mesh segments, the more accurate results for investigating and comparing the models.

11. Size: Model Builder → Mesh 1 and choose *Free Tetrahedral* → Locate the *Element Size* → From the Predefined list, select the mesh that your computer can handle it, for each port should define one size → *Build All*.

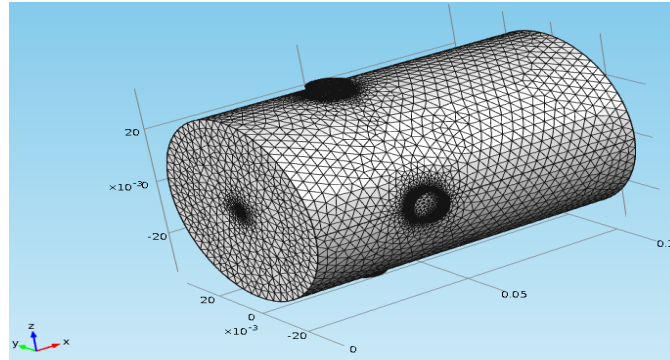


Figure C.4: BPM with finer mesh in Comsol

Frequency domain

12. Model Builder → click Step 1: Frequency Domain → in the Frequencies edit field, type [200-400] with step 100 MHz → right-clicks Study 1 and choose *Compute*.

Derived values

13. Model Builder → right-click Derived Values and choose *Global Evaluation* → choose *Electromagnetic Waves* → S-parameter (emw.S11dB) or *Electromagnetic Waves* → S-parameter (emw.S21dB) → *Evaluate*

In order to find dipole and quadrupole moments, instead of global evaluation should use *line integration* and depend on which moment is of interest suitable formula should be written in the expression box.

According to the Maxwell's equation for this kind of medium, $\rho_s = \text{divergence}(\bar{D})$ Where D is electric flux density and is equal to: $\bar{D} = \epsilon_0 \times \bar{E}$

\bar{E} is electric field and ϵ_0 is the electric permittivity, then surface charge density is:

$$\rho_s = \hat{n} \times \bar{D} = \epsilon_0 \times \hat{n} \times \bar{E} = \epsilon_0 \times (n_z \times E_z + n_y \times E_y)$$

Vacuum permittivity is equal to 8.854e-12.

$$\rho_s = 8.854e-12 \times (\text{emw.ny} \times E_y + \text{emw.nz} \times E_z)$$

For monopole moment line integral of surface charge density is enough while for dipole moments in z and y directions should multiply ρ_s in z and y respectively and for quadruple moments multiply by z^2 and y^2 .

Figure C.5 represents the electromagnetic field distribution. There are two horizontal slices through the pipe illustrates the z component of the field and the vertical slice shows the y component.

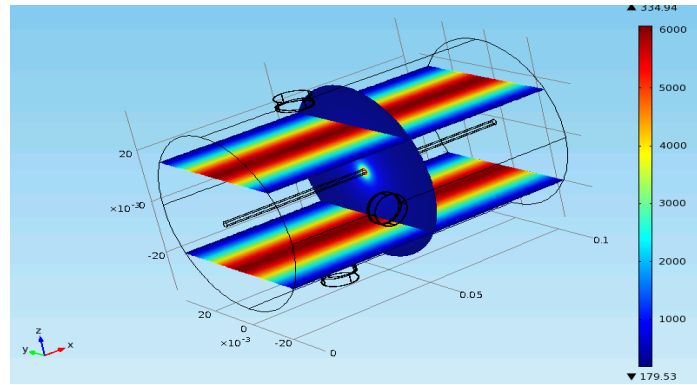


Figure C.5: field distribution inside the BPM, Comsol

CST Microwave Studio:

In CST, there is S-parameter renormalization option, therefore no need to connect 50 ohm coaxial cable on top of the each electrode. CST software sets the units to millimeter and GHz by default. The background material and then all boundaries are defined as PEC.

Geometric Construction

In CST MICROWAVE STUDIO, the results obtain by two techniques: Time domain (hexahedral mesh) and frequency domain (tetrahedral mesh).

1. Set the Units to mm and MHz: Solve → Units.
2. Object → rotate → tab key → enter the coordinates of the pipe → material: *vacuum*

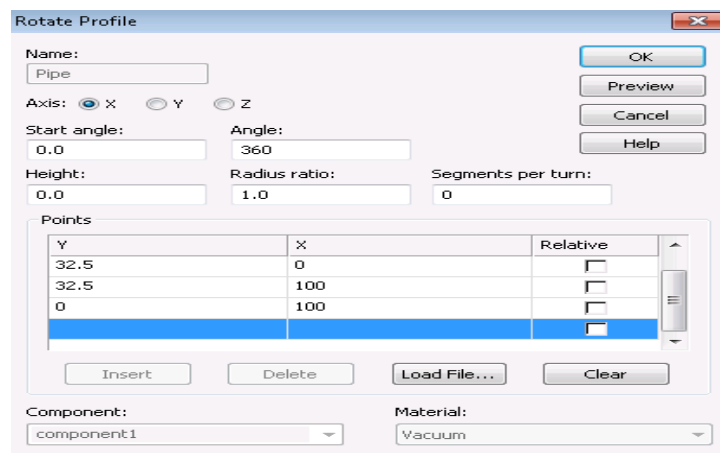


Figure C.6: Geometric parameters, CST

3. In order to draw the electrodes, the local coordinate system should transform for each electrode. WCS → Local Coordinate System

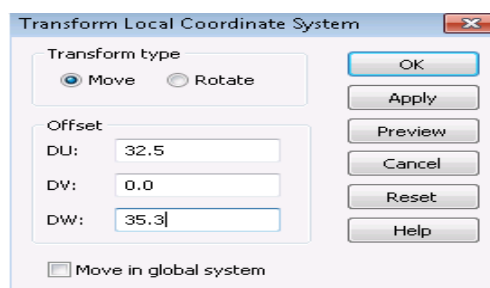


Figure C.7: Transfer local coordinate system, CST

- Objects → Basic Shapes → Cylinder → Shift + tab-key → enter the electrode parameters.

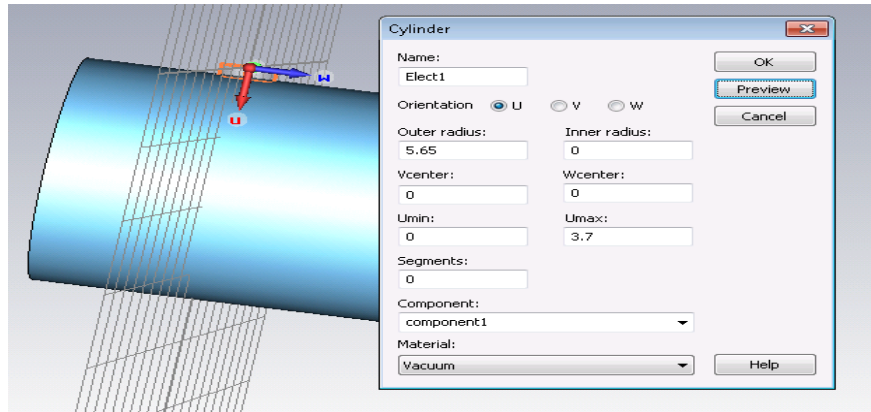


Figure C.8: outer Electrode cylinder parameters, CST

- Inner conductor of the coaxial Cables: Object → rotate → enter the pipe position points (the same way for electrodes) → material: PEC

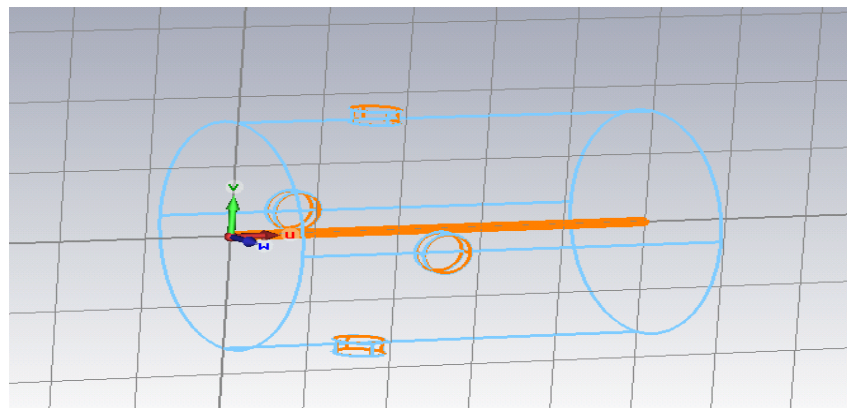


Figure C.9: BPM wireframe visualization, CST

- In the case of coaxial cable, the ports have to completely cover the input-output surfaces. Objects → Pick → Pick Face, f → double-click the substrates *port face*

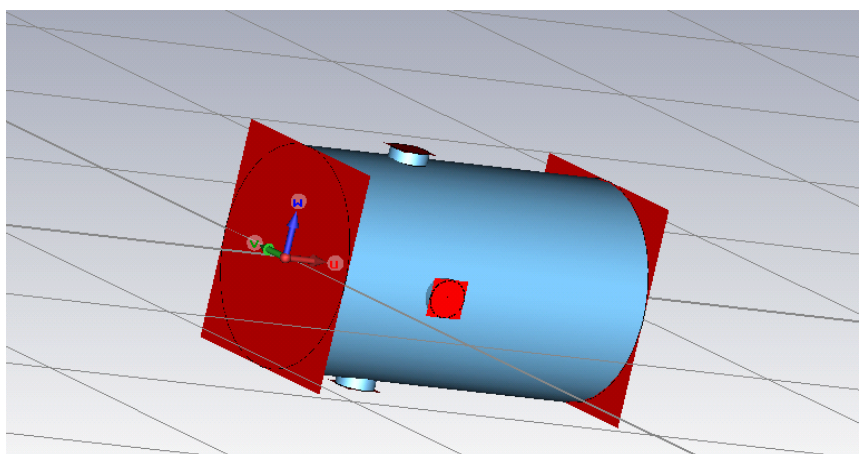


Figure C.10: BPM input and output ports, CST

- Define Boundary conditions: Solve → Boundary Conditions.

All boundary conditions are set to electric meaning that the structure is embedded in a perfect electrically conducting housing.

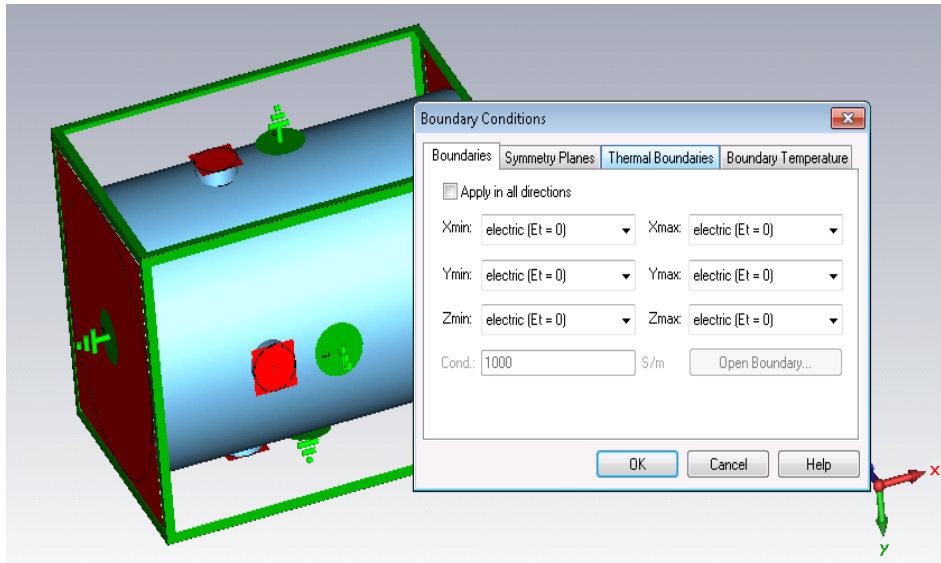


Figure C.11: Boundary perfect electrically conducting housing, CST

8. Define the frequency range: Solve →frequency →enter 200MHz to 400 MHz.
9. Define Field Monitors: CST uses the concept of monitors to specify which field data to store. In addition, it is also possible to choose whether the field is recorded at a fixed frequency or at a sequence of time samples. It is possible to select as many monitors as necessary to obtain the fields at various frequencies. Solve →field monitors

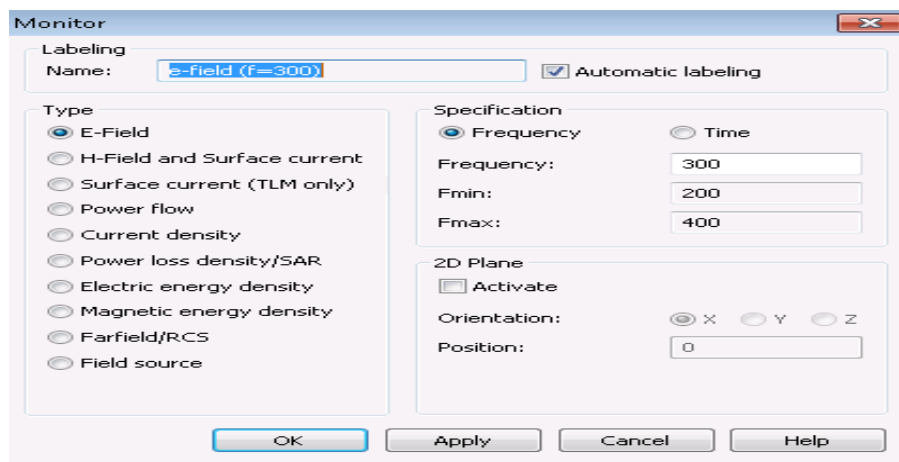


Figure C.12: Field monitors, CST

S-Parameter Calculation

There are two ways to calculate the S-parameters: Transient and frequency domain solvers. The frequency domain calculation uses tetrahedral mesh and the transient simulation is performed with hexahedral mesh. In this project, the frequency domain solver is used.

10. Frequency Domain Solver

The Frequency Domain Solver Parameters dialog box is opened by selecting Solve →*Frequency Domain Solver* from the main menu or by pressing the corresponding icon  in the toolbar. S-

Parameters in the frequency domain are obtained by solving the field problem at different frequency samples → *Start*

11. Results of the Frequency Domain Solver:

- 1D Results → S-Parameters.
- 2D and 3D Results (Port Modes and Field Monitors):
Port Modes → Port1 → To visualize the electric field of the port mode, click on the *e1* folder.
For magnetic field click on *h1*[41].

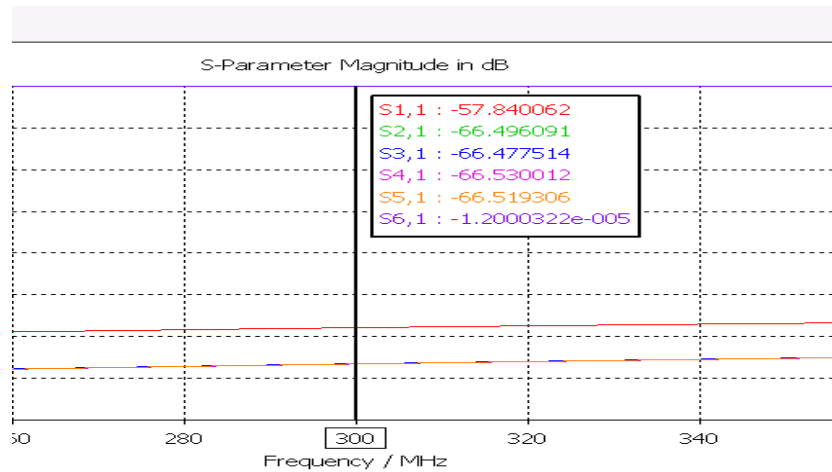


Figure C.13: S-parameters in dB, CST (without renormalization)

Appendix D: Basic considerations

D.1 Mesh:

At the early steps of the work, with regards to the very low memory available (2 GB), all simulations had been done by using extremely coarse mesh being the worse mesh size in Comsol, so the results were not accurate and good enough. As seen in figure D.1.a, there is no uniform electromagnetic distribution inside the vacuum tube; on the other hand, the vertical and horizontal errors in this case are high rather than the case with the best mesh. (Figure D.1.b) .At the next step, by using more RAM, (16 GB), all models repeated by finer mesh size, so the results improve considerable amount. By using finer as the mesh size, there will be a very regular and strong field distribution around the beam as it is depicted in figure D.1.b.

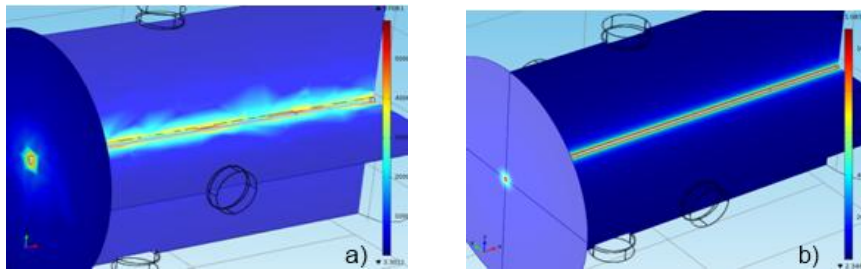


Figure D.1: The field distribution of the beam inside the pipe for two different types of mesh sizes: a) Extremely Coarse mesh and b) Finer mesh

The dissimilarity in electromagnetic distribution inside the pipe is clearly observable for the worse and the best mesh sizes in figure D.1. The electromagnetic distribution around the beam is not uniform and regular for the case with the worse mesh size i.e. extremely coarse.

Table D.1: Element size parameters for extremely coarse and Extra Fine mesh sizes.

Element size parameters	Maximum element size	Minimum element size	Maximum element growth rate	Resolution of curvature	Resolution of Narrow regions	Transmission [dB]	Error [dB]
Extremely coarse	0.05	0.007	2	1	0.1	-53.5167	0.1535
Extra Fine	0.0035	0.00015	1.35	0.3	0.85	-54.5103	0.0004

Table D.1 and D.2 show differences between the element size parameters and the S-parameters for different mesh sizes.

Table D.2: transmission parameters and errors for different meshes

Size	S_{21} [dB]	S_{31} [dB]	S_{41} [dB]	S_{51} [dB]	$ S_{31} - S_{21} $ [dB]	$ S_{51} - S_{41} $ [dB]
Extremely Coarser	-53.5167	-53.547	-53.5394	-53.5296	0.0303	0.0098
Coarser	-54.0257	-54.0197	-54.0172	-54.0223	0.006	0.0051
Normal	-54.5401	-54.5269	-54.5344	-54.5337	0.0132	0.0007
Finer	-54.5103	-54.5099	-54.5098	-54.5102	0.0004	0.0004

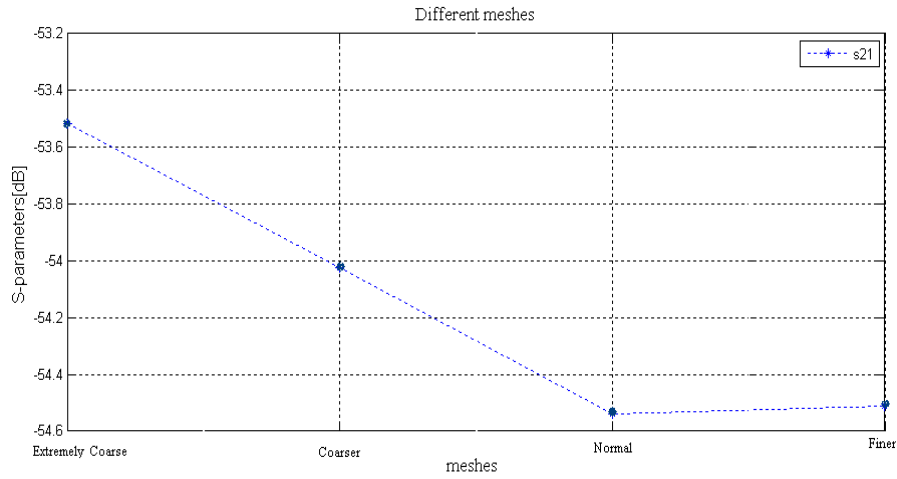


Figure D.2: variation in S-parameter for different meshes

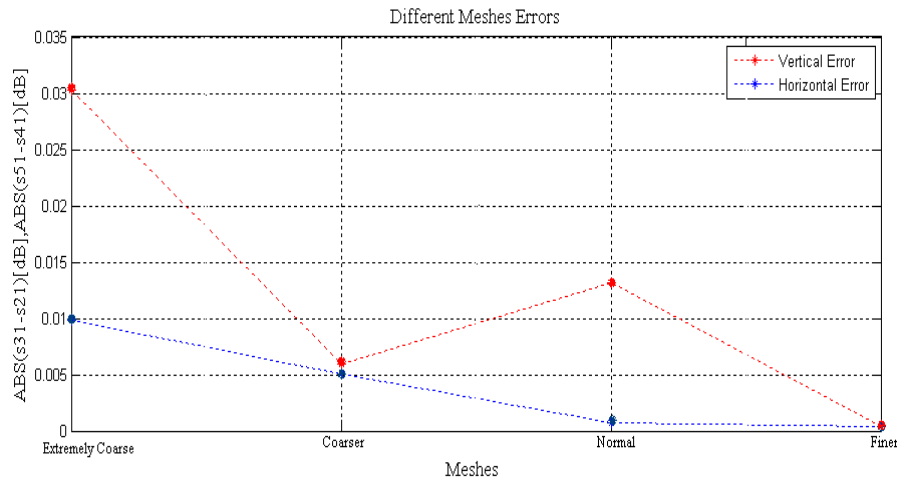


Figure D.3: vertical and horizontal errors for different meshes

One of the most prominent results is that by improving the mesh size toward finer mesh, electromagnetic distribution turns into more oriented shape and the variation in s-parameters becomes smaller, Figure D.2. Consequently the vertical and horizontal errors turn out to be smaller by increasing the mesh size, figure D.3.

D.2 Frequency dependency:

According to the formulas 2.1 and 2.2, the electrode voltage has direct relationship with frequency. The beam current is frequency dependent as follows:

$$I_{beam} = I_p \times T_p \times f_{rep}, \text{ where } T_p, \text{ pulse duration, } I_p \text{ pulse current and } f_{rep}, \text{ the pulse repetition rate. [18]}$$

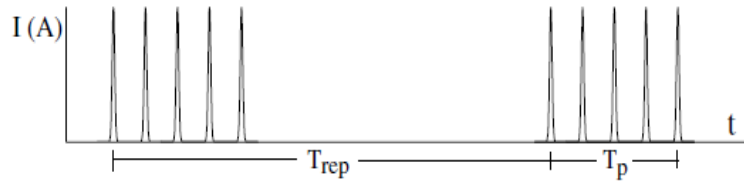


Figure D.4: frequency dependency of the beam current

Table D.3: frequency dependency of S-parameters in BPM

Freq[MHz]	S_{21} [dB]	S_{31} [dB]	S_{41} [dB]	S_{51} [dB]	$ S_{31} - S_{21} $ [dB]	$ S_{51} - S_{41} $ [dB]
200	-57.569	-57.5687	-57.5686	-57.5689	0.0003	0.0003
250	-55.8458	-55.8451	-55.845	-55.8461	0.0007	0.0011
300	-54.5103	-54.5099	-54.5098	-54.5102	0.0004	0.0004
350	-53.448	-53.4476	-53.4475	-53.4479	0.0004	0.0004
400	-52.5858	-52.5861	-52.586	-52.5866	0.0003	0.0006

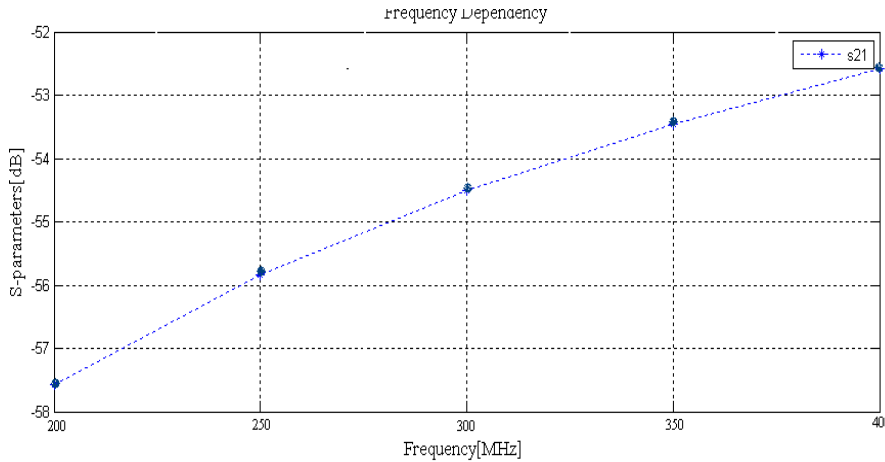


Figure D.5: frequency dependency of S-parameters

Beam frequency is an important parameter in beam position monitoring, because the peak voltages appearing on the pickup electrodes are proportional to both frequency and beam current. As it is clear from table D.3 and figure D.5, by increasing the frequency, transmission through the electrode increases.

D.3 Beam Size:

A particle beam is characterized by a collection of properties. Some of these properties are the same for all particles within the beam and some of them varies from a group of particles to another group like beam intensity or beam size which are the functions of the locations [21].

One of the most important parameters for particle accelerators designing is to have knowledge about the beam size. In this work, with regards to the lack of the facilities to use a real beam as a source, the proton beam was modeled by a narrow perfect electric conductor (PEC) cylinder with a constant potential on its surface.

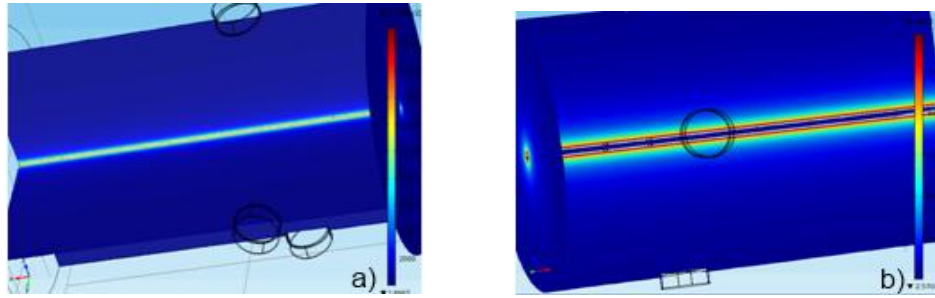


Figure D.6: Two different radiuses of the beam a) $r_p=0.2$ mm and b) $r_p=1$ mm

Different cross section radiuses of the beam for a range of [0.2, 1] millimeter are investigated, table D.4. Due to the restrictions on the mesh size; it is not possible to use very small radiuses.

Table D.4: S-parameters for different beam radiuses

Size r [mm]	S_{21} [dB]	S_{31} [dB]	S_{41} [dB]	S_{51} [dB]	$ S_{31} - S_{21} $ [dB]	$ S_{51} - S_{41} $ [dB]
0.4	-55.5256	-55.5284	-55.527	-55.5257	0.0028	0.0013
0.5	-55.298	-55.2988	-55.2982	-55.2976	0.0008	0.0006
0.6	-55.1047	-55.1039	-55.1042	-55.1045	0.0008	0.0003
0.8	-54.7797	-54.7793	-54.7795	-54.78	0.0004	0.0005
1	-54.5103	-54.5099	-54.5098	-54.5102	0.0004	0.0004

It is noticeable that by increasing the beam size, transmission trough the electrodes increases, figure D.7. This behavior is explicable by using the button voltage formula. As the beam radius increases, the distance between the button pick up cross section and the beam decreases resulting more coupling and more transmission.

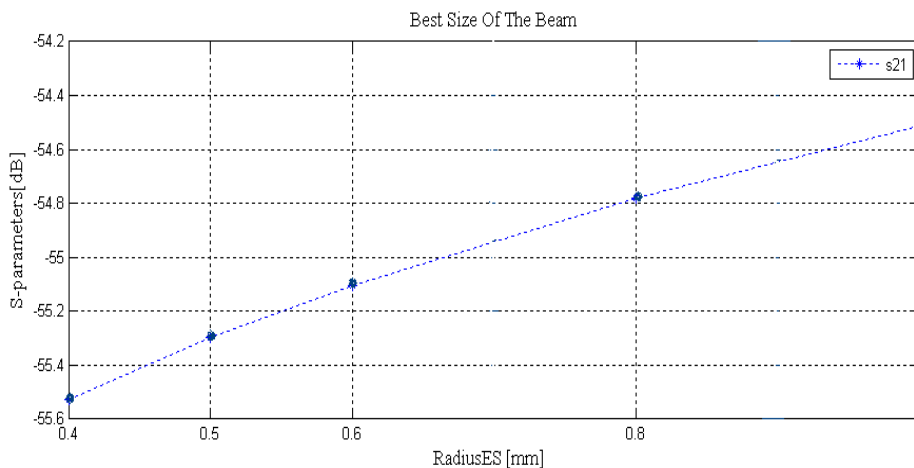


Figure D.7: S-parameters for different radiuses

Appendix E:

S-parameters tables with considering Renormalization

E.1 Variations of electrode outer and inner radius:

Table E.1: S-parameters for different inner and outer radius of electrode number 2, with PEC wire in the pipe center.

Size(mm)	S_{21} [dB]	S_{31} [dB]	S_{41} [dB]	S_{51} [dB]	$ S_{31} - S_{21} $ [dB]	$ S_{51} - S_{41} $ [dB]
Re:5.15,re:4.9	-55.6322	-54.5102	-54.5096	-54.5096	1.1226	0
Re:5.35,re:5.1	-55.1612	-54.5095	-54.5101	-54.5106	0.6511	0.0005
Re:5.55,re:5.3	-54.7127	-54.5097	-54.51	-54.5103	0.2027	0.0003
Re:5.65,re:5.4	-54.5103	-54.5098	-54.5099	-54.5102	0.0004	0.0004
Re:5.75,re:5.5	-54.3424	54.5101	-54.5099	-54.5104	0.1675	0.0003
Re:5.85,re:5.6	-54.3038	54.5107	-54.5101	-54.5101	0.2063	0.0006

Table E.2: S-parameters for different inner and outer radius of electrode number 2, without PEC wire in the pipe center

Size(mm)	S_{21} [dB]	S_{31} [dB]	S_{41} [dB]	$ S_{41} - S_{31} $ [dB]
Re:5.15,re:4.9	-83.9248	-90.5483	-82.8037	1.1211
Re:5.35,re:5.1	-83.4549	-90.5493	-82.8038	0.6511
Re:5.55,re:5.3	-83.0066	-90.5484	-82.8041	0.2025
Re:5.65,re:5.4	-82.8041	-90.5498	-82.8039	0.0002
Re:5.75,re:5.5	-82.6363	-90.5494	-82.8041	0.1678
Re:5.85,re:5.6	-82.5989	-90.5493	-82.8036	0.2047

E.2 Variations of electrode inner radius:

Table E.3: S-parameters for different inner radiuses of electrode number 2, with PEC wire in the pipe center

Size(mm)	S_{21} [dB]	S_{31} [dB]	S_{41} [dB]	S_{51} [dB]	$ S_{31} - S_{21} $ [dB]	$ S_{51} - S_{41} $ [dB]
Re:5.65,re:4.9	-54.8537	54.5096	-54.5102	-54.5098	0.3435	0.0002
Re: 5.65,re:5	-54.6748	-54.5094	-54.5097	-54.51	0.1651	0.0006
Re: 5.65,re:5.1	-54.531	-54.5104	-54.5099	-54.5099	0.0211	0.0005
Re: 5.65,re:5.3	-54.371	-54.5105	-54.5102	-54.5104	0.1392	0.0001
Re:5.65,re:5.4	-54.5103	-54.5098	-54.5099	-54.5102	0.0004	0.0004
Re: 5.65,re:5.5	-55.2874	-54.5103	-54.5097	-54.5103	0.7777	0
Re:5.65,re:5.55	-56.5387	-54.5106	-54.5096	-54.5102	2.0291	0.0004

Table E.4: S-parameters for different inner radiuses of electrode number 2, without PEC wire in the pipe center

Size(mm)	S_{21} [dB]	S_{31} [dB]	S_{41} [dB]	$ S_{41} - S_{31} $ [dB]
Re:5.65,re:4.9	-90.5482	-83.1436	-82.8033	0.3403
Re: 5.65,re:5	-90.5492	-82.9677	-82.8038	0.1639
Re: 5.65,re:5.1	-90.5494	-82.8251	-82.8038	0.0213
Re: 5.65,re:5.3	-90.5497	-82.6637	-82.8039	0.1402
Re:5.65,re:5.4	-90.5498	-82.8041	-82.8039	0.0002
Re: 5.65,re:5.5	-90.5491	-83.5824	-82.8041	0.7783
Re:5.65,re:5.55	-90.5474	-84.8325	-82.804	2.0285

E.3 Variations of electrode outer radius:

Table E.5: S-parameters for different outer radiuses of electrode number 2, with PEC wire in the pipe center

Size(mm)	S_{21} [dB]	S_{31} [dB]	S_{41} [dB]	S_{51} [dB]	$ S_{31} - S_{21} $ [dB]	$ S_{51} - S_{41} $ [dB]
Re:5.45, re:5.4	-60.2644	-54.5099	-54.51	-54.5103	5.7544	0.0004
Re: 5.5, re:5.4	-56.7218	-54.5104	-54.5098	-54.51	2.212	0.0004
Re:5.55, re:5.4	-55.4414	-54.5091	-54.5098	-54.5105	0.9316	0.0014
Re: 5.6, re:5.4	-54.8418	-54.51	-54.5099	-54.51	0.3319	0
Re:5.65, re:5.4	-54.5103	-54.5098	-54.5099	-54.5102	0.0004	0.0004
Re: 5.7, re:5.4	-54.3836	-54.5102	-54.51	-54.5108	0.1264	0.0006
Re:5.75, re:5.4	-54.1604	-54.5092	-54.5095	-54.5103	0.3491	0.0011

Table E.6: S-parameters for different outer radiuses of electrode number 2, without PEC wire in the pipe center

Size(mm)	S_{21} [dB]	S_{31} [dB]	S_{41} [dB]	$ S_{41} - S_{31} $ [dB]
Re:5.45, re:5.4	-90.5487	-88.5585	-82.8034	5.7551
Re: 5.5, re:5.4	-90.5488	-85.0157	-82.8039	2.2118
Re:5.55, re:5.4	-90.5492	-83.736	-82.8048	0.9312
Re: 5.6, re:5.4	-90.5492	-83.1365	-82.8035	0.333
Re:5.65, re:5.4	-90.5498	-82.8041	-82.8039	0.0002
Re: 5.7, re:5.4	-90.5488	-82.5975	-82.8035	0.206
Re:5.75, re:5.4	-90.5489	-82.4545	-82.8047	0.3502

E.5 Insertions of electrode inner cylinder inside the pipe:

Table E.7: S-parameters for different insertions of electrode number 2, with PEC wire in the pipe center

Size(mm)	S_{21} [dB]	S_{31} [dB]	S_{41} [dB]	S_{51} [dB]	$ S_{31} - S_{21} $ [dB]	$ S_{51} - S_{41} $ [dB]
In:0.9	-54.5103	-54.5098	-54.5099	-54.5102	0.0004	0.0004
In:1.1	-67.1171	-54.5101	-54.5096	-54.5106	12.6075	0.0004
In:1.3	-70.0607	-54.5109	-54.51	-54.5105	15.5507	0.0004
In:1.5	-71.5267	-54.5113	-54.5104	-54.512	17.0163	0.0007
In:1.7	-72.3894	-54.5122	-54.5107	-54.5126	17.8787	0.0004
In:1.9	-72.8983	-54.5119	-54.5103	-54.5128	18.388	0.0009

Table E.8: S-parameters for different insertions of electrode number 2, without PEC wire in the pipe center

Size(mm)	S_{21} [dB]	S_{31} [dB]	S_{41} [dB]	$ S_{41} - S_{31} $ [dB]
In:0.9	-90.5498	-82.8041	-82.8039	0.0002
In:1.1	-90.5504	-95.34	-82.8043	12.5357
In:1.3	-90.552	-98.3558	-82.8042	15.5516
In:1.5	-90.5546	-99.5546	-82.8051	16.7495
In:1.7	-90.5559	-100.6748	-82.8048	17.87
In:1.9	-90.5583	-101.1701	-82.8057	18.3644

E.6 Displacements of electrode inner cylinder, radially:

Table E.9: S-parameters for different radial displacements of electrode number 2, with PEC wire in the pipe center

Size(mm)	S_{21} [dB]	S_{31} [dB]	S_{41} [dB]	S_{51} [dB]	$ S_{31} - S_{21} $ [dB]	$ S_{51} - S_{41} $ [dB]
Disp :0.05	-54.539	-54.5101	-54.5098	-54.5103	0.0292	0.0002
Disp :0.1	-54.6314	-54.51	-54.51	-54.5101	0.1214	0.0001
Disp :0.15	-54.8502	-54.5098	-54.5101	-54.5106	0.3401	0.0008
Disp :0.2	-55.4839	-54.51	-54.5101	-54.5108	0.9738	0.0008

Table E.10: S-parameters for different radial displacements of electrode number 2, without PEC wire in the pipe center, clockwise

Size(mm)	S_{41} [dB]	S_{21} [dB]	S_{31} [dB]	$ S_{31} - S_{21} $ [dB]
Disp :0.05	-90.5491	-82.8499	-82.8048	0.0451
Disp :0.1	-90.5496	-82.962	-82.8035	0.1585
Disp :0.15	-90.549	-83.2019	-82.8036	0.3983
Disp :0.2	-90.5498	-83.8671	-82.8037	1.0634

Table E.11: S-parameters for different radial displacements of electrode number 2, without PEC wire in the pipe center, counter clockwise

Size(mm)	S_{21} [dB]	S_{31} [dB]	S_{41} [dB]	$ S_{31} - S_{21} $ [dB]
Disp :0.05	-82.8142	-82.8048	-90.5498	0.0094
Disp :0.1	-82.8894	-82.8044	-90.5487	0.085
Disp :0.15	-83.0859	-82.8025	-90.5485	0.2834
Disp :0.2	-83.6887	-82.8037	-90.5482	0.885

E.6 Displacements of electrode inner cylinder, longitudinally:

Table E.12: S-parameters for different longitudinal displacements of electrode number 2, with PEC wire in the pipe center

Displacement [mm]	S_{21} [dB]	S_{31} [dB]	S_{41} [dB]	S_{51} [dB]	$ S_{31} - S_{21} $ [dB]	$ S_{51} - S_{41} $ [dB]
0.05	-54.536	-54.51	-54.5097	-54.5098	0.026	0.0001
0.1	-54.6199	-54.5097	-54.5096	-54.5103	0.1102	0.0007
0.15	-54.8204	-54.51	-54.51	-54.5101	0.3104	0.0001
0.2	-55.3786	-54.5097	-54.5099	-54.5098	0.8689	0.0001

Table E.13: S-parameters for different longitudinal displacements of electrode number2, without PEC wire in the pipe center

Size(mm)	S_{21} [dB]	S_{31} [dB]	S_{51} [dB]	$ S_{21} - S_{31} $ [dB]
0.05	-82.8282	-82.8032	-90.5493	0.025
0.1	-82.9138	-82.8037	-90.5482	0.1101
0.15	-83.294	-82.8037	-90.5497	0.4903
0.2	-83.6724	-82.8032	-90.5488	0.8692

E.7 The inner pipe displacements along the vertical axis

Table E.14: S-parameters for different beam displacements on vertical axis by connecting to 50Ω

Displacement (mm)	S_{21} [dB]	S_{31} [dB]	S_{41} [dB]	S_{51} [dB]	$ S_{31} - S_{21} $ [dB]	$ S_{51} - S_{41} $ [dB]
0.25 mm	-54.3767	-54.6432	-54.5104	-54.5108	0.2665	0.0004
0.5 mm	-54.2439	-54.7762	-54.5138	-54.514	0.5323	0.0002
0.75 mm	-54.1089	-54.909	-54.5186	-54.5188	0.8001	0.0002
1 mm	-53.9756	-55.0421	-54.5251	-54.5254	1.0665	0.0003
1.25 mm	-53.8412	-55.1752	-54.5334	-54.5344	1.334	0.0001
1.5 mm	-53.707	-55.308	-54.5438	-54.5438	1.601	0
2 mm	-53.4387	-55.5738	-54.5704	-54.5701	2.1351	0.0003

Table E.15: Linear S-parameters for different displacements of the inner pipe on the vertical axis by using lumped port

Displacement	S_{21} [dB]	S_{31} [dB]	S_{41} [dB]	S_{51} [dB]	$ S_{31} - S_{21} $ [dB]	$ S_{51} - S_{41} $ [dB]
0.25 mm	-54.2223	-54.4886	-54.3566	-54.3562	3.3350e-5	8e-8
0.5 mm	-54.0884	-54.6223	-54.3585	-54.3601	6.6870e-5	2.4e-7
0.75 mm	-53.9553	-54.7558	-54.3645	-54.3640	1.0028e-4	7e-8
1.25 mm	-53.6874	-55.0206	-54.3792	-54.3792	1.6706e-4	0
1.5 mm	-53.5538	-55.1533	-54.3901	-54.3890	2.0054e-4	1.8e-7

Table E.16: Multipole moments for different displacements of the beam on the vertical axis, lumped port

Displacement (mm)	Dipole $ P_y $	Dipole $ P_z $	Quadrupole $ Q_{yy} $	Quadrupole $ Q_{zz} $	Quadrupole $ Q_{yz} $	Quadrupole $ (Q_{yy} - Q_{zz}) $
0.25 mm	8.43790951e-18	4.02261432e-14	8.0524482e-17	9.06537915e-17	2.11847496e-20	1.01293095e-17
0.5 mm	1.10200925e-17	8.05758358e-14	8.04989089e-17	1.20833147e-16	1.08163669e-20	4.03342383e-17
0.75 mm	1.44365374e-18	1.20903915e-13	8.05201027e-17	1.71287776e-16	4.05360632e-21	9.07676733e-17
1.25 mm	8.23304341e-17	2.01691152e-13	8.06202411e-17	3.32935805e-16	1.40479144e-19	2.52315564e-16
1.5 mm	2.41734619e-18	2.41901101e-13	8.05484896e-17	4.4375105e-16	1.08841657e-20	3.6320256e-16

Table E.17: Multipole moments for different displacements on vertical axis, extra electrode

Displacement (mm)	Dipole $ P_y $	Dipole $ P_z $	Quadrupole $ Q_{yy} $	Quadrupole $ Q_{zz} $	Quadrupole $ Q_{yz} $	Quadrupole $ (Q_{yy} - Q_{zz}) $
0.25 mm	1.1892e-17	4.0305e-14	8.054e-17	9.0628e-17	7.211e-21	1.0088e-17
0.5 mm	1.0783e-17	8.0597e-14	8.052e-17	1.2086e-16	1.0666e-20	4.0344e-17
0.75 mm	5.865e-19	1.2108e-13	8.059e-17	1.7155e-16	1.198e-20	9.0956e-17
1 mm	3.2996e-17	1.6134e-13	8.0567e-17	2.421e-16	6.281e-20	1.6154e-16
1.25 mm	6.865e-17	2.0163e-13	8.0616e-17	3.3278e-16	4.4348e-20	2.5216e-16
1.5 mm	7.2171e-17	2.4217e-13	8.0627e-17	4.4432e-16	1.4909e-19	3.6369e-16
2 mm	5.0383e-18	3.2271e-13	8.0599e-17	7.2659e-16	1.1208e-20	6.4599e-16

E.8 The inner pipe displacements along a line between the horizontal and vertical axes

Table E.18: linear S-parameters for different displacements of the inner pipe, lumped port

Displacement (mm)	S_{21} [dB]	S_{31} [dB]	S_{41} [dB]	S_{51} [dB]	$ S_{31} - S_{21} $ [dB]	$ S_{51} - S_{41} $ [dB]
0.25 mm	-54.2233	-54.4897	-54.2233	-54.4893	3.339e-5	3.326e-5
0.5 mm	-54.0884	-54.6223	-54.3585	-54.3601	6.68e-5	6.683e-5
0.75 mm	-53.9637	-54.7633	-53.9636	-54.7640	1.0004e-4	1.0016e-4
1.25 mm	-53.7122	-55.0443	-53.7118	-55.0435	1.6651e-4	1.6643e-4
1.5 mm	-53.5883	-55.1856	-53.5888	-55.1862	1.9952e-4	1.9947e-4

Table E.19: S-parameters for different beam displacements along a line between the horizontal and vertical axes

Displacement (mm)	S_{21} [dB]	S_{31} [dB]	S_{41} [dB]	S_{51} [dB]	$ S_{31} - S_{21} $ [dB]	$ S_{51} - S_{41} $ [dB]
0.25	-54.3779	-54.644	-54.3773	-54.6449	0.2661	0.2676
0.5	-54.2473	-54.78	-54.2473	-54.7809	0.5327	0.5336
0.75	-54.1183	-54.9172	-54.1181	-54.9177	0.7989	0.7996
1	-53.9908	-55.057	-53.9911	-55.0569	1.0662	1.0658
1.25	-53.8656	-55.1982	-53.8654	-55.1982	1.3326	1.3328
1.5	-53.7433	-55.3397	-53.743	-55.3408	1.5964	1.5978
2	-53.503	-55.6312	-53.5012	-55.6311	2.1282	2.1299

Table E.20: Multipole moments for different displacements along a line between the horizontal and vertical axes

Displacement (mm)	Dipole $ P_y $	Dipole $ P_z $	Quadrupole $ Q_{yy} $	Quadrupole $ Q_{zz} $	Quadrupole $ Q_{yz} $	Quadrupole $ (Q_{yy} - Q_{zz}) $
0.25	4.036e-14	4.0409e-14	9.0698e-17	9.071e-17	1.6149e-10	1.2482e-20
0.5	8.0625e-14	8.0618e-14	1.2089e-16	1.2089e-16	4.0347e-17	3.4853e-22
0.75	1.2096e-13	1.2096e-13	1.7136e-16	1.7138e-16	9.0829e-17	2.2593e-20
1	1.6128e-13	1.6129e-13	2.4199e-16	2.4201e-16	1.6144e-16	2.1822e-20
1.25	2.0162e-13	2.0164e-13	3.3282e-16	3.3286e-16	2.5227e-16	3.985e-20
1.5	2.4202e-13	2.4204e-13	4.4397e-16	4.4402e-16	3.6339e-16	5.0141e-20
2	3.2313e-13	3.2307e-13	7.2769e-16	7.274e-16	6.4684e-16	2.885e-19

Table E.21: Multipole moments for different displacements of the beam along a line between the horizontal and vertical axes

Displacements (mm)	Dipole $ P_y $	Dipole $ P_z $	Quadrupole $ Q_{yy} $	Quadrupole $ Q_{zz} $	Quadrupole $ Q_{yz} $	Quadrupole $ (Q_{yy} - Q_{zz}) $
0.25 mm	4.02578428e-14	4.03041072e-14	9.05538458e-17	9.05829891e-17	1.00912167e-17	2.91433035e-20
0.5 mm	8.0603e-14	8.0595e-14	1.2086e-16	1.2085e-16	4.0335e-17	3.584e-21
0.75 mm	1.20868715e-13	1.20920829e-13	1.71256316e-16	1.7127977e-16	9.07254545e-17	2.34537107e-20
1.25 mm	2.01566044e-13	2.01582579e-13	3.327327e-16	3.32773674e-16	2.52203406e-16	4.09744462e-20
1.5 mm	2.42031116e-13	2.42064072e-13	4.43899363e-16	4.43971932e-16	3.63354456e-16	7.25688253e-20

E.9 Elliptic beam

Table E.22: S-parameters for Elliptic beam with semimajor axis a and semiminor axis b, lumped port

Elliptic Inner (mm)	S_{21} [dB]	S_{31} [dB]	S_{41} [dB]	S_{51} [dB]	$ S_{31} - S_{21} $ [dB]	$ S_{51} - S_{41} $ [dB]	$(S_{51} + S_{41}) - (S_{31} + S_{21})$
a:1 , b:1	-54.3563	-54.3566	-54.3559	-54.3560	3e-4	1e-4	0.0010
a:1.1 , b:0.9	-54.3596	-54.3600	-54.3528	-54.3527	4e-4	1e-4	0.0141
a:1.25 , b:0.74	-54.3707	-54.3705	-54.3544	-54.3544	2e-4	0	0.0324
a:1.4 , b:0.6	-54.3692	-54.3702	-54.3427	-54.3439	1e-3	0.0012	0.0528
a:1.7 , b:0.31	-54.3772	-54.3763	-54.3315	-54.3324	9e-4	9 e-4	0.0896
a:1.85 , b:0.16	-54.3808	-54.3810	-54.3255	-54.3253	2 e-4	2 e-4	0.1110

Table E.23: S-parameters for Elliptic beam with semimajor axis a and semiminor axis b by connecting to 50Ω .

Elliptic Inner (mm)	S_{21} [dB]	S_{31} [dB]	S_{41} [dB]	S_{51} [dB]
a:1 , b:1	-54.2809531	-54.281532	-54.2744757	-54.2769517
a:1.1 , b:0.9	-54.2809531	-54.28153198	-54.27447573	-54.27695166
a:1.25 , b:0.74	-54.2861672	-54.286233	-54.2690327	-54.2713441
a:1.4 , b:0.6	-54.29060685	-54.29150566	-54.26566514	-54.26707986
a:1.7 , b:0.31	-54.29774362	-54.29725255	-54.25179299	-54.25480179
a:1.85 , b:0.16	-54.29976297	-54.30030973	-54.24425589	-54.24742219

Table E.24: Multipole moments for different displacements elliptic beam, 300MHz, Lumped port

Beam radiuses (mm)	Dipole $ P_y $	Dipole $ P_z $	Quadrupole $ Q_{zz} $	Quadrupole $ Q_{yy} $	Quadrupole $ Q_{yz} $	Quadrupole $ (Q_{yy} - Q_{zz}) $
a:1, b:1	2.1422e-18	4.9772e-18	8.0483e-17	8.0502e-17	3.1877e-21	1.900e-20
a:1.1, b:0.9	1.1036e-16	9.9752e-17	6.5309e-17	9.6577e-17	1.2053e-19	3.1268e-17
a:1.25 ,b:0.74	2.0592e-16	4.2366e-17	4.4365e-17	1.2187e-16	1.9523e-19	7.7505e-17
a:1.4, b:0.6	1.4654e-15	1.51808e-16	2.9725e-17	1.5193e-16	4.9711e-19	1.2221e-16
a:1.7, b:0.31	1.2346e-15	1.6392e-16	7.9789e-18	1.9248e-16	1.4560e-19	1.8450e-16
a:1.85, b:0.16	4.8904e-15	5.5057e-17	2.1062e-18	2.1212e-16	1.0867e-19	2.1001e-16

Table E.25: Multipole moments for different displacements elliptic beam, 300MHz, extra piece

Beam radiuses (mm)	Dipole $ P_y $	Dipole $ P_z $	Quadrupole $ Q_{zz} $	Quadrupole $ Q_{yy} $	Quadrupole $ Q_{yz} $	Quadrupole $ (Q_{yy} - Q_{zz}) $
a:1, b:1	1.6868057e-18	2.7115835e-16	6.5467274e-17	9.6655839e-17	9.7350827e-20	3.11885652e-17
a:1.1, b:0.9	1.6868124e-18	2.7115832e-16	6.5467274e-17	9.6655839e-17	9.7350821e-20	3.1188565e-17
a:1.25 ,b:0.74	5.7701895e-17	6.1073583e-17	4.4366087e-17	1.2212182e-16	2.685213e-19	7.7755732e-17
a:1.4, b:0.6	1.1289179e-15	5.8366331e-17	2.963541e-17	1.5236828e-16	1.9627668e-19	1.2273287e-16
a:1.7, b:0.31	1.9972403e-15	1.9164894e-16	7.9711297e-18	1.9270815e-16	2.3524867e-19	1.8473702e-16
a:1.85, b:0.16	3.4667325e-15	1.2853316e-16	2.1034056e-18	2.1762516e-16	7.5635644e-18	2.1552176e-16

Appendix F

Simulations without renormalization:

F.1. Variations of electrodes radius

F.1.1 Variations of electrode outer and inner radius

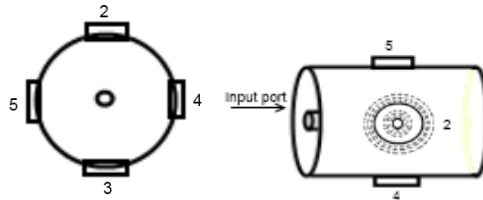


Figure F.1: Variation of both inner and outer radius of electrode number 2 with pipe as input port

Table F.1: S-parameters for different inner and outer radius of electrode number 2 (see Figure F.1).

Size(mm)	S21	S31	S41	S51	S31 – S21	S51 – S41
Re:5.15 , re:4.9	-67.2037	-66.301	-66.3007	-66.3008	0.9027	0.0001
Re:5.35 ,re:5.1	-66.8348	-66.3008	-66.3006	-66.3008	0.5340	0.0002
Re:5.55 ,re:5.3	-66.4772	-66.3006	-66.3001	-66.3012	0.1766	0.0011
Re:5.65 ,re:5.4	-66.3007	-66.301	-66.3008	-66.3009	0.0003	0.0001
Re:5.75 ,re:5.5	-66.1299	-66.301	-66.3014	-66.3004	0.1711	0.0010
Re:5.85 ,re:5.6	-65.9624	-66.3005	-66.301	-66.301	0.3381	0
Re:5.95 ,re:5.7	-65.7972	-66.3006	-66.3007	-66.3007	0.5034	0

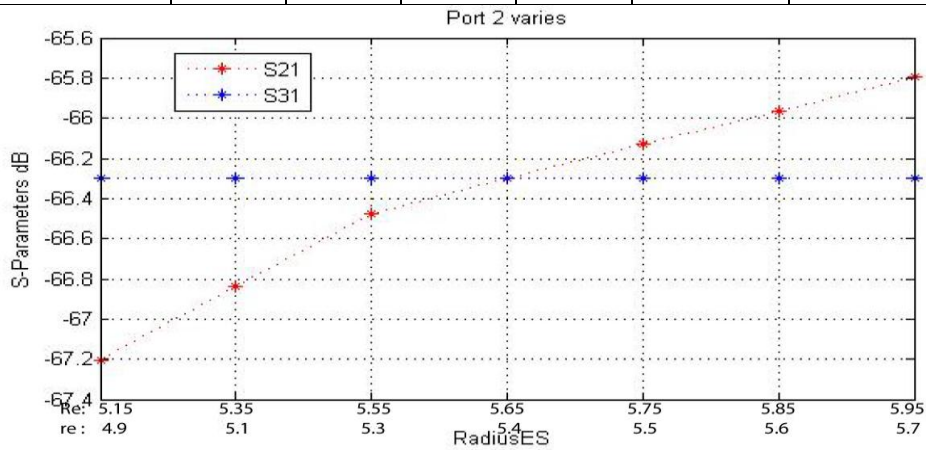


Figure F.2: S-parameters for different inner and outer radius of electrode number 2 (see Figure F.1).

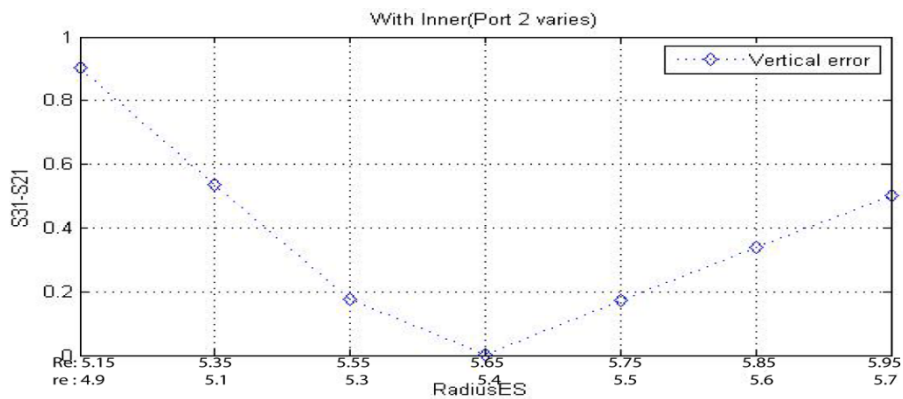


Figure F.3: Horizontal errors for different inner and outer radius of electrode number 2 (see Figure F.1)

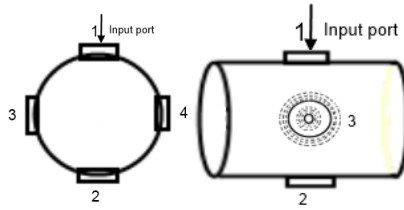


Figure F.4: Variation of both inner and outer radius of the electrode number 3 with electrode as input port

Table F.2: S-parameters for different inner and outer radius of electrode number 3 (see Figure F.4)

Size(mm)	S21	S31	S41	S41-S31(H)
Re:5.15 , re:4.9	-114.1319	-107.2873	-106.3857	0,9016
Re:5.35 , re:5.1	-114.1291	-106.9195	-106.386	0,5335
Re:5.55 , re:5.3	-114.1319	-106.5608	-106.3858	0,175
Re:5.65 , re:5.4	-114.1313	-106.3843	-106.3849	0.0006
Re:5.75 , re:5.5	-114.1328	-106.2163	-106.3851	0,1688
Re:5.85 , re:5.6	-114.1321	-106.0469	-106.3848	0,3379
Re:5.95 , re:5.7	-114.133	-105.8835	-106.3846	0,5011

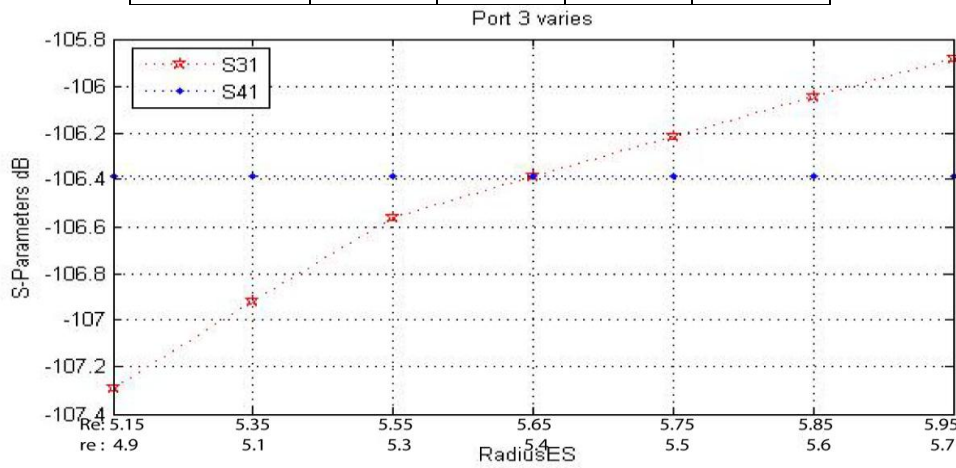


Figure F.5: S-parameters for different inner and outer radius of electrode number 3 (see Figure F.4)

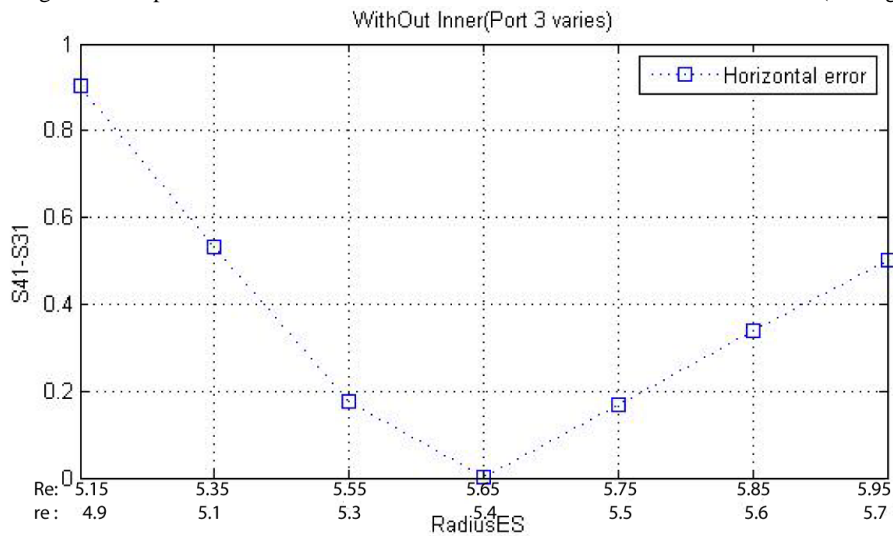


Figure F.6: The horizontal errors for different inner and outer radius of electrode number 3 (see Figure F.4)

F.1.2 Variations of electrode inner radius

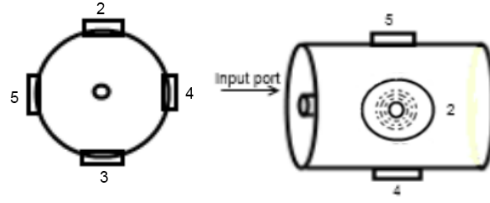


Figure F.7: Variation of inner radius of electrode number 2 with pipe as input port

Table F.3: S-parameters for different inner radius of electrode number 2 (see Figure F.7)

Size(mm)	S21	S31	S41	S51	S31-S21	S51-S41
Re:5.65 , re:4.9	-62.3908	-66.301	-66.3003	-66.3012	3.9102	0.0009
Re: 5.65 , re:5	-62.8393	-66.301	-66.3001	-66.3001	3.4617	0
Re: 5.65 ,re:5.1	-63.4051	-66.3005	-66.3009	-66.3005	2.8954	0.0004
Re: 5.65, re:5.3	-65.0186	-66.301	-66.3012	-66.3011	1.2824	0,0001
Re:5.65 , re:5.4	-66.3007	-66.301	-66.3008	-66.3009	0.0003	0.0001
Re: 5.65, re:5.5	-68.3373	-66.3014	-66.3009	-66.3012	2.0359	0.0003
Re:5.65,re:5.55	-70.006	-66.3015	-66.3004	-66.3002	3.7045	0.0002

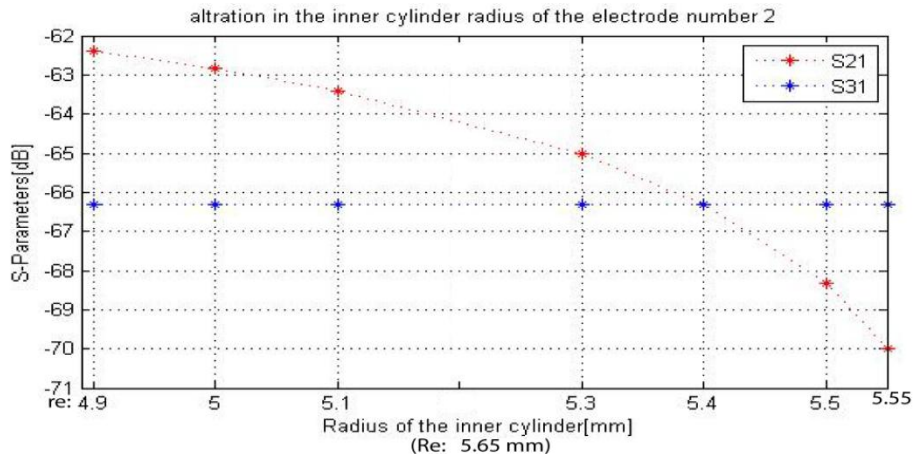


Figure F.8: S-parameters for different inner radius of electrode number 2 (see Figure F.7)

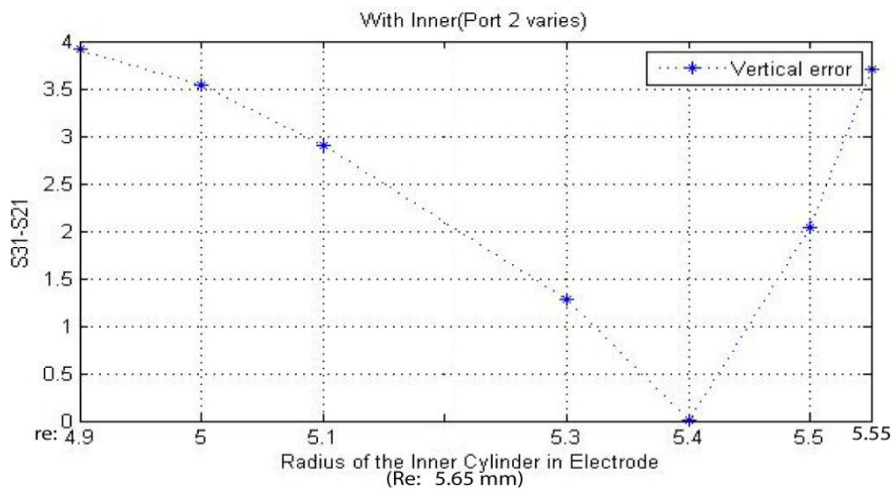


Figure F.9: The horizontal errors for different inner and outer radius of electrode number 2 (see Figure F.7)

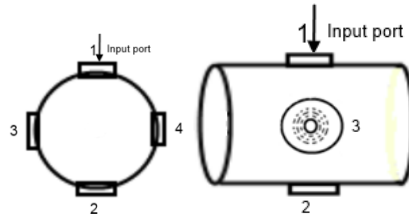


Figure F.10: Variation of inner radius of electrode number 3 with electrode as input port

Table F.4: S-parameters for different inner radius of electrode number 3 (see Figure F.10)

Size(mm)	S21	S31	S41	S41-S31	S21-S31	S21-S41
Re:5.65 ,re:4.9	-114.1312	-102.4608	-106.3853	3.9245	11,6704	7,7459
Re: 5.65 ,re:5	-114.1324	-102.9231	-106.386	3,4629	11,2093	7,7464
Re: 5.65 ,re:5.1	-114.1296	-103.486	-106.3861	2,9001	10,6436	7,7435
Re: 5.65, re:5.3	-114.1289	-105.1028	-106.3859	1,2831	9,0261	7,743
Re: 5.65,re:5.4	-114.1313	-106.3843	-106.3849	0,0006	7.7470	7.7464
Re: 5.65,re:5.5	-114.1319	-108.4225	-106.3842	2,0383	5,7094	7,7477
Re: 5.65 ,re:5.55	-114.1311	-110.0894	-106.3842	3,7052	4,0417	7,7469

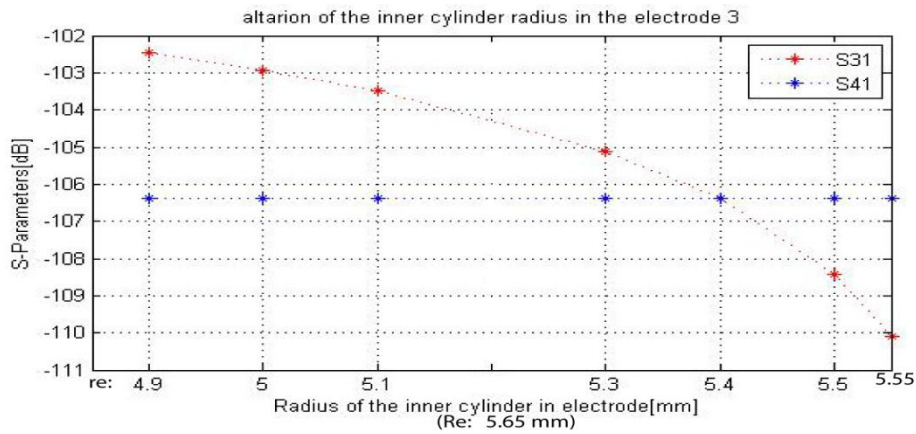


Figure F.11: S-parameters for different inner radius of electrode number 3 (see Figure F.10)

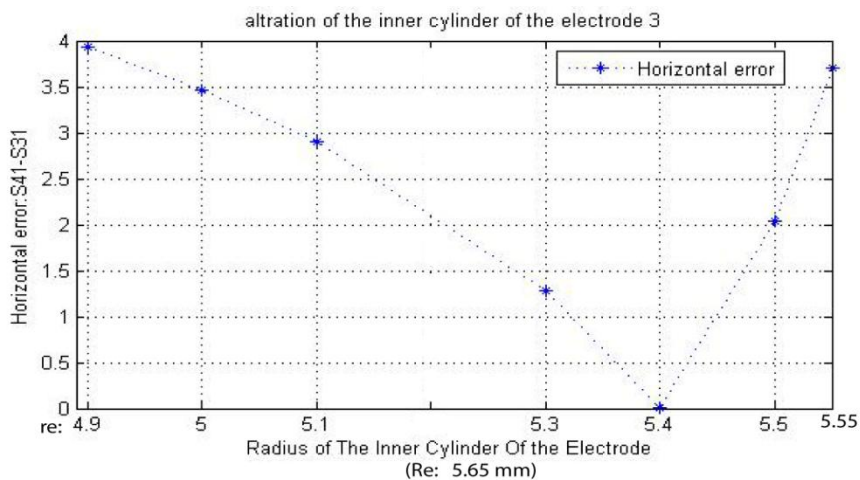


Figure F.12: Horizontal Error for different inner radiuses of electrode number 3 (see Figure F.10)

F.1.3 Variations of electrode outer radius

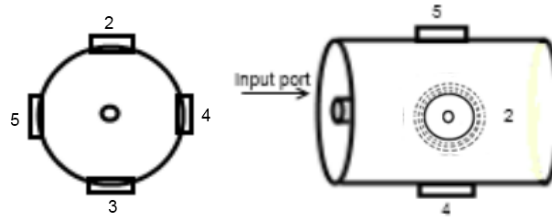


Figure F.13: Variation of outer radius of electrode number 2 with pipe as input port

Table F.5: S-parameters for different outer radiuses of electrode number 2 (see Figure F.13)

Size(mm)	S21	S31	S41	S51	S31-S21	S51-S41
Re:5.45,re:5.4	-73.2547	-66.3008	-66.3009	-66.3015	6.9539	0.0006
Re: 5.5,re:5.4	-70.258	-66.3006	-66.3005	-66.301	3.9574	0.0005
Re: 5.55,re:5.4	-68.5075	-66.3011	-66.3012	-66.3012	2.2064	0
Re: 5.6,re:5.4	-67.2656	-66.3005	-66.3008	-66.3014	0.9651	0.0006
Re: 5.65,re:5.4	-66.3007	-66.301	-66.3008	-66.3009	0.0003	0.0001
Re: 5.7,re:5.4	-65.5137	-66.3011	-66.3007	-66.3004	0.7874	0.0003
Re: 5.75,re:5.4	-64.844	-66.3011	-66.3012	-66.3008	1.4571	0.0004

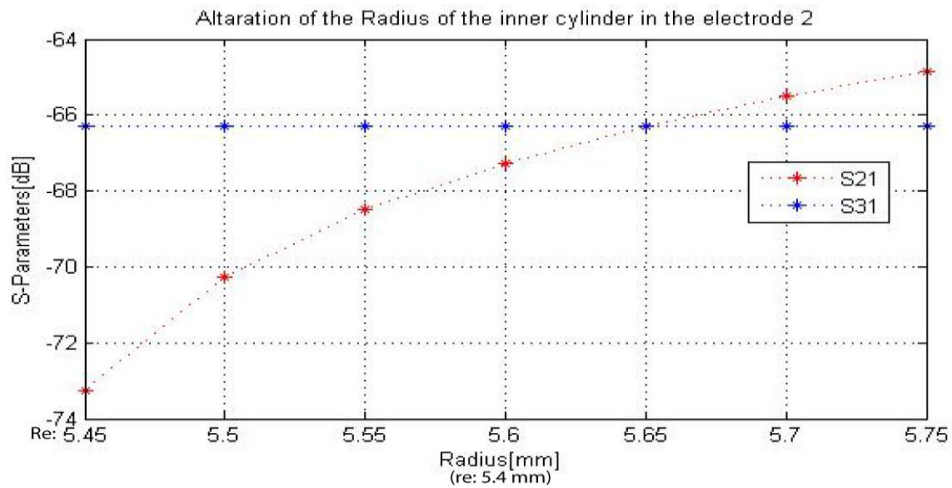


Figure F.14: S-parameters for different outer radiuses of electrode number 2 (see Figure F.13)

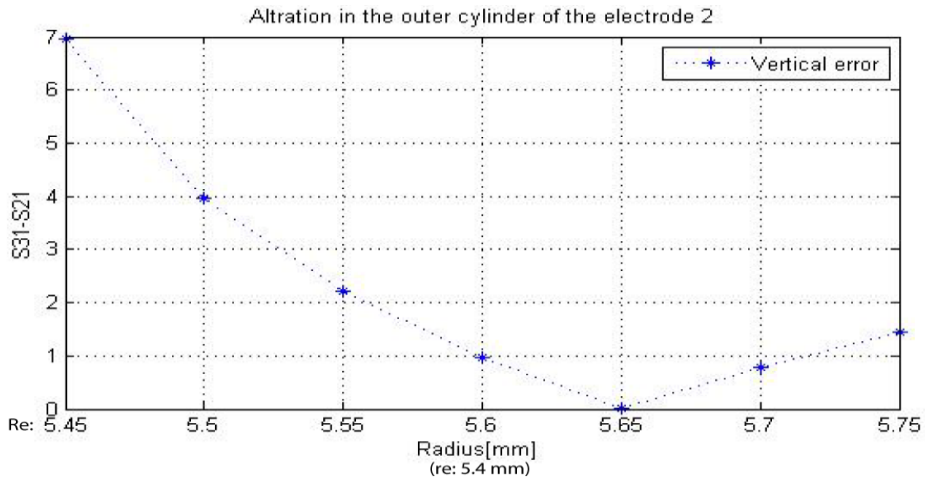


Figure F.15: Horizontal errors for different outer radiuses of electrode number 2 (see Figure F.13)

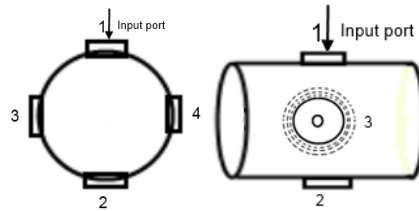


Figure F.16: Variation of outer radius of electrode number 3 with electrode is input port

Table F.6: S-parameters for different outer radius of electrode number 3 (see Figure F.16)

Size(mm)	S21	S31	S41	S41-S31(H)	S21-S31	S21-S41
Re:5.45, re:5.4	-114.0873	-112.5532	-106.3648	6,1884	1,5341	7,7225
Re: 5.5, re:5.4	-114.1315	-110.3425	-106.3855	3,957	3,789	7,746
Re:5.55, Re: 5.4	-114.1319	-108.5927	-106.3856	2.2071	5.5392	7.7463
Re: 5.6, re:5.4	-114.1315	-106.3842	-106.3842	0	7,7473	7,7473
Re: 5.65, re:5.4	-114.1299	-106.3855	-106.3857	0,0002	7,7444	7,7442
Re: 5.7, re:5.4	-114.1297	-105.5983	-106.3849	0,7866	8,5314	7,7448
Re: 5.75, re:5.4	-114.1293	-104.9301	-106.3858	1,4557	9,1992	7,7435

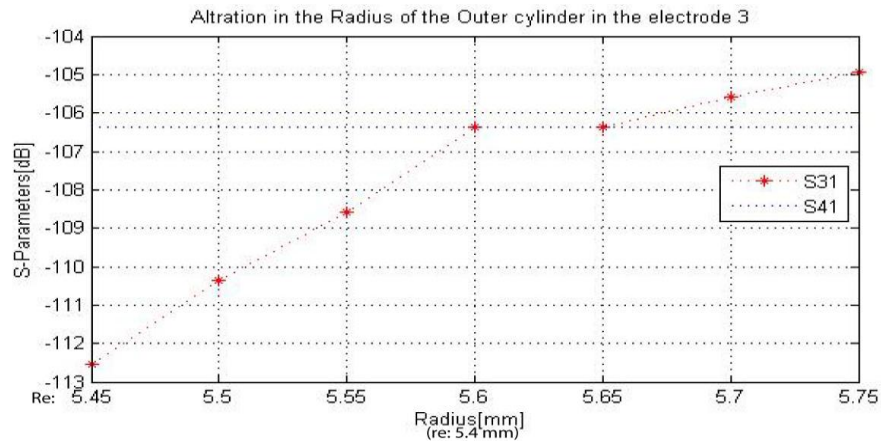


Figure F.17: S-parameters for different outer radius of electrode number 3 (see Figure F.16)

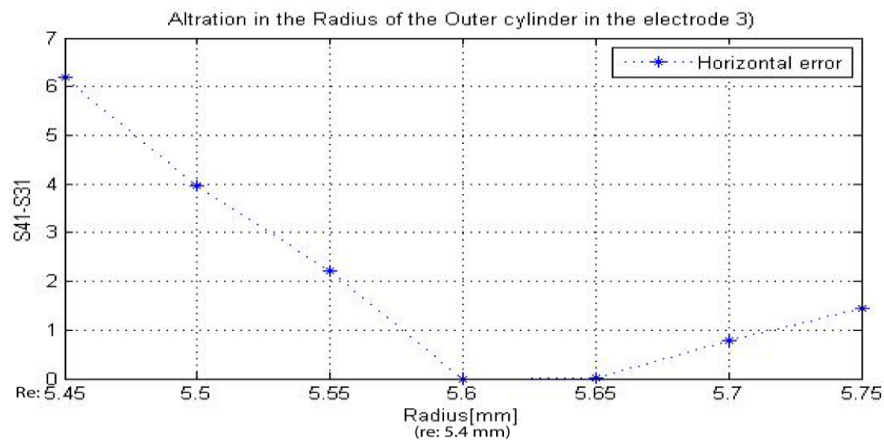


Figure F.18: Horizontal errors for different outer radiuses of electrode number 3 (see Figure F.16)

F.2 Insertion of the inner electrode inside the pipe

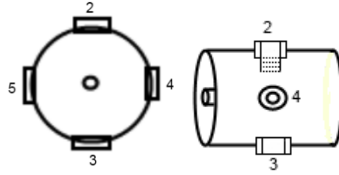


Figure F.19: Insertion of the inner cylinder of electrode 2 inside the pipe, pipe as input port.

Table F.7: S-parameters for different insertions of electrode number 2 (see Figure F.19).

Size(mm)	S21	S31	S41	S51	S31-S21	S51-S41
In:0.9	-66.3007	-66.301	-66.3008	-66.3009	0.0003	0.0001
In:1.1	-65.6176	-66.3009	-66.3013	-66.3019	0.6833	0.0006
In:1.3	-64.9737	-66.3018	-66.302	-66.3019	1.3281	0.0001
In:1.5	-64.3735	-66.3016	-66.303	-66.3028	1.9281	0.0002
In:1.7	-63.8119	-66.3016	-66.3034	-66.304	2.4897	0.0006
In:1.9	-63.278	-66.3017	-66.3052	-66.3056	3.0237	0.0004

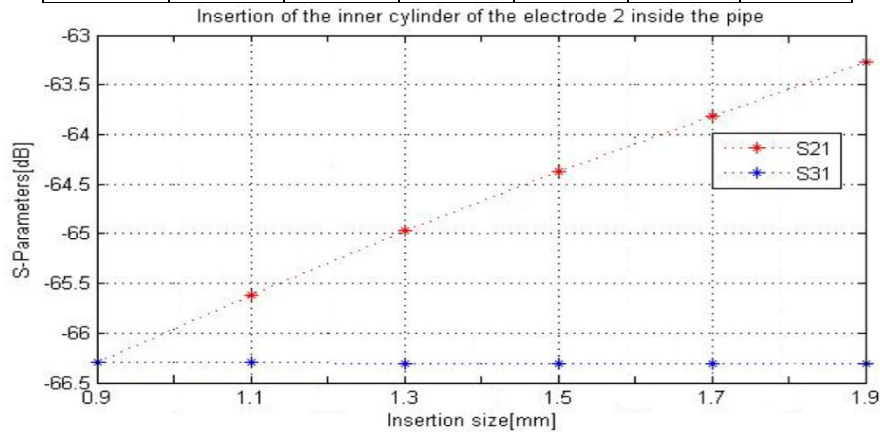


Figure F.20: S-parameters for different insertions of electrode number 2 (see Figure F.19).

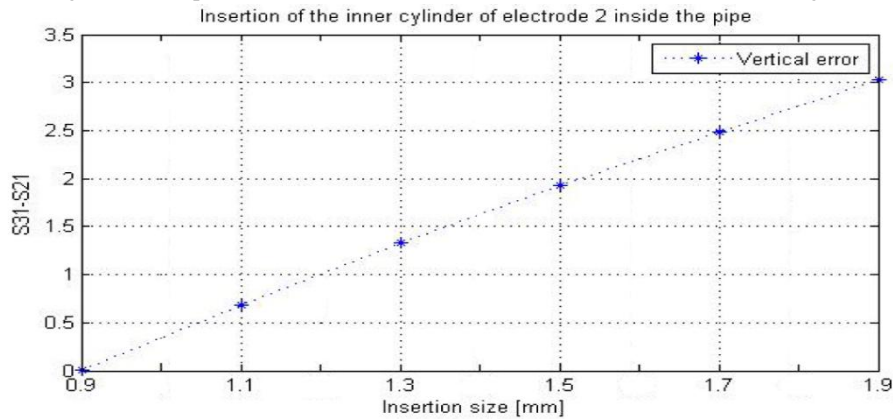


Figure F.21: Horizontal errors for different insertions of electrode number 2 (see Figure F.19).

F.3 Inner electrode displacements

F.3.1 Radially displacements

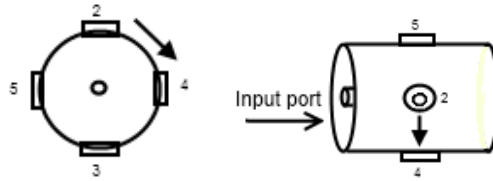


Figure F.22: Radial displacements of the inner cylinder of electrode number 2 toward port 4

Table F.8: S-parameters for different radial displacements of electrode number 2 (see Figure F.22).

Displacement [mm]	S21	S31	S41	S51	S31-S21	S51-S41
0.05	-66.3901	-66.301	-66.3009	-66.3017	0.0891	0.0008
0.1	-66.6796	-66.3013	-66.301	-66.3015	0.3783	0.0005
0.15	-67.268	-66.3008	-66.3008	-66.3016	0.9672	0.0008
0.2	-68.5138	-66.3005	-66.3008	-66.3014	2.2133	0.0006

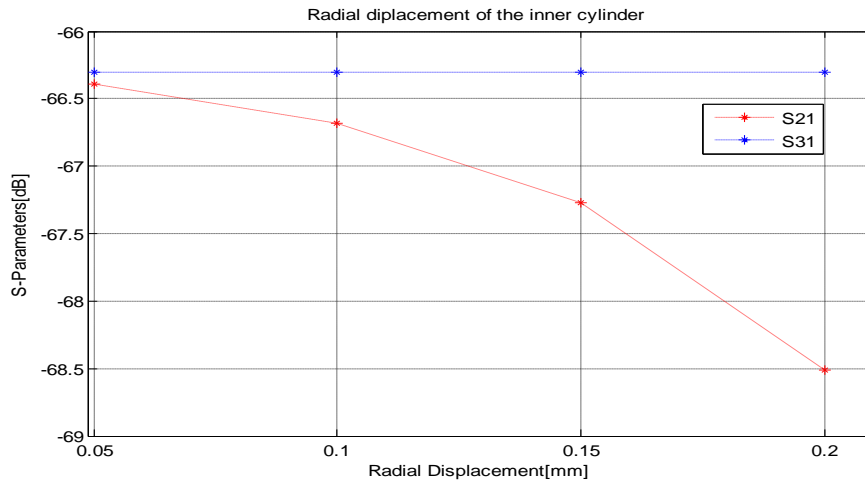


Figure F.23: S-parameters for different radial displacements of electrode number 2 (see Figure F.22).

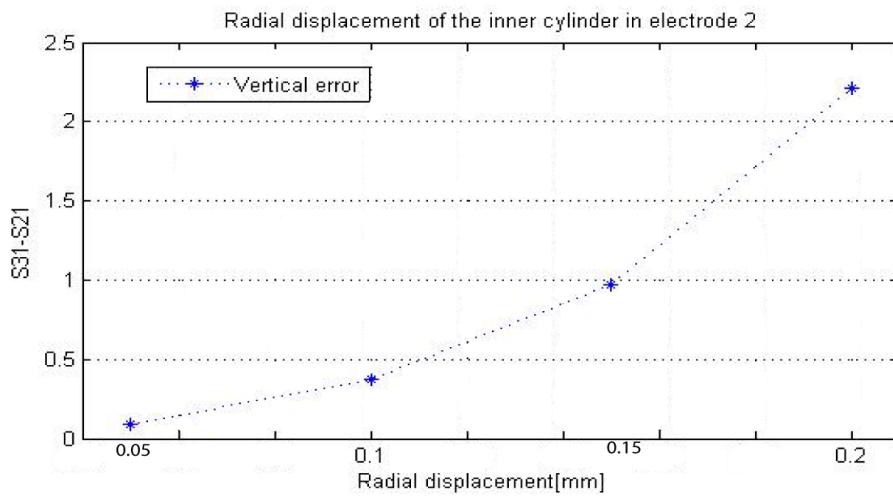


Figure F.24: Horizontal errors for different radial displacements of electrode number 2 (see Figure F.22).

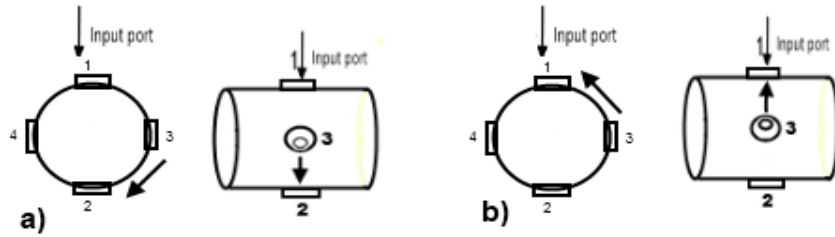


Figure F.25: Radial displacements of the inner cylinder of electrode number 3: a) Clockwise and b) counter Clockwise

Table F.9: S-parameters for different radial displacements of electrode number 3, clockwise (see Figure F.25a).

Displacement [mm]	S21	S31	S41	S41-S31	S21-S31	S21-S41
0.05	-114.1312	-106.4848	-106.3853	0.0995	7.6464	7.7459
0.1	-114.1317	-106.7847	-106.3863	0.3984	7.347	7.7454
0.15	-114.1315	-107.3916	-106.385	1.0066	6.7399	7.7459
0.2	-114.1327	-108.6504	-106.3849	2.2655	5.4823	7.7478

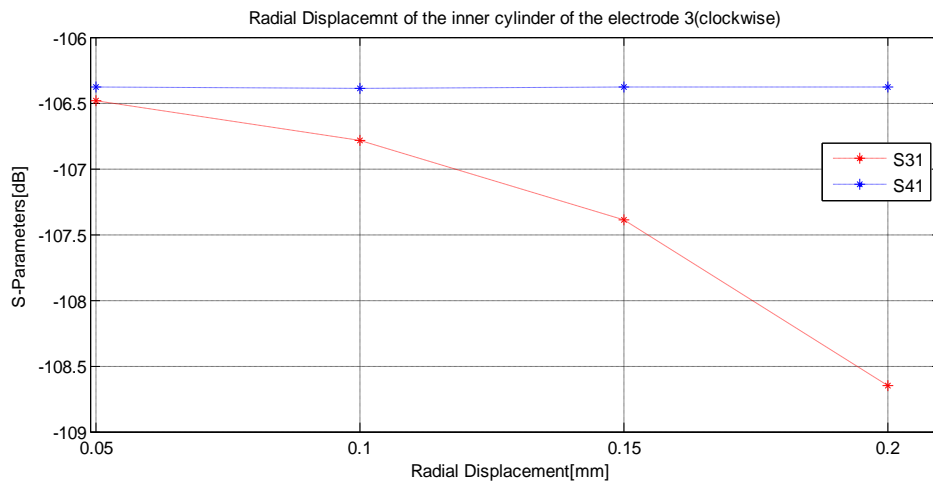


Figure F.26: S-parameters for different radial displacements of electrode number 3, clockwise (see Figure F.25a).

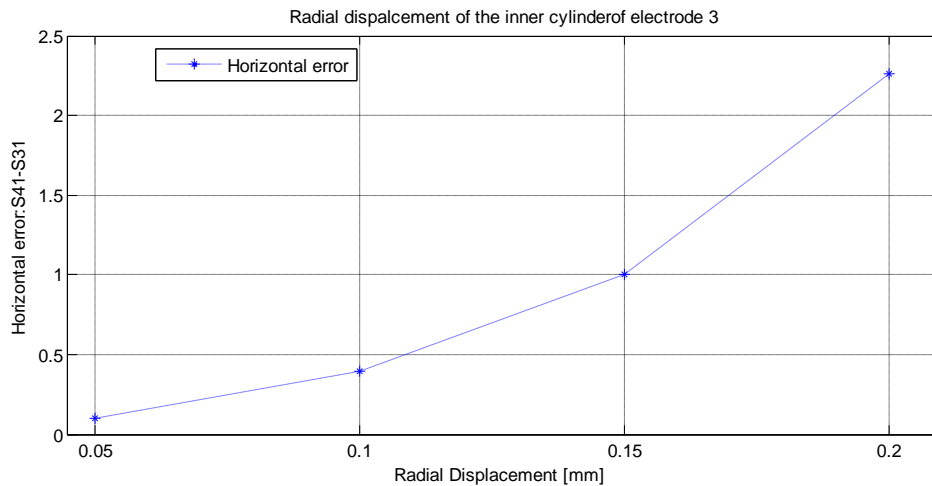


Figure F.27: Horizontal errors for different radial displacements of electrode number 3, clockwise (see Figure F.25a).

Table F.10: S-parameters for different radial displacements of electrode number 3, counter clockwise (see Figure F.25a).

Displacement [mm]	S21	S31	S41	S41-S31	S21-S31	S21-S41
0.05	-114.1323	-106.4627	-106.3842	0.0785	7.6696	7.7481
0.1	-114.1318	-106.7393	-106.3845	0.3548	7.3925	7.7473
0.15	-114.1326	-107.3157	-106.3856	0.9301	6.8169	7.747
0.2	-114.1325	-108.5479	-106.3842	2.1637	5.5846	7.7483

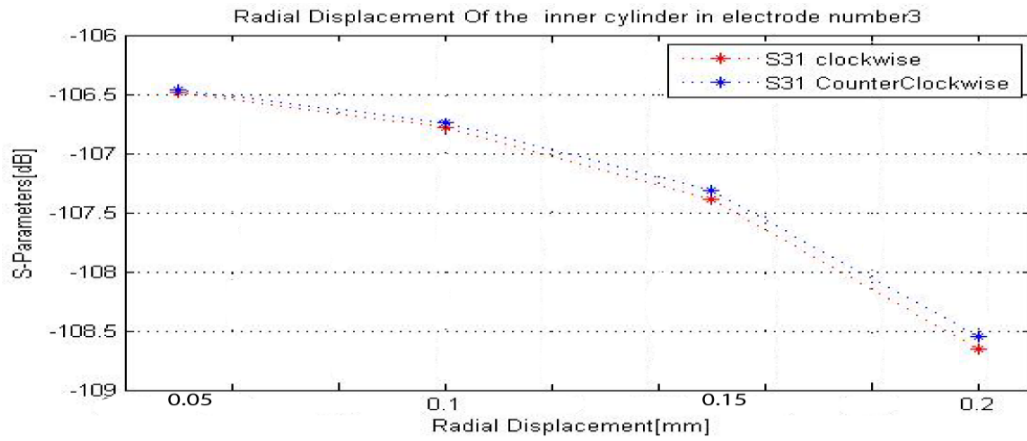


Figure F.28: Comparison between clock wise and counter clockwise radial displacements of electrode number 3 (see Figure 5.26).

F.3.2 Longitudinally displacements

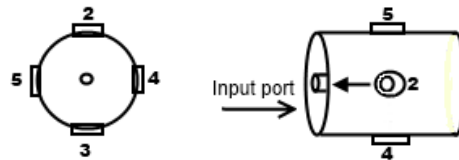


Figure F.29: Longitudinal displacements of the inner cylinder of electrode number 2 toward input port, for the case with pipe as input port

Table F.11: S-parameters for different longitudinal displacements of electrode number 2 (see Figure F.29).

Displacement [mm]	S21	S31	S41	S51	S31-S21	S51-S41
0.05	-66.3907	-66.2999	-66.3006	-66.3011	0.0908	0.0005
0.1	-66.6791	-66.3012	-66.3014	-66.3012	0.3779	0.0002
0.15	-67.2682	-66.3014	-66.3013	-66.3008	0.9668	0.0005
0.2	-68.5133	-66.3015	-66.3012	-66.3013	2.2118	0.0001

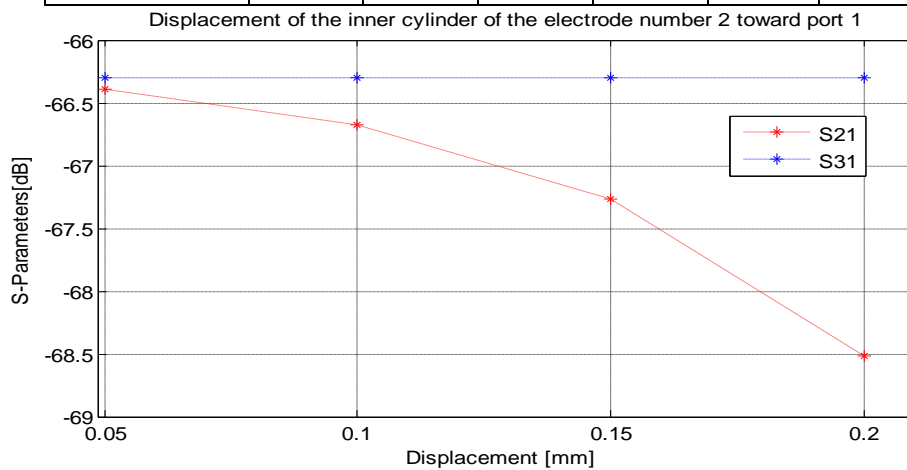


Figure F.30: S-parameters for different longitudinal displacements of electrode number 2 (see Figure F.29).

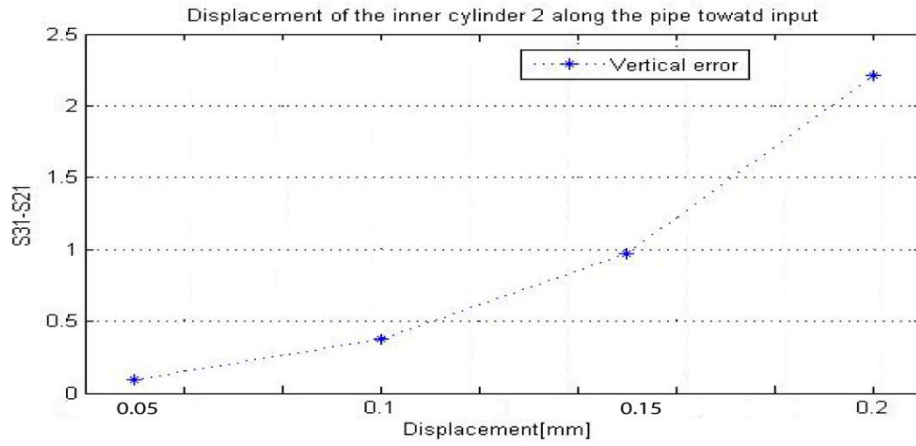


Figure F.31: Horizontal errors for different longitudinal displacements of electrode number 2 (see Figure F.29).

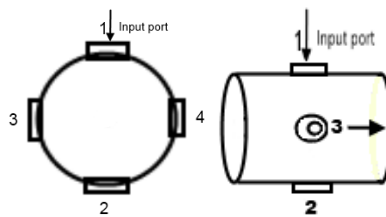


Figure F.32: Longitudinal displacements of the inner cylinder of electrode number 3 for the case electrode as input port
 Table F.12: S-parameters for different longitudinal displacements of electrode number 3 (see Figure F.32).

Displacement [mm]	S21	S31	S41	S41-S31	S21-S31	S21-S41
0.05	-114.1317	-106.4753	-106.384	0.0913	7.6564	7.7477
0.1	-114.1319	-106.7638	-106.3843	0.3795	7.3681	7.7476
0.15	-114.1324	-107.3525	-106.3837	0.9688	6.7799	7.7487
0.2	-114.1315	-108.5965	-106.3845	2.212	5.535	7.747

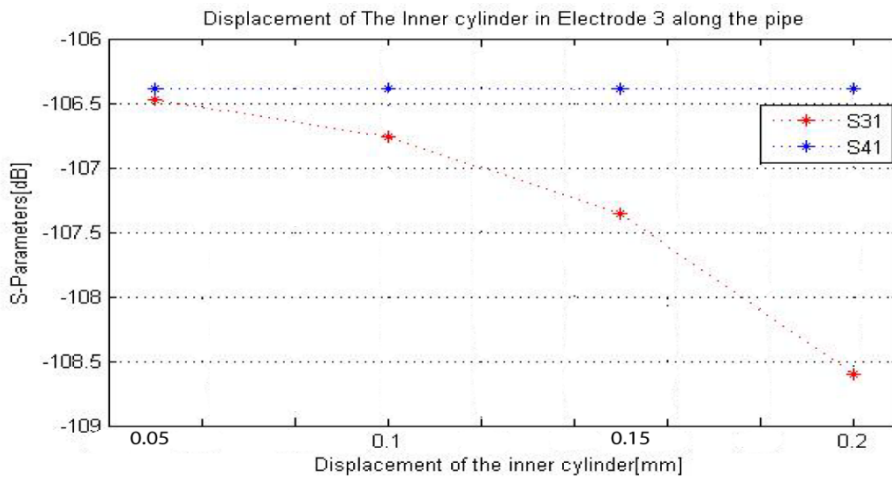


Figure F.33: S-parameters for different longitudinal displacements of electrode number 3 (see Figure F.32).

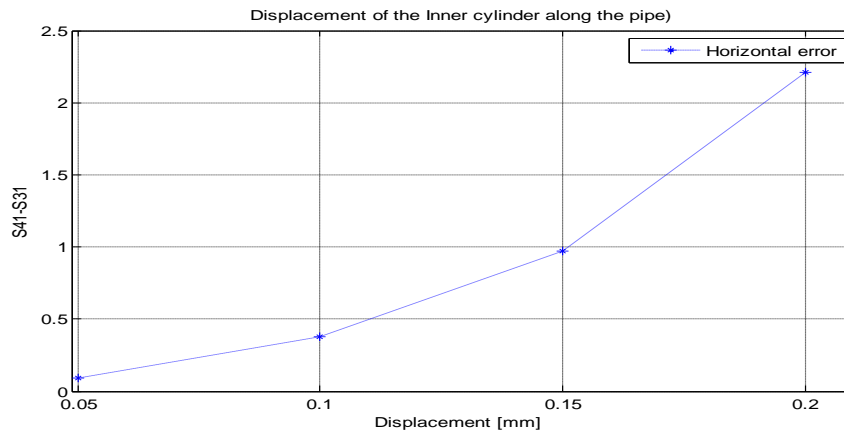


Figure F.34: Horizontal errors for different longitudinal displacements of electrode number 3 (see Figure F.32).

F.4. The inner pipe displacements

5.4.1. Beam displacements along the vertical axis

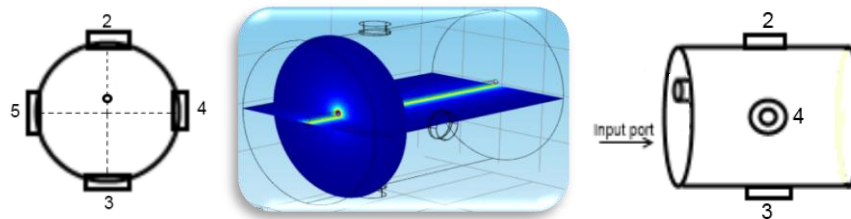


Figure F.35: Displacement of the inner pipe along the vertical axis z

Table F.13: S-parameters for different displacements of the beam along the vertical axis

Displacement to port 2	S21	S31	S41	S51	S31 – S21	S51 – S41
0.25 mm	-66.1675	-66.4339	-66.3018	-66.3014	0.2664	0.0004
0.5 mm	-66.0336	-66.5675	-66.3037	-66.3054	0.5339	0.0017
0.75 mm	-65.9005	-66.7012	-66.3097	-66.3092	0.8007	0.0005
1 mm	-65.7671	-66.8335	-66.3157	-66.3161	1.0664	0.0004
1.25 mm	-65.6326	-66.9659	-66.3245	-66.3244	1.3333	0.0001
1.5 mm	-65.499	-67.0986	-66.3354	-66.3342	1.5996	0.0012
2 mm	-65.2291	-67.3652	-66.3608	-66.3617	2.1361	0.0009

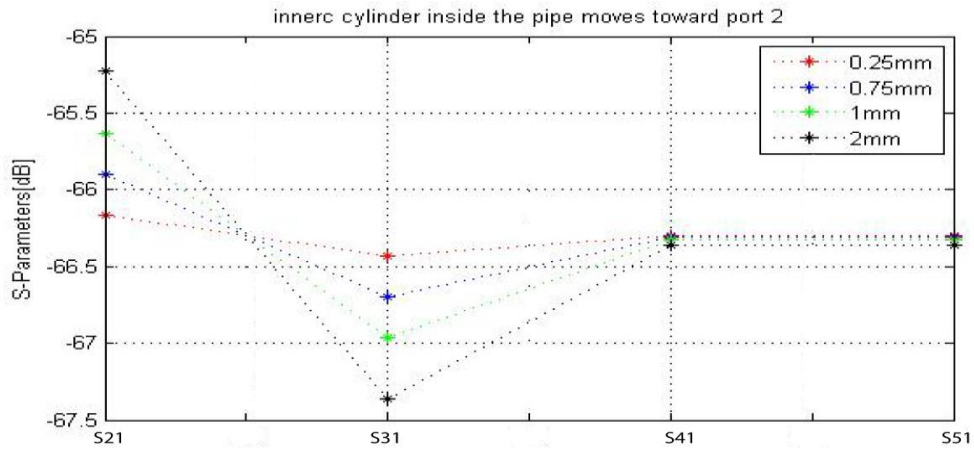


Figure F.36: S-parameters for different displacements of the beam along the vertical axis (See figure F.35).

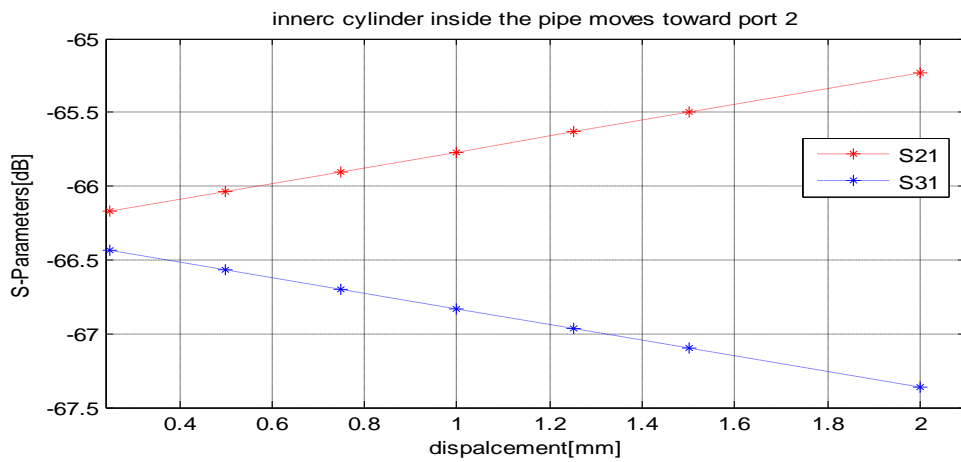


Figure F.37: Transmission through buttons 2 and 3 for different displacements of the beam along the vertical axis (See figure F.35).

Table F.14: Linear charge (Monopole) on the inner pipe surface for different displacements of the beam along the vertical axis (See figure F.35).

Linear charge	0.25 mm	0.5 mm	0.75 mm	1 mm	1.25 mm	1.5 mm	2 mm
ρ_l	1.6114e-9	1.6102e-9	-1.6105e-9	1.6112e-9	1.6118e-9	1.6106e-9	1.6115e-9

Table F.15: multipole moments for different displacements of the beam along the z-axis

Displacement [mm]	Dipole in y direction	Dipole in z direction	quadrupole in y direction	quadrupole in z direction	quadrupole $\rho_s \times y * z$	quadrupole $\rho_s \times (y^2 - z^2)$
0.25	-8.4378e-18	-4.0226e-14	8.0524e-17	9.0653e-17	2.1185e-20	1.0129e-17
0.5	-1.102e-17	-8.0576e-14	8.0499e-17	1.2083e-16	1.0816e-20	4.0334e-17
0.75	-1.4436e-18	-1.209e-13	8.052e-17	1.7129e-16	4.0536e-21	9.0767e-17
1	9.6854e-19	-1.6119e-13	8.0528e-17	2.4185e-16	4.8785e-21	1.6132e-16
1.25	-8.233e-17	-2.0169e-13	8.062e-17	3.3293e-16	1.4048e-19	2.5231e-16
1.5	2.4174e-18	-2.419e-13	8.0548e-17	4.4375e-16	1.0884e-20	3.632e-16
2	1.1586e-17	-3.2261e-13	8.0575e-17	7.2638e-16	1.7759e-20	6.458e-16

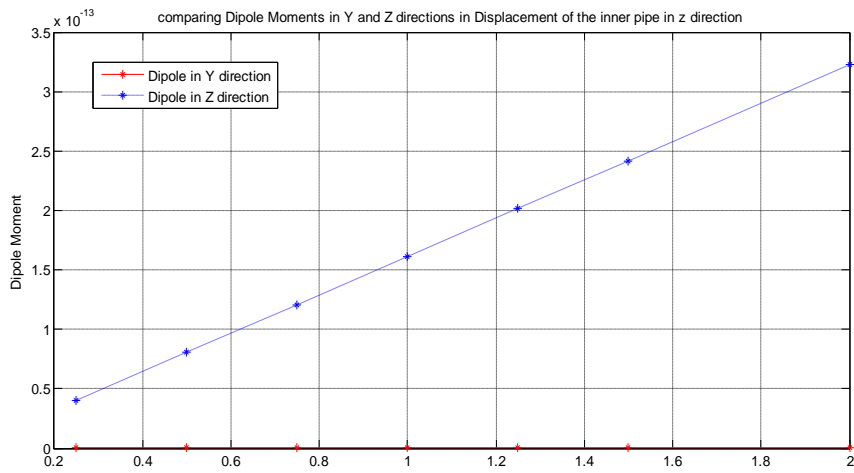


Figure F.38: Dipole moments for different displacements of the beam along the z-axis (See Figure F.35).

F.4.2. Beam displacements along a line between the horizontal and vertical axes

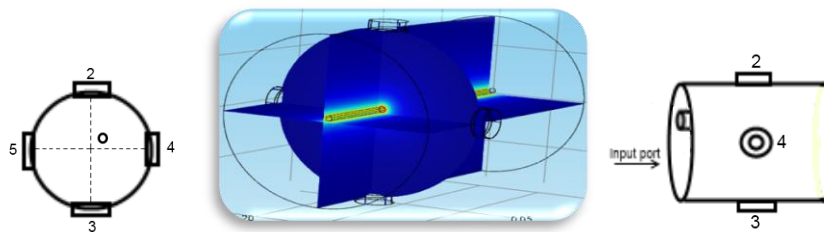


Figure F.39: Displacement of the inner pipe along the line $y=z$.

Table F.16: S-parameters for different displacements of the beam along the line $y=z$ (see figure F.39).

Displacement [mm]	S21	S31	S41	S51	S31-S21	S51-S41
(0.25,0.25)	-66.1685	-66.435	-66.1685	-66.4345	0.2665	0.2660
(0.5,0.5)	-66.0379	-66.5716	-66.0373	-66.5712	0.5337	0.5339
(0.75,0.75)	-65.909	-66.7086	-65.9088	-66.7093	0.7996	0.8005
(1,1)	-65.7815	-66.8482	-65.7816	-66.8484	1.0667	1.0668
(1.25,1.25)	-65.6574	-66.9897	-65.657	-66.9888	1.3323	1.3318
(1.5,1.5)	-65.5334	-67.1309	-65.534	-67.1315	1.5975	1.5975
(2,2)	-65.2933	-67.4219	-65.293	-67.4217	2.1286	2.1287

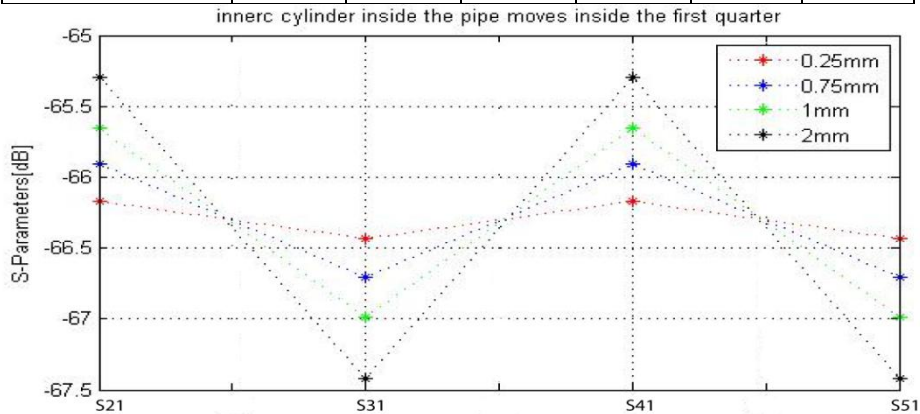


Figure F.40: S-parameters for different displacements of the beam along the line $y=z$ (see figure F.39).

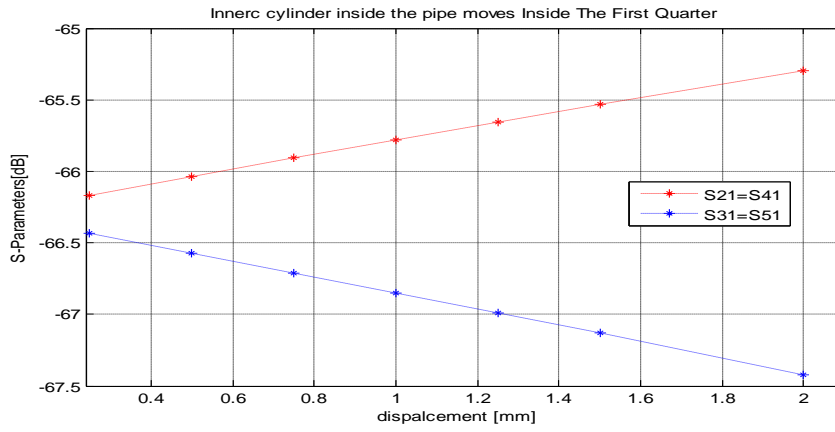


Figure F.41: Transmission through port 2 and 3 for different displacements of the beam along the line $y=z$ (see figure F.39).

Table F.17: Linear charge (Monopole) on the inner pipe surface for different displacements of the beam along the line $y=z$.

Linear charge	0.25 mm	0.5 mm	0.75 mm	1 mm	1.25 mm	1.5 mm	2 mm
ρ_l	1.6099e-9	1.6104e-9	1.6112e-9	1.6127e-9	1.3042e-9	1.6126e-9	1.6139e-9

Table F.18: multipole moments for different displacements of the beam along the line $y=z$ (see figure F.39).

Displacement [mm]	Dipole in y direction	Dipole in z direction	quadrupole in y direction	quadrupole in z direction	quadrupole $\rho_s \times y * z$	quadrupole $\rho_s \times (y^2 - z^2)$
(0.25,0.25)	4.0258e-14	-4.0304e-14	9.0554e-17	9.0583e-17	1.0091e-17	2.9143e-20
(0.5,0.5)	8.0602e-14	-8.0594e-14	1.2086e-16	1.2085e-16	4.0334e-17	-3.584e-21
(0.75,0.75)	1.2087e-13	-1.2092e-13	1.7126e-16	1.7128e-16	9.0725e-17	2.3454e-20
(1,1)	1.6126e-13	-1.6152e-13	2.4193e-16	2.4234e-16	1.6143e-16	4.0982e-19
(1.25,1.25)	1.6306e-13	-1.6307e-13	2.6909e-16	2.6909e-16	2.0394e-16	7.7982e-22
(1.5,1.5)	2.4203e-13	-2.4206e-13	4.439e-16	4.4397e-16	3.6335e-16	7.2569e-20
(2,2)	3.2297e-13	-3.2316e-13	7.2702e-16	7.2777e-16	6.4665e-16	7.4174e-19

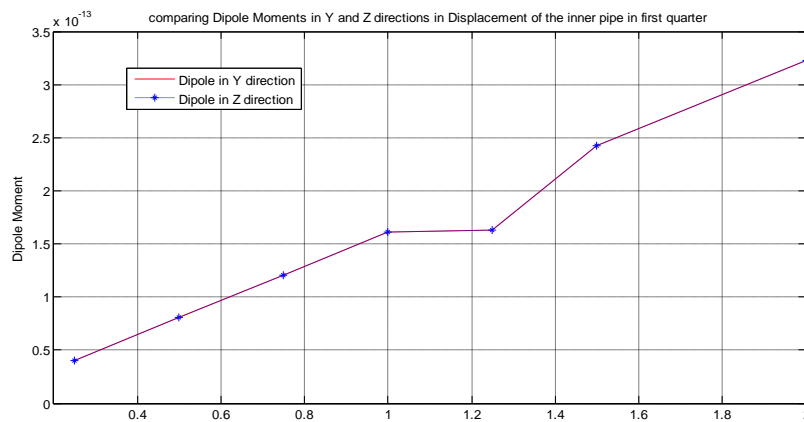


Figure F.42: Dipole moments for different displacements of the beam along the line $y=z$ (see figure F.39).

F.5 Elliptic beam

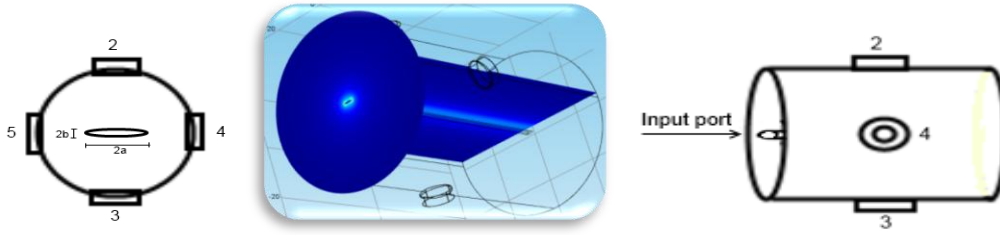


Figure F.43: Ellipse shape of the beam with the horizontal diameter $2a$ and vertical diameter $2b$

Table F.19: Buttons transmissions on vertical and horizontal axis (see figure F.43)

Elliptic Inner (mm)	S21	S31	S41	S51	$ S21 - S31 $	$ S41 - S51 $
a:1 , b:1	-66.3016	-66.3019	-66.3011	-66.3012	3e-4	1e-4
a:1.1 , b:0.9	-66.3048	-66.3054	-66.298	-66.2979	6e-4	1e-4
a:1.25 , b:0.75	-66.3096	-66.3093	-66.293	-66.2927	3e-4	3e-4
a:1.4 , b:0.6	-66.3145	-66.3155	-66.288	-66.2891	0,0010	0,0011
a:1.55 , b:0.45	-66.318	-66.3179	-66.2826	-66.2821	1e-4	5e-4
a:1.7 , b:0.31	-66.3223	-66.3214	-66.2762	-66.2775	9e-4	0.0013
a:1.85 , b:0.16	-66.3262	-66.3264	-66.2712	-66.2707	2e-4	5e-4
a:2 , b:0.02	-66.312	-66.3123	-66.2456	-66.2447	3e-4	9e-4

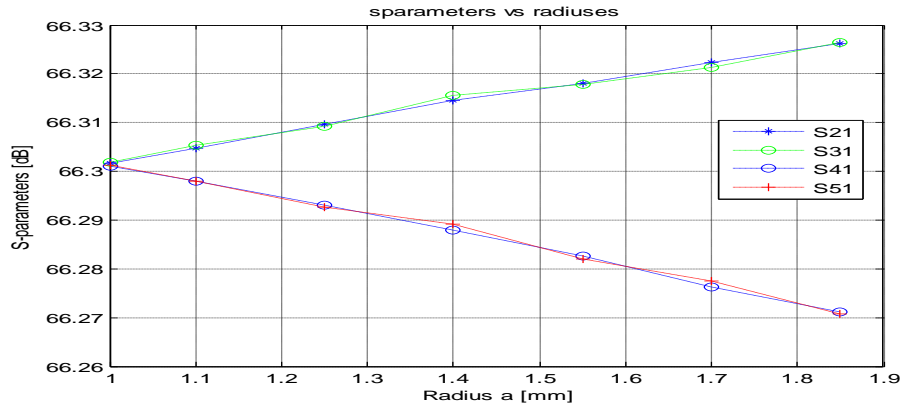


Figure F.44: Buttons transmissions on vertical and horizontal axis (see figure F.43)

Table F.20: multipole moments for Ellipse shape of the beam with the horizontal diameter $2a$ and vertical diameter $2b$

Elliptic Inner (mm)	Dipole in y direction $\rho_s \times y$	Dipole in z direction $\rho_s \times z$	quadrupole in z direction $\rho_s \times z^2$	quadrupole in z direction $\rho_s \times y^2$	quadrupole in z direction $\rho_s \times y * z$	$ (Q_{yy} - Q_{zz}) $
a:1.1 , b:0.9	1.1036e-16	9.9751e-17	6.5309e-17	9.6577e-17	1.2053e-19	3.1268e-17
a:1.25 , b:0.75	4.9826e-16	7.7985e-17	4.5184e-17	1.2142e-16	3.9774e-19	7.6232e-17
a:1.4 , b:0.6	1.4655e-15	1.518e-16	2.9726e-17	1.5194e-16	4.9712e-19	1.2221e-16
a:1.55 , b:0.45	4.0938e-16	1.2265e-16	-1.6871e-17	-1.729e-16	3.6141e-19	1.5603e-16
a:1.7 , b:0.31	-1.2347e-15	-1.6392e-16	-7.9789e-18	-1.9248e-16	1.456e-19	1.8451e-16
a:1.85 , b:0.16	-4.8904e-15	-5.506e-17	-2.1063e-18	-2.1212e-16	1.0867e-19	2.1002e-16

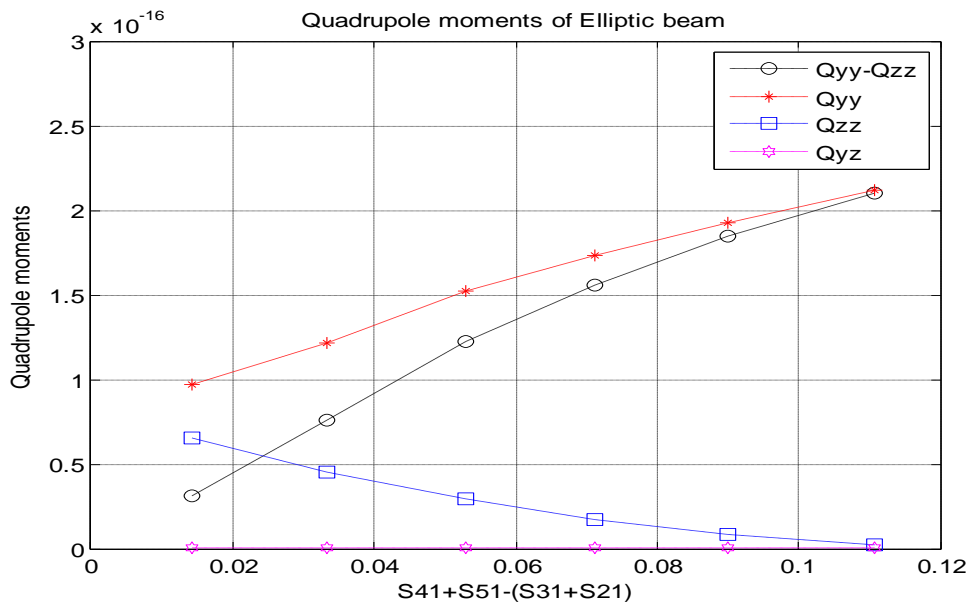


Figure F.45: The quadrupole moments of Elliptic beam with different semimajor axis a , and semiminor axis b , in horizontal and vertical axes vs the quadrupole signals $[(|S_{41}|_{dB}+|S_{51}|_{dB})-(|S_{21}|_{dB}+|S_{31}|_{dB})]$, (see figure F.43)

References:

- [1] Rahul Gaur[#], P.K. Jana and Purushottam Shrivastava Pulsed High Power Microwave Section Raja Ramanna Centre for Advanced Technology, Indore, RF CAVITY DESIGN OF 352.2 MHz, 3 MeV RFQ
- [2] M. Wendt. OVERVIEW OF RECENT TRENDS AND DEVELOPMENTS, FOR BPM SYSTEMS. Fermilab, Batavia, IL 60510, U.S.A.
- [3] Gil A. Travish. Transverse beam break-up in linear electron accelerators, Work supported by the Office of Energy Research, U.S. Dept of Energy, under Contract No. DE-AC03-76SF00098
- [4] Marcel Ruf, Siegfried Martius, Stefan Setzer and Sven Muller. Beam Position Monitoring in Electron Accelerators. *Frequenz* 63 (2009) 5–6.
- [5] Robert W Hamm. Marianne E Hamm. INDUSTRIAL ACCELERATORS AND THEIR APPLICATIONS. ISBN: 978-981-4307-04-8. Winter 2011.
- [6] pegas S, Bousson B, Calaga R, plans for the ESS LINAC, 2010.
- [7] <http://ess-scandinavia.eu/press>.
- [8] Quadrupole magnet at SLAC, **A094/0038** Rights Managed, **Credit: [STANFORD LINEAR ACCELERATOR CENTER/SCIENCE PHOTO LIBRARY](#)** and Photo courtesy SLAC
- [9] F. Hinode, H. Hayano, M. Tejima, N. Terunuma and J. Urakawa. A BEAM TEST OF BUTTON-TYPE BEAM POSITION MONITOR FOR THE ATF DAMPING RING. KEK, National Laboratory for High Energy Physics, 1-1 Oho, Tsukuba-shi, Ibaraki-ken, 305 Japan.
- [10] Robert E. Shafer. BEAM POSITION MONITORING. Los Alamos National Laboratory, Los Alamos, NM 87545.
- [11] Helmuth Spieler. Introduction to Radiation Detectors and Electronic. Lecture Notes - Physics 198, Spring Semester 1998 – UC Berkeley.
- [12] Robert W Hamm. Marianne E Hamm. INDUSTRIAL ACCELERATORS AND THEIR APPLICATIONS. ISBN: 978-981-4307-04-8. Winter 2011.
- [13] Helmut Wiedemann. Particle Accelerator Physics (book). Third Edition. ISBN-13 978-3-540-64504-7 Vol. 2 2nd ed. Springer Berlin Heidelberg New York
- [14] Peter Forck. Lecture Notes on Beam Instrumentation and Diagnostics. Joint University Accelerator School January – March 2011.
- [15] S.R. Marques[#], J.B. Gonzalez, P.F. Tavares, O.R. Bagnato, M.J. Ferreira, R.H.A. Farias, C. Rodrigues. *DESIGN OF BUTTON BEAM POSITION MONITOR FOR THE BRAZILIAN SYNCHROTRON LIGHT SOURCE LNSLS*. Campinas, Brazil, SP 13083-100
- [16] V. Ziemann. *Accelerator Physics and Technology*. Uppsala University. October 22, 2008
- [17] N. Akasaka, M. Arinaga, S. Hiramatsu, T. Jeiri, H. Ishii, K. Mori, T. Obina, T. Shintake, and M. Tejima. Design of Beam Position Monitor System for KEKB. KEK, Tsukuba, JAPAN.
- [18] Vorgelegt von, Dipl.-Ing Vahagn Sargsyan aus Jerewan. Cavity Beam Position Monitor for the TESLA-cryomodule. Cross-Talk minimization. Berlin 2003.

- [19] P. Kowina, P. Forck, W. Kaufmann, P. Moritz, GSI Darmstadt, F. Wolfheimer, T. Weiland, TU Darmstadt. *FEM SIMULATIONS – A POWERFUL TOOL FOR BPM DESIGN*. Germany.
- [20] Helmut Wiedemann. *Particle Accelerator Physics* (book). Third Edition. ISBN-13 978-3-540-64504-7 Vol. 2 2nd ed. Springer Berlin Heidelberg New York
- [21] Peter Forck. *Lecture Notes on Beam Instrumentation and Diagnostics*. Joint University Accelerator School January – March 2011
- [22] M. Minty. *DIAGNOSTICS*. Deutsches Elektronen Synchrotron (DESY), Hamburg, Germany.
- [23] Seadat Varnasseri. *BPM PICK UP POSITIONING FOR SESAME VACUUM CHAMBER*. Amman, June 2, 2005
- [24] Peter Forck, Piotr Kowina, Dmitry Liakin. *Beam Position Monitors*. Gesellschaft für Schwerionenforschung GSI, Darmstadt, Germany
- [25] Stephen R. Smith. *Beam Position Monitor Engineering*. Stanford Linear Accelerator Center, Stanford University, Stafiord, California 94309. July 1996
- [26] T. Moreno, *Microwave Transmission Design Data*, Great Neck, N.Y., Sperry gyroscope Co. [1945]
- [27] A. Jansson*, D. J. Williams. *A NEW OPTIMISED QUADRUPOLE PICK-UP DESIGN USING MAGNETIC COUPLING*. 2001
- [28] George B. Arfken, Hans J. Weber, Frank Harris, *Mathematical Methods for Physicists*, Sixth Edition, Academic Press, 2005.
- [29] N. Barov#, J.S. Kim, A.W. Weidemann, FAR-TECH, Inc., San Diego, CAR.H. Miller, C.D. Nantista, SLAC, Menlo Park, CA. *HIGH-PRECISION RESONANT CAVITY BEAM POSITION, EMITTANCE AND THIRD-MOMENT MONITORS*. 2005.
- [30] A. Jansson*, D. J. Williams. *A NEW OPTIMISED QUADRUPOLE PICK-UP DESIGN USING MAGNETIC COUPLING*. 2001.
- [31] Ronald Lorenz. *Cavity Beam Position Monitors*. DESY Zeuthen, Platanenallee 6, D-15738 Zeuthen
- [32] Vorgelegt von ,Dipl.-Ing Vahagn Sargsyanaus Jerewan. *Cavity Beam Position Monitor for the TESLA-cryomodule. Cross-Talk minimization*. Berlin 2003.
- [33] <http://ess-scandinavia.eu/>.
- [34] http://neutron.neutron-eu.net/n_ess/n_the_history_of_ess.
- [35] Myron D. Fanton, PE. *Transmission Line for Broadcast Applications*. ERITechnical Series, Vol. 6, April 2006.
- [36] Anders Karlsson. Gerhard Kristensson. *Microwave Theory*. Lund 1996-2009.
- [37] Peter A. Rizzi. *microwave engineering passive circuits*, ISBN 0-13-581711-0-1988.
- [38] Stanley Humphries, Jr. *Principles of Charged Particle Acceleration*. QC787.P3H86 1986 ISBN 0-471-87878-2.

[39] V. Ziemann. Accelerator Physics and Technology. Uppsala University. October 22, 2008.

[40] R. H. MILLER, J. E. CLENDENIN, hf. B. JAMES, J. C. SHEPPARD. NONINTERCEPTING EMITTANCE MONITOR. Stanford Linear Accelerator Center . August 1933.

[41] N. Barov¹, C.D. Nantista², and R.H. Miller², J.S. Kim¹. High-Efficiency Resonant Cavity Quadrupole Moment Monitor. FAR-TECH, Inc., 10350 Science Ctr. Dr, Bldg. 14, Ste. 150, San Diego, CA 92121 Stanford Linear Accelerator Center, Menlo Park, CA.